VILNIUS GEDIMINAS TECHNICAL UNIVERSITY

Regimantas RAMANAUSKAS

PRIMARY CRACK SPACING MODEL OF REINFORCED CONCRETE ELEMENTS

DOCTORAL DISSERTATION

TECHNOLOGICAL SCIENCES,
CIVIL ENGINEERING (T 002)

VGTU
LEIDYKLA
TECHNIKA
Vilnius 2019

Doctoral dissertation was prepared at Vilnius Gediminas Technical University in 2015–2019.

Supervisor

Prof. Dr Habil. Gintaris KAKLAUSKAS (Vilnius Gediminas Technical University, Civil Engineering – T 002).

The Dissertation Defence Council of Scientific Field of Civil Engineering of Vilnius Gediminas Technical University:

Chairman

Prof. Dr Juozas VALIVONIS (Vilnius Gediminas Technical University, Civil Engineering – T 002).

Members:

Dr Valentin ANTONOVIČ (Vilnius Gediminas Technical University, Material Engineering – T 008),
Dr Nicholas FANTUZZI (University of Bologna, Italy, Civil Engineering – T 002),
Assoc. Prof. Dr Olga KURASOVA (Vilnius University, Informatics Engineering – T 007),
Assoc. Prof. Dr Vladimir POPOV (Vilnius Gediminas Technical University, Civil Engineering – T 002).

The dissertation will be defended at the public meeting of the Dissertation Defence Council of Civil Engineering in the Senate Hall of Vilnius Gediminas Technical University at **1 p. m. on 8th of November 2019**.

Address: Saulėtekio al. 11, LT-10223 Vilnius, Lithuania.
Tel.: +370 5 274 4956; fax +370 5 270 0112; e-mail: doktor@vgtu.lt

A notification on the intent to defend the dissertation was sent on 7th of October 2019. A copy of the doctoral dissertation is available for review at VGTU repository http://dspace.vgtu.lt and at the Library of Vilnius Gediminas Technical University (Saulėtekio al. 14, LT-10223 Vilnius, Lithuania).

VGTU leidyklos TECHNIKA 2019-046-M mokslo literatūros knyga

ISBN 978-609-476-199-7

regimantas.ramanauskas@vgtu.lt

VILNIAUS GEDIMINO TECHNIKOS UNIVERSITETAS

Regimantas RAMANAUSKAS

ATSTUMO TARP PAGRINDINIŲ PLYŠIŲ ARMUOTO BETONO ELEMENTUOSE MODELIS

DAKTARO DISERTACIJA

TECHNOLOGIJOS MOKSLAI,
STATYBOS INŽINERIJA (T 002)

VGTU
LEIDYKLA
TECHNIKA
Vilnius 2019

Disertacija rengta 2015–2019 metais Vilniaus Gedimino technikos universitete.

Vadovas

prof. habil. dr. Gintaris KAKLAUSKAS (Vilniaus Gedimino technikos universitetas, statybos inžinerija – T 002).

Vilniaus Gedimino technikos universiteto Statybos inžinerijos mokslo krypties disertacijos gynimo taryba:

Pirmininkas

prof. dr. Juozas VALIVONIS (Vilniaus Gedimino technikos universitetas, statybos inžinerija – T 002).

Nariai:

dr. Valentin ANTONOVIČ (Vilniaus Gedimino technikos universitetas, medžiagų inžinerija – T 008),
dr. Nicholas FANTUZZI (Bolonijos universitetas, Italija, statybos inžinerija – T 002),
doc. dr. Olga KURASOVA (Vilniaus universitetas, informatikos inžinerija – T 007),
doc. dr. Vladimir POPOV (Vilniaus Gedimino technikos universitetas, statybos inžinerija – T 002).

Disertacija bus ginama viešame Statybos inžinerijos mokslo krypties disertacijos gynimo tarybos posėdyje **2019 m. lapkričio 8 d. 13 val.** Vilniaus Gedimino technikos universiteto senato posėdžių salėje.

Adresas: Saulėtekio al. 11, LT-10223 Vilnius, Lietuva.
Tel.: (8 5) 274 4956; faksas (8 5) 270 0112; el. paštas doktor@vgtu.lt

Pranešimai apie numatomą ginti disertaciją išsiusti 2019 m. spalio 7 d.

Disertaciją galima peržiūrėti VGTU talpykloje http://dspace.vgtu.lt ir Vilniaus Gedimino technikos universiteto bibliotekoje (Saulėtekio al. 14, LT-10223 Vilnius, Lietuva).

Abstract

The intention of the present study is to develop a unified approach for serviceability analysis reinforced concrete tensile and flexural elements, with a focus on mean crack spacing. The current research is mainly quantitative in nature, with the development of the strain compliance approach based on collected data of 170 tensile and 96 flexural specimens. Furthermore, statistical analysis and individual physical parameter impact on the crack spacing and accuracy in general are provided. The key feature of the proposed strain compliance concept is the merging of two distinct cracking analysis methods, referred to as the stress transfer and the mean deformation approaches. Compatibility is ensured by equating the mean reinforcement strains, as estimated by the referred techniques individually. Thus, the lack of knowledge on the spatial strain distribution in the mean deformation approach is addressed by the stress transfer technique, which contains such knowledge.

The technique has been derived for tensile elements with the inclusion of a reference element notion, that is defined by reference values of bar diameter and reinforcement ratio. Moreover, the mean crack spacing must also be known. Consequently, the bond stresses can be evaluated for this reference case and the predictions can then be extended to alternative configurations of ratios of reinforcement and bar diameters.

The concept has been extended with modifications to the assumed strain profile for flexural elements. The notion of the reference element has been eliminated with bond stresses accounted for directly from selected models, such as design codes. A central zone concept is introduced, which governs the averaged behaviour of the reinforcement strains within the middle between consecutive primary cracks. A constitutive length model was derived. In-depth comparisons with experimental data and parametric investigations were carried out.

With the rise of machine learning in the field of civil engineering, it is imperative that research stays ahead of the trend to be able to analyse the implications. A multipurpose study was carried out, resulting in the development of an artificial neural network for estimating the spacing between cracks with very good generalisation abilities, good adequacy in terms of accuracy and consistency. Incidentally, the gathered experimental data was validated for robustness and the general features of the strain compliance method were found to be in good agreement with the neural network predictions and the experimental results.

The research concludes with the validation of the strain compliance technique as a more adequate approach in terms of scatter and accuracy than the present design codes. Moreover, the concept has been shown to be mechanically sound.

Reziumė

Šios disertacijos tyrimų pagrindinis tikslas nukreiptas į unifikuoto fizikinio metodo sukūrimą gelžbetoninių tempiamų bei lenkiamų konstrukcinių elementų tinkamumo ribinio būvio analizei, ypač atstumų tarp plyšių prognozavimui. Šis tyrimas didžiąja dalimi yra kiekybinis, paremtas surinktais eksperimentiniais duomenimis, kuriuos sudaro 170 tempiamų elementų bei 96 lenkiamų sijų ir plokščių. Darbe pateikta supaprastinta šių duomenų statistinė analizė, išskiriant esmines geometrines bei mechanines charakteristikas turinčias didžiausią poveikį atstumams tarp plyšių. Remiantis šiais duomenimis pasiūlytas suderintas deformacijų metodas, kurio esminis principas yra dviejų pleišėjimo analizės metodų – vidutinių deformacijų ir diskrečiųjų plyšių – apjungimas per šiais metodais apskaičiuotų vidutinių armatūros deformacijų lygybę.

Sukurtas metodas tempiamiems armuotiems betoniniams elementams, kurių akcentas yra etaloninio elemento sąvoka. Ji aprašo tempiamą elementą, kurio armavimo procentas, armatūros skersmuo bei vidutinis atstumas tarp pagrindinių plyšių yra žinomi. Pagal pasiūlytą metodą nustatomi armatūros ir betono sukibimo įtempiai prie pasirinkto apkrovimo lygio. Žinant sukibimo įtempius, armatūros skersmenį bei armavimo procentą, galima įvertinti bet kurios kitos konfigūracijos tempiamo elemento vidutinį atstumą tarp plyšių.

Ši koncepcija išplėtota lenkiamiems gelžbetoniniams elementams, pritaikius supaprastintą armatūros deformacijų tarp dviejų pagrindinių plyšių kreivę. Šiam metodui nebereikalinga etaloninio elemento sąvoka, armatūros ir betono sukibimo įtempiai įvertinami tiesiogiai. Armatūros deformacijos aprašomos tiesėmis, darant prielaidą, kad centrinė dalis tarp gretutinių plyšių gali būti reprezentuojama horizontalia linija, taip akcentuojant vidutinę deformacijų elgseną. Šiai centrinei zonai pasiūlytas fizikinis modelis, priklausantis nuo efektyvaus konstrukcijos aukščio ir neutraliosios ašies. Vidutinis atstumas tarp plyšių įvertinamas remiantis vidutinių armatūros deformacijų sulyginimu kaip ir tempiamiems elementams. Tyrimo rezultatai ir palyginimai pateikti išsamiose lentelėse ir grafikuose.

Šiame tyrime buvo išvystytas dirbtinis neuroninis tinklas, leidžiantis itin tiksliai ir su minimalia sklaida prognozuoti vidutinius atstumus tarp plyšių lenkiamiems elementams. Atlikta studija leido įvertinti surinktų eksperimentinių duomenų adekvatumą bei pagrįsti suderintų deformacijų metodą, kuris buvo sukurtas naudojant tuos pačius duomenis. Taip pat pademonstravo galimas pasiūlyto metodo tikslumo bei rezultatų sklaidos ribas, kurias būtų įmanoma pasiekti toliau plėtojant suderintų deformacijų metodą.

Disertacijos tyrimų metu sukurtas suderintų deformacijų metodas pasižymi geresniu skaičiavimo rezultatų tikslumu bei sklaida palyginus su projektavimo normomis. Metodas ir jo prielaidos pasižymi tvirtu fizikiniu pagrindimu.

Notations

Symbols

ε_c – concrete strain;
ε_{cr} – concrete cracking strain;
ε_s – steel strain;
ε_{sm} – mean reinforcement strains;
ξ – strain correlation coefficient;
ρ – reinforcement ratio in percentage;
σ_c – concrete stress;
σ_s – steel reinforcement stress;
τ – bond stress;
A_c – area of plain concrete net section;
A_s – area of bar reinforcement;
E_c – elasticity modulus of concrete;
E_s – elasticity modulus of steel reinforcement;
I – moment of inertia;
L – element length;
M – bending moment;
M_{cr} – cracking bending moment;
M_u – ultimate bending moment;
N_c – axial force of concrete;

N_s – axial force of steel reinforcement;
P – load;
P_{cr} – cracking load;
P_u – ultimate load;
b – element section width;
c – concrete cover;
d – the effective depth of a reinforced concrete section;
f_c – compressive strength of concrete;
f_{cm} – mean compressive strength of concrete;
f_{ct} – tensile strength of concrete;
f_{ctm} – mean tensile strength of concrete;
f_s – yield strength of steel reinforcement;
f_u – ultimate tensile strength of reinforcement;
h – section height;
l_c – *central zone* length;
l_d – *debonding zone* length;
l_{eff} – *effective bond zone* length;
l_{tr} – bond stress transfer length;
s – slip between concrete and reinforcement bar;
s_{rm} – mean crack spacing;
t – time in days;
w_m – mean crack width;
w_{max} – maximum crack width;
y_0 – distance to the neutral axis from the top of the element;
Ø – diameter of bar reinforcement.

Abbreviations

ANN – artificial neural network;
EC2 – European code for design of reinforced concrete structures;
FE – finite element;
FFBP – feed forward back propagation (neural network type);
FFNN – feed-forward neural network;
FRP – fibre reinforced polymer;
MC 2010 – design code of the International Federation for Structural Concrete;
RC – reinforced concrete.

Contents

[1] The annexes are supplied in the attached compact disc.

Introduction

Problem Formulation

With the construction industry progressively aiming for higher levels of sustainability, reinforced concrete as the most widely used construction material is gaining increased attention. Numerous actions can be taken to improve the sustainability of concrete, most common ones target the reduction of CO_2 emissions from the manufacturing process. Other solutions are targeting the increase of the durability of the material over time. Improving the service life of reinforced concrete structures can have a profound long-term impact, particularly when large scale projects such as infrastructure objects are in question. The control of concrete cracking can partially help address the issue. Whereas the ultimate limit state governs the load carrying capacity of structural components, the serviceability limit state is intended to ensure the expected life-cycle of the structure. As the concrete cracks, environmental factors, such as rain, freeze-thaw cycles, begin to affect the reinforcing bars, which begin to corrode and if left unattended. Such structures risk not achieving their expected design life or risk premature collapse. A core issue lies in the design process, the design code implementations of cracking models. In order to mitigate cracking, it is imperative to understand the cracking phenomena well enough to adequately estimate the widths and spacings of cracks. Design codes employ numerous empirical notions,

that inherently lead to increased scatter of calculation results. The incompatibility of available techniques in terms of width, the spacing of cracks and deformations have provided the motivation for the present study. Which attempts to solve the need for a compatible approach with greatly controlled scatter of predictions by developing the strain compliance concept for cracking analysis.

Due to the highly scattered results of design codes, engineers are increasingly more reliant on various numerical based solution. The gradual increase in available computer processing power has given rise to the adoption of machine learning within the fields of architecture, engineering and construction. Although neural networks have been around for a while, widespread adoption is yet to be reached. There is limited research on neural network application for serviceability analysis purposes and the few that target spacing between cracks have significant shortcomings. The present research aims to utilise neural networks for a multitude of purposes, the numerical and statistical analysis of the collected experimental cracking data, as a form of sensitivity analysis of the impact of various physical parameters on the spacing value and, finally, for the purpose of creating a tool yielding highly consistent estimations.

Relevance of the Thesis

One of the core issues, particularly for large span structures, such as bridges, and very long structural beams is not related to the load carrying capacity, but the extensive cracking and crack widths exceeding limits as defined by serviceability analysis. This partly occurs due to inadequately performing cracking models present in design codes. Accuracy of predictions and, more significantly, the consistency have to be improved. However, the techniques present in design codes are permeated with empirical aspects, further increasing the scatter of results. Furthermore, the methods are not compatible in terms of strain behaviour and cracking phenomena estimation. In order to improve the adequacy of predictions and reduce the scatter, a unified approach must be developed. As the width of a crack is dependent on the spacing between adjacent primary cracks, known from the bond behaviour of reinforced concrete structures, it is imperative to prioritise accurate crack spacing estimations that will, in turn, affect the width estimations. Investigating the mean crack spacing enables to account for the scatter and statistically derive characteristic values in the future. Investigation of analytical and numerical techniques such as artificial neural networks allows for better insight on the significance of the various aspects governing cracking.

Object of the Research

The object of this research is the average spacing between primary consecutive cracks of both tensile and flexural reinforced concrete elements under service loading at the stabilized cracking stage.

Aim of the Thesis

This study is dedicated to the development of a new technique for the investigation of cracking behaviour of tensile and flexural reinforced concrete members and the validation of this technique through the application of artificial neural networks.

Tasks of the Thesis

In order to achieve the aim of the thesis, the following tasks are established:

1. To identify the drawbacks of existing crack spacing prediction models, investigate the state-of-the-art approaches and their key characteristics.
2. To carry out an in-depth investigation of available experimental data on tensile and flexural concrete elements, where sufficient records on key characteristics exist, such as geometric and mechanical properties, loading conditions, the distance between cracks.
3. To propose an approach for estimating the average crack spacing of reinforced concrete tension members, when loading conditions are ensured the element being in the stabilized cracking stage.
4. To adapt the developed theoretical approach for reinforced concrete beams subjected to bending.
5. To verify the adequacy of the proposed approaches for predicting crack spacing against experimental data and carry out a systematic comparative study with existing design codes and selected best performing existing methods and the influence of parameters.
6. To create an artificial neural network for the prediction of crack spacing values of flexural elements, analyse the collected data in terms of quality.
7. To compare the performance of the neural network with the proposed approach.

Research Methodology

The methodology adopted for the present research covers the collection and statistical analysis of experimental cracking results of tensile and flexural elements available in published literature, analysis of available cracking models and development of a new approach for crack spacing predictions by analytical and numerical means. *Matlab* software was employed for these tasks to carry out regression analyses and apply numerical iterative methods. An artificial neural network was calibrated in *Matlab* to analyse the quality of the collected data as a form of statistical and numerical analysis. The nature of the present research is quantitative, relying on a database of results to develop and validate new prediction techniques. The methodology enabled the development of a new crack spacing estimation approach with increased certainty in its prediction accuracy.

Scientific Novelty of the Thesis

1. The fundamental concept of the strain compliance approach is applicable to both, the tensile and flexural reinforced concrete elements. The harmonisation of the approach in terms of adequate predictions for both cases enables to overcome the shortcomings of previous research studies.
2. The proposed strain compliance concept is able to provide an adequate estimation of crack spacings, provided reasonable approximations of the strain distribution are considered. The flexibility of the concept enables for the inclusion of multiple local effects, alternative strain shape functions, sectional geometries and alternative materials. The results of the approach are compatible in terms of deformations and crack spacings, as per the equality of mean strains from smeared crack and stress transfer techniques condition that must be enforced in the approach.
3. Artificial neural network predictions indicate that the bar diameter, ratio of reinforcement, effective section height are the key parameters having the largest impact on the crack spacing predictions. With concrete cover playing a reduced part and the mean concrete compressive strength having a negligible impact for primary cracks.

Practical Value of the Research Findings

1. A new method for predicting the mean crack spacing values in a compatible way with strain behaviour has been developed. The technique

can be employed in predicting the mean crack spacing of any structural element subjected to bending or applied to experimental tensile specimens. By relating the crack spacing to the maximum spacing, the maximum crack width could be predicted.

2. An artificial neural network has been developed and tuned for the collected experimental data of flexural reinforced concrete elements. The network enables accurate and consistent predictions of mean crack spacing values based on 6 key inputs, the diameter of tensile bars $Ø_s$, the ratio of reinforcement ρ, effective section height d, concrete compressive strength f_{cm}, the concrete cover c and the neutral axis position y_0. The network can serve as a tool for more controlled experimental programme development, with better knowledge of the expected outcome beforehand.

The Defended Statements

1. The developed strain compliance concept enables accurate predictions of the mean crack spacing values of both tensile and flexural reinforced concrete elements in a mechanically robust way and minimal reliance on empirical notions, provided equality of mean reinforcement strains as obtained by the stress transfer and mean deformations approaches is ensured.
2. With a meticulous calibration process, a neural network model can be trained from relatively scattered and limited reinforced concrete cracking data to predict the distance between cracks with a high degree of accuracy and certainty, while maintaining the ability to generalise to newly introduced samples.

Approval of the Research Findings

The author has published 11 scientific research papers on the topic of the dissertation (three of them in journals with an Impact Factor and one in conference proceedings indexed by the *Clarivate Analytics Web of Science,* eight in international conference proceedings). Over the course of the PhD studies (2015–2019) dissertation results were published or presented at 5 conferences:

- 2017. 2nd International RILEM/COST Conference on *Early Age Cracking and Serviceability in Cement-based Materials and Structure*s (EAC-02), Brussels, Belgium.

- 2016. 24th Australasian Conference on the *Mechanics of Structures and Materials* (ACMSM24), Perth, Australia.
- 2016. fib Symposium 2016 *Performance-based approaches for concrete structures*, Cape Town, South Africa.
- 2016. International RILEM Conference on *Materials, Systems and Structures in Civil Engineering*, Lyngby, Denmark.
- 2015. 10th International Conference on *Mechanics and Physics of Creep, Shrinkage, and Durability of Concrete and Concrete Structures* (CONCREEP 10), Vienna, Austria.

Structure of the Dissertation

The dissertation consists of an introduction, four chapters, general conclusions, reference list of cited sources (105), list of the author's publications on the dissertation research (11 publications), summary in Lithuanian and 8 annexes. The volume of the dissertation is 145 pages, with 51 figures and 11 tables.

Acknowledgements

The author is infinitely grateful for the support, patience and encouragement on the path to this doctoral thesis to the two most important people in his life, his wife Skaistė Ardavičiūtė-Ramanauskienė and his mother Genovaitė Ramanauskienė.

For consultation and guidance in preparing this thesis, the author would like to express his gratitude to his supervisor, Prof. Dr Habil. Gintaris Kaklauskas of the Department of Reinforced Concrete Structures and Geotechnics.

In addition, the author expresses his appreciation for the advice, comments and assistance in the preparation of this thesis to Dr Viktor Gribniak of the Department of Steel and Composite Structures. Dr. Pui Lam NG for his valuable comments and shared experience, also Prof. Dr Darius Bačinskas and Dr Eugenijus Gudonis of the Department of Reinforced Concrete Structures and Geotechnics, Dr Aleksandr Sokolov of the Laboratory of Innovative Building Materials. The author is grateful to the staff of the Department of Reinforced Concrete Structures and Geotechnics, to the fellow PhD students with who we have shared this doctoral experience. For remarks and valuable feedback on the thesis, the author extends gratitude to Dr Remigijus Šalna, Dr Vladimir Popov and Dr Gintautas Skripkiūnas. The author of the thesis expresses his gratitude to the Research Council of Lithuania for the financial support during doctoral studies.

1

Background on Cracking Behaviour and Serviceability of Concrete

The fundamental background on the behaviour of reinforced concrete (RC), particularly in relation to its complex cracking nature, as well as the literature survey on the topic of predicting crack spacing is presented in this chapter. Various existing crack spacing prediction approaches have been investigated, including both, available in design codes and in published scientific papers. Origins of different methods are covered, and their key assumptions outlined. The strengths and drawbacks are compared. Although the core of the present study is focused on developing more accurate and consistent ways to estimate crack spacing, bond behaviour and its significance on reinforcement and concrete strain distributions are examined as well. From the key observations, the main objective and tasks for the current research are presented at the end of this chapter. This chapter includes the material presented in journal publications Kaklauskas et al. (2017a, 2019a, 2019b) and conference proceedings Gudonis et al. (2017), Kaklauskas et al. (2015, 2016, 2017b), Kaklauskas & Ramanauskas (2016a, 2016b).

1.1. Deformation Behaviour of a Cracked Reinforced Concrete Element

Reinforced concrete is a material with a highly universal application and intricate working mechanics. Nonlinearity is present throughout all aspects of RC behaviour. From complex expressions governing the relation between material and geometrical properties. As RC structures are mostly designed for ultimate limit state conditions, the peculiarities of serviceability limit state analyses can be overlooked on how complicated and inconsistent they are among different design codes and methods proposed by various researchers. Cracking of concrete can be considered the most complex of all phenomena affecting the material. The nature of it is not fully understood to this day, with a great number of influencing physical parameters present in the available approaches highlighting the ongoing debate in the field of serviceability analysis of RC.

Cracking phenomenon is deeply related to the contact of reinforcement and concrete. The boundary layer between them is the source of most cracking in the element. Goto (1971) has observed and shown with his research the inner crack pattern of an RC element that was not observed before. Special ink was used to infiltrate the cracks that left even the smallest ones visible after the specimens were cut longitudinally. The pattern was cleared and revealed very dense small cracks surrounding the reinforcement bar ribs (shown schematically in Fig. 1.1). The described cracks, stemming from the ribs are now referred to as secondary cracks or internal Goto cracks. The extension of these internal cracks further deteriorates the bond actions between the bar and concrete and this behaviour describes the stabilized cracking stage (Goto 1971). In contrast to ribbed bars for which the larger part of bond action is controlled by their ribs, plain bars do not exhibit such cracking behaviour as the primary source of compatible action is ensured by adhesion and friction (Tepfers 1979).

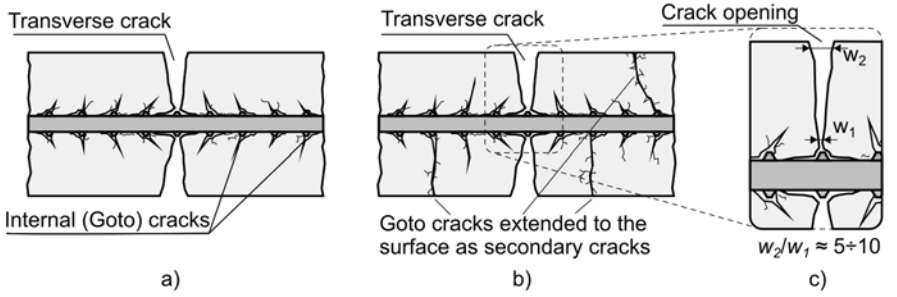

Fig. 1.1. Reinforced concrete cracking phenomena: a) secondary cracks, often call Goto cracks, localised around bar ribs, b) as secondary cracks reaching the surface of an element, c) crack width increase further away from the bar.

With sufficient increase in applied load, the radial cracks will extend towards the surface of the concrete (Fig. 1.1b). Depending on this distance, the width of the crack will vary along with the height of the element (see Fig. 1.1c), within a significantly large range of up to 10 times the width at the origin (Broms 1965, Broms & Lutz 1965). Moreover, Broms (1965) has observed that crack widths at the surface of an RC element can be linearly related to the tensile.

1.1.1. Reinforced Concrete Cracking Stages

Generally, the behaviour of reinforced concrete elements is expressed by three stages depending on loading levels (Model Code 2010). Similarly, Somayaji & Shah (1981) have discerned four stages, with the initial three being identical to the Model Code provision and the last one called the fracture stage, where the reinforcement yields. Figure 1.2a conveys these stages visually, with letters A, B and C denoting the beginning/end of cracking stages. The first is the *elastic stage*, defined by *OA*, where the structural response is fully linearly elastic. Local effects are limited to the ends of the element, where minor slippage can occur between reinforcement and concrete.

After exceeding the cracking load P_{cr}, the element enters the *crack formation stage AB*. Usually, after the first crack appears, subsequent cracks form close to instantaneously, without significant increase of the load. Reinforcement strain values immediately shift right, as the compatibility between concrete and reinforcement strains is not sustained. Hence, the tensile force (in case of axially loaded RC elements) is transferred mainly by the steel bar at the position of the crack. Effects such as tension-softening can play a significant role in the amount of the load the concrete part is able to carry within the crack. Often the tension-softening effect is neglected for simplicity, by considering the entirety of the concrete section to be cracked. At the crack formation stage, the bond behaviour plays a key role, as with the further increase of the load, the tensile stresses continue to increase, and the amount transferred to the surrounding concrete from the reinforcement bar depends on the bond. After a specific distance denoted as the transfer length l_{tr} (Beeby 2004), concrete and reinforcement strains become compatible again, provided there is enough physical length remaining in the actual segment between normal cracks. If compatibility is reached, new cracks may continue to appear. The discussed concrete and reinforcing bar interaction is defined as the stress-transfer approach (Saliger 1936), part of the discrete crack based models. The transfer length l_{tr}, which defines the distance required to achieve complete bond action between concrete and reinforcement can be evaluated from the condition of equilibrium of concrete cracking force and the force transmitted by bond:

$$A_c f_{ct} = n\pi \emptyset_s \int_0^{l_{tr}} \tau(x)dx., \tag{1.1}$$

When the length of the remaining concrete blocks becomes sufficiently short that l_{tr} cannot be reached, the element can be considered to have reached the *stabilized cracking* stage *BC*. However, Model Code 2010, also proposes the stabilized cracking phase is entered when the load exceeds $1.3P_{cr}$. In general, the spacing between normal cracks s_r falls within the range $l_{tr} \leq s_r < 2l_{tr}$. The average crack spacing value is declared to be in the range of $1.3l_{tr} \leq s_r < 1.5l_{tr}$ by various authors (Bigaj 1999, Borosnyói & Balázs 2005, Barre et al. 2016).

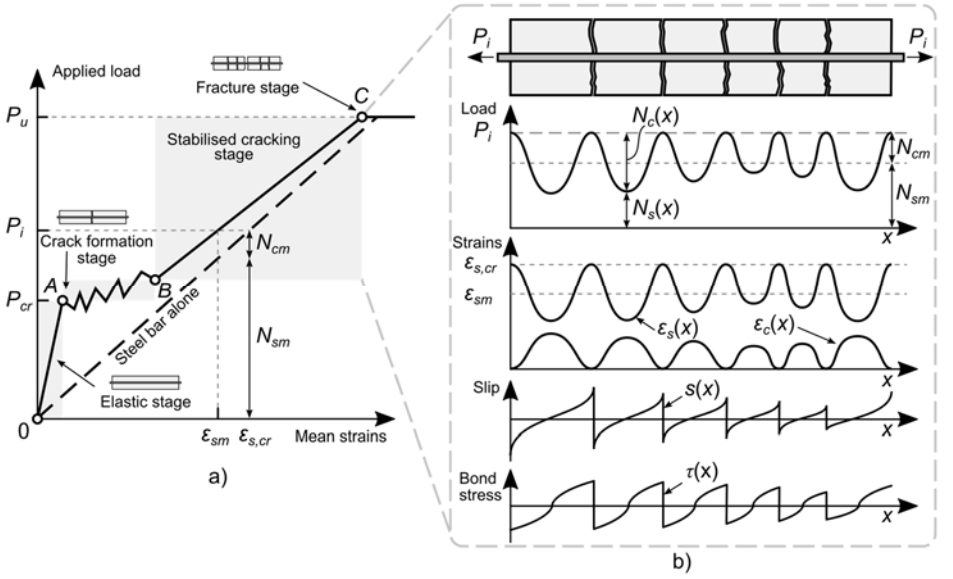

Fig. 1.2. Reinforced concrete loading and cracking schematics: a) **c**racking stages; b) load-sharing concept

The mechanics of bond interaction between the embedded bar and the surrounding concrete are presented in Figure 1.2b for a given load in the stabilized cracking stage. The relation between the strains of reinforcement $\varepsilon_s(x)$ and concrete $\varepsilon_c(x)$, bond stress $\tau(x)$ and slippage $s(x)$ are controlled by the governing equation (Ruiz et al. 2007):

$$\frac{d\varepsilon_s(x)}{dx} = \frac{4}{E_s \emptyset_s}\tau(x). \tag{1.2}$$

Saliger (1936) had assumed the bond stress to be constant in order to simplify the expression and its solution. The reinforcement strain distribution was thus

expressed linearly and was subsequently incorporated in many approaches and design codes as discussed Section 1.2. The result of this simplification was the expression of transfer length ltr in terms of the well-known $Ø/\rho_{ef}$ ratio. Moreover, the governing Equation (1.2) also provides the link to the crack width w by:

$$w = \Delta\varepsilon_m = \int_{s_r} (\varepsilon_s - \varepsilon_c)\, dx, \tag{1.3}$$

where ε_s and ε_c are the reinforcement and concrete strains, respectively.

1.1.2. Experimental Investigations of Strain Distribution

Ordinary investigation of the bond behaviour of reinforced concrete elements is based on reinforcement bar pull-out from concrete experiments and RILEM-RC5 4 point bending tests (RILEM 1982). The common test types are shown schematically in Figure 1.3. With load-displacement recording being the primary source of data. Such tests enable obtaining the average bond stress distribution within anchorage length in relation to the displacement. Nevertheless, the results have been unreliable due to unnatural behaviour of the specimen, like compression stresses which are not representative of likely scenarios (FIB 2000). The standardised pull-out tests are not adequate for determining bond-slip relationships or strain distributions within an element, for that matter (Ashtiani et al. 2013).

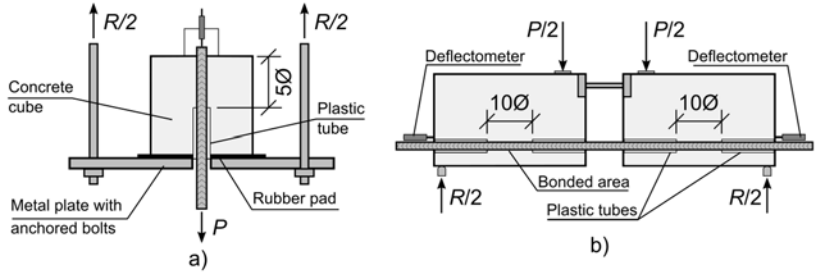

Fig. 1.3. Common bond test types: a) pull-out test; b) RILEM-RC5 four-point bending test with a hinge at the top and exposed bar at the bottom

With the introduction of electrical strain gauges, it was possible to record strains directly from the reinforcement of a cast reinforced concrete element. Therefore, bond stress versus slippage could be estimated from the spatial distribution. The technique for installing gauges directly on the reinforcement have largely remained complicated and demanding of meticulous precision, yet it remains among the most reliable ways to investigate the bond interactions of concrete and reinforcement (Scott & Gill 1987) and more significantly in the

context of the present research, a way to provide more insight on the actual strain profile and its governing shape function.

First attempts to record measurements in the above way resulted in strain gauges being glued to the external boundary of the reinforcement bars, yet this reduced the bond area between reinforcement and concrete and inadvertently altered the readings. To overcome this, Mains (1951) has developed a technique whereby the bar was split into two parts longitudinally and strain gauges were installed along the middle, along the axis. A groove held the gauges and the wires. This did have an effect on the reduced bar area, which had a relatively increased impact on results for a smaller bar, hence the early research adopted large bar diameter for such tests. Further experimental studies with the technique were carried out by Houde (1974), Scott & Gill (1987), Kankam (1997), with studies exploring both longer elements and shorter elements and bars as small as 12 mm in diameter. Examples of tensor strain installation layouts are given in Figure 1.4, as employed in Kaklauskas et al. (2019b), Kaklauskas et al. (2016) and Gudonis et al. (2017).

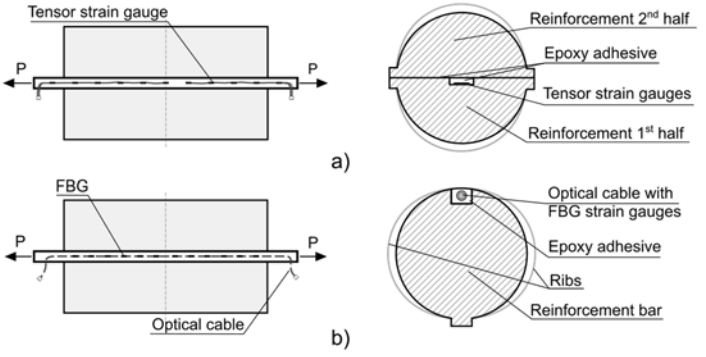

Fig. 1.4. Layouts of tensor strain gauge or optical sensor cable installation: a) 2 bars milled and glued back together with the sensor in the middle groove and b) sensors installed on the outside of the bar where damage to ribs can be minimized

Kankam (1997) has obtained reinforcement strain readings for short 200 mm long RC tie specimens, that has yielded detailed insight on the strain distribution profile. Moreover, he has suggested bond-slip relationships from the research findings. Very large diameter bars (Ø50mm) were prepared with inner strain gauges by Wenkenbach (2011). Recently, with advances in optical sensing techniques, strain measurement has become more detailed with the ability to measure data points with increased density (Davis et al. 1997). The principles remain similar to earlier experimental studies, the optical wires are inserted either within a groove on the outside or the middle of the bar. Fibre Bragg grating (FBG)

based optical sensors were employed by Kenel et al. (2005), and Kaklauskas et al. (2019). Both studies had the FBG sensors in 10 mm intervals, providing denser results than most previous tensor strain gauge tests. More sophisticated research with optical frequency domain reflectometry (OFDR) based solutions (Henault et al. 2012, Monsberger et al. 2018), or alternatively encountered as distributed sensing, have provided the ability to record strain data over potentially thousands of points within the element. This resulted in excessively detailed strain profiles that have greatly contributed to the formulation of key concepts and assumptions in the present study. Moreover, the strain data has been presented and investigated in Chapters 2 and 3.

The described experimental programmes have provided direct insight on the actual distribution shape of the reinforcement strains, enabling future development of more accurate bond models (Jakubovskis 2015) and the present research on crack modelling through the principle of strain compatibility.

1.2. Cracking Models of Concrete

The majority of cracking models can be summed up into three groups:

- Models based on empirical notions
- Models based on mean strains
- Models based on stress transfer concept

The first group contains the largest number of proposed models that are often based on very early experimental research of the middle of the previous century. The great number of experimental tests have been used to derive various empirical constants and notions with some still being considered today.

The second group is comprised of both analytical and semi-analytical models dedicated to mean deformation analysis. Borosnyói & Balázs (2005) suggest four groups, however, both models discussed herein share the core principles, hence are presented as a single group. Furthermore, these models are often encountered in numerical approaches such as FE based analysis by the name of smeared crack models. In general, these models are simple to implement and are hence adopted for design codes (Model Code 2010, Eurocode 2). Where the method lacks is the ability to explicitly account for complicated geometry or individual cracks and the ensuing stress redistributions without averaging these aspects out.

The last group originated from research by Saliger (1936) and later Kuuskoski (1950), Rehm (1961). The key feature is the reliance on bond-slip models to transmit the stresses from the reinforcement to the surrounding concrete, enabling distinct representation of the cracks and redistributed stresses within the RC element. Therefore, the approach is significantly more robust in

terms of mechanics than the previously mentioned ones. For the purpose of design, simplifications such as the *classical bond theory* are relatively well established. The approach is considered to be the most flexible and versatile way to carry out serviceability analysis (Ma and Kwan 2015).

Considering the above aspects in the context of serviceability analysis as presently governed in design codes such as Eurocode 2. It is essential to highlight the importance of crack widths, that often govern the design of certain structures as opposed to the ultimate limit state. An example of this are long span reinforced concrete beams that are not prestressed. In order to prolong the lifespan of RC structures, these crack widths should be controlled to certain widths as defined by design codes. When crack widths increase too much, water begins to penetrate towards the reinforcement, and if the concrete cover is fully cracked, the embedded steel bars will begin to rust. Naturally, rust will build up, further expanding and damaging the concrete around it and widening the crack, creating a circular deterioration mechanism. While design codes propose crack width prediction methods, they are highly scattered, as shown further in this thesis. While directly studying crack widths can partially help increase the accuracy of prediction methods, it is unlikely the scatter levels will be controlled if the cause is not addressed. The present research, hence, tackles the mean crack spacing, as shown further in this chapter, are related to the width of a crack. By targeting the mean spacing value, the scatter levels can be more easily assessed and, in the future, reliability analysis can be applied to establish characteristic values.

An array of models from classical research and the latest research are presented further in this section. As will be shown, the serviceability models are lacking uniformity between them and range greatly in their degree of complexity, adequacy and founding principles. From the previous subsections, the average strain behaviour of an RC member can be estimated with considerable precision, in contrast to the cracking phenomenon related predictions, particularly crack widths, spacing that is highly localised. The predictions, as will be discussed further, are highly scattered and are impacted by an extensive list of variables. The abundance of empirical notions in the serviceability models inhibits compatibility of the methods, particularly when it comes to predicting crack widths, spacing and deformations. The models are not able to provide adequate outcomes for all three outputs simultaneously and rarely provide results in the vicinity of the stress-transfer based predictions.

1.2.1. Crack Spacing Models

Various cracking models retrieved from research literature are gathered and presented in this section. The models are presented in chronological order, with

notations adjusted from the originals to conform with the ones employed in the present study.

Among the first equations for predicting crack spacing was suggested by Saliger (1936) and extended in Saliger (1950), it was based on the stress transfer principles, including the bond stress τ in the equation. The expression also accounted for the concrete compressive strength f_{cm}. While originally proposed as part of a crack width solution, the model, in general, is limited due to the use of weak concrete grade with strength not exceeding 15 MPa. The expression for the maximum crack spacing is as follows:

$$s_{rm} = 0.157 \frac{Ø}{4\rho} \cdot \frac{f_{cm}}{\tau_{b,max}}. \tag{1.4}$$

A simple empirical equation was proposed by Broms (1965), that is related to the position of the reinforcement bar within the element. This approach was derived from a set of 37 tension and 10 bending specimen tests. With the maximum crack spacing being twice the distance between the axis of the embedded bar and concrete surface:

$$s_{rm} = 2(c + 0.5Ø). \tag{1.5}$$

Significant modifications to the model were introduced by Broms & Lutz (1965), with a new concept as the effective thickness of concrete cover t_e, and accounting for the distance between reinforcement bars along the section:

$$s_{rm} = 2t_e, \tag{1.6}$$

where the effective concrete cover is estimated by:

$$t_e = \sqrt{\left(\frac{s}{4}\right)^2 + (h-d)^2}. \tag{1.7}$$

The nowadays well-known relation of the reinforcement bar diameter to the reinforcement ratio $Ø/\rho_{ef}$ was originally established by Borges (1965). The ratio has become very popular in the scientific community studying the cracking phenomena and can be encountered in present design codes such as Model Code 2010 and Eurocode 2. Furthermore, the proposed equation included concrete cover as a variable:

$$s_{rm} = 1.5c + 0.04 \frac{Ø}{\rho_{ef}}, \tag{1.8}$$

the effective reinforcement ratio ρ_{ef} is a concept that is highly empirical and is controversial to this day. Borges (1965) provided the following conditions for evaluating ρ_{ef} which is based on the effective concrete area in tension $A_{c,ef}$:

$$A_{c,ef} = \begin{cases} bh & -\,tensile\ elements \\ b(h-y_0) & -\,flexural\ elements \end{cases}. \tag{1.9}$$

A relationship for crack spacing relying on the principles of stress transfer approach was derived by Noakowski (1985). For this reason, the following differential bond-slip expression was solved:

$$\tau(x) = 0.95 \cdot {f_{cm,cube}}^{0.66} \cdot s(x)^{0.12}, \tag{1.10}$$

where *s(x)* is the slip between reinforcement and concrete, expressed by the difference of respective strain values. The resulting crack spacing model is:

$$s_{rm} = 2.33 \left(\frac{\left(k_1 \frac{f_{ctm}}{\rho}\right)^{0.88}}{{f_{cm,cube}}^{0.66}} \emptyset \right)^{0.89}, \tag{1.11}$$

where k_1 is a stress redistribution coefficient, taken as $k_1 = 0.5$ for tensile elements and $k_1 = 0.22$ for flexural elements.

A greatly simplified equation was proposed by Janovic and Kupfer (1986), with only the spacing between bars required:

$$s_{rm} = 50 + 0.75s. \tag{1.12}$$

More exotic formulations have been proposed based on fracture mechanics principles (Oh and Kang 1987). The proposed expression was further refined through a significant quantity of experimental data to come up with the equation:

$$\frac{s_{rm}}{\emptyset} = 25.7 \left(\frac{h-d}{h-y_0}\right)^{4.5} + 1.66 \left(\frac{1}{n}\frac{A_{c,ef}}{A_s}\right)^{1/3} + \frac{0.236 \times 10^{-6}}{{\varepsilon_s}^2}, \tag{1.13}$$

where n is the number of tensile reinforcement bars, $A_{c,ef}$ is the effective area of concrete in tension, estimated by:

$$A_{c,ef} = b\frac{(h-y_0)^3}{9(d-y_0)^2}. \tag{1.14}$$

Jankó (1994) has suggested an expression which takes the stresses of the reinforcement and concrete into account:

$$s_{rm} = \frac{1}{2}\frac{\sigma_s}{\alpha\sigma_c}\emptyset_s, \tag{1.15}$$

where σ_s is the stress in the reinforcement and σ_c is the stress in the concrete, and α is the ratio of average and minimum crack spacing.

The greater part of the models presented above originated as part of expressions for crack width predictions. The early crack width expressions were all based on the relation between the crack spacing and the difference between

reinforcement and concrete strains (Borosnyói & Balázs 2005, Lapi et al. 2018). With the characteristic crack width given in the following form:

$$w_k = \beta w_m = \beta s_{rm} \Delta\varepsilon_{m,}, \tag{1.16}$$

where β is a factor often suggested to be between 1.5 and 2, w_m is the mean crack width, s_{rm} represents the mean crack spacing value and $\Delta\varepsilon_m$ is the average difference between reinforcement and concrete strains within an element.

A number of variables can be highlighted from the above expressions that are common to many of the approaches, namely the cover of concrete c, steel bar diameter Ø, spacing between reinforcing bars, ratio of reinforcement ρ, or more often, the $Ø/\rho_{ef}$ ratio. Due to the multiple parameters and variations of expressions and widely scattered crack prediction results, it can be inferred, that the cracking behaviour is highly complex and multiple factors affecting it. Among the influencing aspects is the bond interaction of concrete and the embedded bar, aggregate particle sizes, particularly their boundaries, along which cracks propagate, general brittleness of the material, microcracks due to chemical processes and the stress redistribution complexities after initial cracks form within the element and the stochastic nature of concrete in general (Kaklauskas et al. 2016). By no means is the list of potential causes is complete. Neglecting these factors in classical theories, as well as reliance on perfect bond assumptions, lead to inaccurate estimations of widths and spacings of cracks. Maintaining bond properties closer to actual physical behaviour can significantly contribute to improved serviceability analysis (Oehlers et al. 2012, Pérez Caldentey et al. 2013).

An extensive investigation on the cracking models, their origins were carried out by Borosnyói & Balázs (2005) and Lapi et al. (2018). While the present research has focused on more distinctive models, the aforementioned studies examine a wider spectrum, with both crack width and crack spacing models of multiple authors, highlighting the general trends and clustering the models into appropriate groups, similarly to the ones presented in the present work. However, state-of-the-art techniques are not widely covered, such as models developed through numerical means. Among these is the model developed by Wang et al. (2017), that is tailored specifically to the mean crack spacing estimation. The foundation of the approach relies on the fracture energy-based approach. Instead of providing a single equation to cover both flexural and tensile cases, separate models are derived:

$$s_{rm} = \begin{cases} \frac{1}{\alpha} \sqrt[4]{A_e} \cdot f_{cm}^{-0.4} \left[-29.1 \left(\frac{c}{Ø} \right)^2 + 228 \left(\frac{c}{Ø} \right) + 18.9 \right] & tension \\ \frac{1}{\alpha} \sqrt[4]{A_e t} \cdot f_{cm}^{-0.3} (134170\rho^2 - 10958\rho + 339) & flexure \end{cases}, \tag{1.17}$$

where α is the ratio of bond stress to tensile concrete strength, A_e is the effective cracking area, c is the clear concrete cover, t is the concrete cover taken from the bar axis. The approach has been shown to be more accurate than the fracture mechanics based Oh & Kang (1987) model, however, the expression remains to be prohibitively complex for everyday usage.

While numerical techniques rarely propose a simplified model, they serve as a specific workflow with the inclusion of complex concepts to produce highly detailed cracking behaviour analyses. Ng et al. (2015) have proposed a new technique to carry out FE analysis of RC elements. The key feature was to approach the analysis through the ordinary smeared crack approach, with a dedicated algorithm controlling the insertion of cracks into the element. The proposed algorithm handles the redistribution of stresses after each load step, checking if conditions are reached to introduce a single new crack at a certain finite element. Limiting the number of cracks forming to one per load step, the size of which is controlled dynamically. This approach enables to simulate stress redistribution with high levels of accuracy, much like the Extended Finite Element Method (XFEM). Which by nature is similar however is based on very sophisticated fracture mechanics (Li et al. 2018). Another numerical method for reinforced concrete cracking analysis is developed by Kurumatani et al. (2019). Again, the foundation is on fracture mechanics. The method was able to provide adequate results in terms of cracking behaviour of RC beam without shear reinforcement. Furthermore, the benefit of the developed method was the lack of dependency on the size of the mesh. Leading to more optimal computation time, without the need to artificially inflate the number of finite elements.

1.2.2. Design Code Methods for Crack Spacing

The concepts included in the design codes stem from the earlier attempts by researchers. Some of the ideas have been successfully incorporated and are present in the codes up to this day, as will be shown further in the section.

One of the first design codes to distinctively characterise the mean crack spacing s_{rm} as opposed to just empirical crack width w_k models is Model Code 1978 (CEB 1978) of the Comite Euro-International du Beton:

$$s_{rm} = 2(c + 0.1s) + k_1 k_2 \frac{\emptyset}{\rho_{ef}}, \tag{1.18}$$

where k_1 and k_2 are the coefficients for the bond properties of the embedded bars (high bond, ribbed prestressing wires or plain bars) and the type of loading condition (pure bending or tension).

The Architectural Institute of Japan (AIJ 1986) have made modifications to the k_1 and k_2 coefficients, replacing them with a constant value of 0.1:

$$s_{rm} = 2(c + 0.1s) + 0.1\frac{Ø}{\rho_{ef}}. \quad (1.19)$$

More significant alterations can be found in Model Code 1990 (CEB-FIP 1993), namely the removal of the cover of concrete as a variable that reduced the model's ability to predict experimental results with sufficient adequacy (Lapi et al. 2018). The simplified spacing equation is given by:

$$s_{rm} = \frac{2}{3} \cdot \frac{Ø}{3.6\rho_{ef}}. \quad (1.20)$$

The Japanese Society of Civil Engineers (JSCE 1997) has published an empirical expression based on the diameter and spacing between reinforcing bars:

$$s_{rm} = k[4c + 0.7(s - Ø)], \quad (1.21)$$

where k is an empirical coefficient. The newer version (JSCE 2007) has maintained the form, with changes concerning only the empirical factors.

The Eurocode 2 design code (CEN 2004) and later version include the following expression, based on Model Code equations:

$$s_{r,max} = 3.4c + 0.425k_1k_2\frac{Ø}{\rho_{ef}}, \quad (1.22)$$

where k_1, k_2 are coefficients for bond and loading conditions, same as for Equation (1.18). As the present implementation is not suitable for predicting the mean crack spacing, the previous edition of EC 2 (CEN 1992) was employed in the present research as discussed in Chapter 3. Moreover, the version given in Equation (1.22) is not able to account well for tensile members reinforced with a single centrally located bar due to the inclusion of concrete cover and effective area of concrete in tension. The cover values for tensile members exceed the scope of the intended implementation of the above expression, as compared to flexural elements.

The latest edition of the Model Code 2010 (FIB 2012) implements the stress-transfer concept. The equation is provided by solving the differential bond-slip expression with an assumption for constant bond $\tau = const$ like in classical approaches. The crack spacing is obtained from the transfer length l_{tr}:

$$s_{rm} = \frac{2}{1.5}l_{s,max} = \frac{2}{1.5} \cdot \left(k \cdot c + \frac{1}{4}\frac{f_{ctm}Ø}{\tau_{bm}\rho_{ef}}\right), \quad (1.23)$$

where $l_{s,max}$ is the maximum transfer length, τ_{bm} is the bond stress, taken as constant, k is an empirical coefficient, normally taken as 1.0 and c is the cover of concrete, taken as less or equal than 75 mm ($c \leq 75$ mm). The ratio 2/1.5 relates the maximum crack spacing to the mean spacing. In contrast to provisions by Balázs et al. (2013), it has been suggested by Debernardi & Taliano (2016) that the corrective term kc could be dropped completely from the equation for

improved accuracy. This consideration is taken into account when comparing tensile and flexural results as removing the *kc* term improves accuracy for RC ties, as will be shown in Chapter 2.

The common notion between the Eurocode 2 and Model Code 2010 is the effective area of concrete in tension $A_{c,ef}$ which is employed for effective reinforcement ratio ρ_{ef} estimation (Figure 1.5).

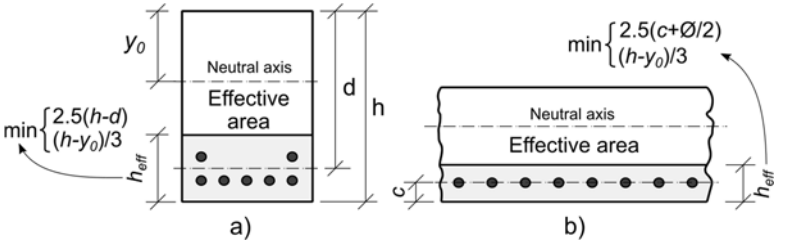

Fig. 1.5. The effective area of concrete in tension according to Model Code 2010 provisions: a) beam section; b) slab section

The term is a topic of controversy among researchers (Borosnyói & Balázs 2005, Windisch 2016, Debernardi & Taliano 2016). It was argued that the $Ø/\rho_{ef}$ term is not adequate in terms of impact on the maximum transfer length $l_{s,max}$ Equation (1.23). The opinion was further endorsed by Beeby (2004), stating that the spacing between cracks is not dependent on the diameter to effective reinforcement percentage ratio $Ø/\rho_{ef}$. Moreover, Beeby (2004) demonstrated the spacing between bars to have a greater impact on the crack spacing value than the mentioned ratio.

1.3. Artificial Neural Networks Investigations

Neural networks have been around for some time, nevertheless, significant attention to machine learning has only been given since approximately 2010 when research papers on the topic began to increase at a faster pace than before. Circumstances limiting the reach of ANNs in the past can be attributed to a lack in computer processing power, which has continued to grow by means of multithreading and increased performance per clock instruction (Ekman et al. 2005).

The present research is not intended to propose any modifications to neural networks, as the sole purpose is to attempt implementation of the state-of-the-art knowledge to develop an ANN for crack spacing predictions and compare its performance against the proposed strain compliance concept. For this reason, an in-depth background on neural networks is substituted with the introduction of

core concepts and the state of their implementation for reinforced concrete element structural behaviour modelling.

The general architecture of a feed forward back propagation neural network is shown in Figure 1.6a. The construct is defined by the following features: input, hidden and output layers, individual neurons and their connections. Each layer contains a set number of neurons, which in turn have dedicated structure comprised of inputs, weights, activation function (or transfer function), biases (Fig. 6b). The activation function controls whether and what fraction of the data gets output further and they can be of a variety of types, ranging from linear to sigmoid curves to step functions and other non-continuous functions (Fig. 1.6c). In order to add more control to the neural network, biases are introduced that essentially shift the activation function to the side. The weights represent the parameter strength, influence on the connection between neurons governing how much impact an input has on the output. Training a neural network means finding values for these weights, the larger number of variables per sample the more samples are required to obtained good generalisation. A single change in weight will alter all connecting neurons, hence the difficulty of training grows exponentially. The problem is known as "the curse of dimensionality" (Verleysen & Damien 2005, Stathakis 2009).

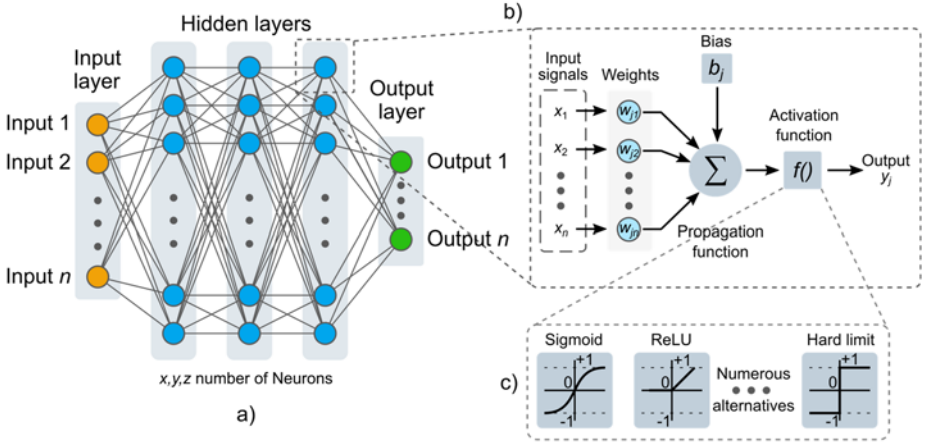

Fig. 1.6. Common artificial neural network structure: a) a feed-forward neural network; b) neuron substructure; c) activation function types

The application of ANNs for modelling reinforced concrete element behaviour are still somewhat infrequent. Early attempts to predict concrete behaviour were related more to reinforced concrete material properties, such as the strength of concrete. Vanluchene & Sun (1990) have discussed the early attempts of neural network application for reinforced concrete and structural

engineering in general. Ghaboussi et al. (1991) have highlighted the advantages of modelling material behaviour with knowledge infused models. Later studies were more refined, aiming to predict the strength properties of costly high-performance concrete and deep beams (Kasperkiewicz et al. 1995, Sanad & Saka 2001). Both studies attempted to implement ANNs to simulate relatively expensive experiments.

One of the primary reasons why neural networks have not been as widely employed in structural engineering, particularly reinforced concrete behaviour modelling is the lack of data. While hundreds of experiments have been carried out over the last decades, the majority of experimental results of RC beams are underreported in terms of geometrical, material characteristics. Often the initial data and outcomes are not compatible from different experimental studies, with diverse aims different needs arise for which data is significant enough to be recorded.

Normally, neuron networks require excessively large datasets in the order of thousands of data points to provide truly adequate and consistent results. Nevertheless, techniques have been proposed and been proven to generate adequate ANNs with knowledge of reliability and consistency levels to generalise a small data set by Shaikhina & Khovanova (2017). Increasing neural network prediction accuracy in terms of generalisation of features is often approached through the concept of removing random neurons and their connections from the network (Srivastava et al. 2014), yet this technique is only viable for larger data sets, as it was shown to decrease the performance of small data neural networks.

Studies targeting cracking of concrete focus more on crack detection from image sources (Moon & Kim 2011, Cha et al. 2017) than serviceability related phenomena such as cracking of concrete. Several studies have developed neural networks for crack width predictions (Ince 2004, Elshafey et al. 2013a), however, research on crack spacing and neural networks is extremely limited. One study that has attempted to develop an ANN for predicted the mean spacing between normal cracks (Elshafey et al. 2013b) is flawed by lack of data and no investigation on the variability of the ANN or any attempt to analyse the neural network scatter. In the present research, a multivariate and iterative investigation of neural networks for crack spacing is carried out, with aims of calibrating the neural network to adequate levels in terms of accuracy and consistency. Furthermore, the multivariate and multiple training approaches will yield insight into the sensitivity of the material and geometrical parameters of the collected experimental data.

1.4. Conclusions of Chapter 1 and Formulation of the Objectives of the Thesis

After carrying out a literature survey on the topics of reinforced concrete cracking and modelling crack spacing, the following observations can be summarised:

1. The investigated smeared crack based analytical and semi-analytical methods for estimating crack spacing are very diverse and are permeated with a variety of empirical notions, as shown in this chapter. This diversity can be attributed as the cause for inconsistent and scattered cracking results.
2. Stress transfer techniques and analytical or semi-analytical models based on it are able to account for distinct cracks, hence can provide insight on the spatial distribution of strains within a cracked element. However, the application of the techniques is highly complex and reliant on additional relationships describing bond stress and slip interaction, which in itself, is highly dependent on reinforcing bar, concrete properties and loading levels. More simplified models in this category rely on constant bond assumptions and are considered classical approaches. These methods are still not devoid of empiricism, which can be encountered in the form of the bar diameter to reinforcement ratio parameter $Ø/\rho_{eff}$.
3. The wide variety of variables implemented the numerous cracking models do not contribute to the unification of the cracking approaches and the high scatter of crack spacing predictions. Leading to the conclusion, that lack of harmonisation in the models is a threshold to be passed first before assessing and planning further necessary actions for improving cracking prediction adequacy.
4. Crack spacing models presented in design codes have limitations on which types of structural behaviour they can model. Eurocode 2, specifically, is highly unsatisfactory in this regard. Furthermore, the models are heavily reliant on the empirical effective area of concrete in tension A_{eff} feature, which in turn depends on a multitude of conditional checks.
5. Artificial neural networks have been employed for predicting crack spacing, however their scope of application remains limited. Moreover, the influence of the naturally limited data set on the adequacy of predictions is not investigated. The reviewed research is inconclusive in terms of accuracy, lack of parametric variations and network calibration in general. Due to the prohibitive costs of RC experiments, research on ANNs for cracking behaviour can potentially deliver new opportunities to

study concrete parameter interactions, provided the network can be developed with sufficient adequacy.

The present research constitutes the development of an alternative crack spacing prediction methodology as the key aim with tensile and flexural RC elements as the main object of the study. In order to address the shortcomings asserted above, the following tasks are defined:

1. Collect experimental test data of tensile and flexural RC elements tested with sufficient mechanical, geometrical properties and cracking patterns to analyse and formulate primary crack spacing models and validate subsequent results.
2. Develop a primary crack spacing evaluation framework for tensile and flexural RC members subjected to loading levels equivalent of the stabilized cracking stage, while maintaining principles of simplicity, mechanical soundness and minimal reliance on empiricism.
3. Validate the proposed primary crack spacing prediction approach against collected experimental data and design codes for tensile RC elements and flexural RC beams and slabs.
4. Analyse the collected experimental data with artificial neural networks and statistical modelling to substantiate the existence of parametric relationships for the data specimens and, in turn, the proposed primary crack spacing prediction approach, derived from this data.
5. By training and calibrating a neural network for primary crack spacing predictions, establish a benchmark for the achievable prediction performance in terms of accuracy and scatter levels for future research.

2

Investigation of Reinforced Concrete Tensile Element Cracking Behaviour by the Strain Compliance Approach

The investigation of cracking and deformation behaviour of tensile RC specimens is presented in this chapter. Fundamentally distinct methods for analysing cracking, the mean strain and discrete crack-based techniques have been integrated into a novel framework that promises to yield more consistent results. Synergy is obtained by equating the mean reinforcement strains of the embedded bars as estimated by any mean strain approach with the average strain value provided by the stress transfer approach. The advantage provided by the mean strain approach over the knowledge of the average behaviour of the RC element enables the crack spacing value to be determined from the stress transfer approach. Hence the outcome is a new way of investigating cracking, named the *Strain Compliance* approach. The concept has been detailed in this chapter from conception, the main assumptions to an analysis of experimental data. Comparisons with Model Code 2010 and Eurocode 2 design code predictions have been carried out and the findings discussed. The chapter includes content from journal papers Kaklauskas et al. (2017a), Kaklauskas et al. (2019a, 2019b) and conference proceedings Kaklauskas et al. (2016, 2016, 2017b), Kaklauskas & Ramanauskas (2016a, 2016b).

2.1. Methodology and Assumptions of the Tensile Element Primary Crack Spacing Prediction Approach

The cracking analysis technique presented in this chapter is primarily focused on higher loading levels. The RC tie is considered to have a fully developed normal crack pattern that extends from the reinforcing bar to the surface of the covering concrete. This behaviour is characteristic of the Model Code 2010 definition of the stabilized cracking stage, where only secondary cracks continue to increase in both size and width but normally do not reach the level of the primary normal cracks. The service load equivalent of $0.6f_s$ is taken as the loading level. Resulting in a reinforcement strain value of $\varepsilon_s = 0.0015$ when steel reinforcement of $f_s =$ 500 MPa yield strength and elasticity modulus of $E_s = 200$ GPa are considered. This provided strain level in the embedded bar is considered for the reference data point, which is required for the crack spacing analysis of RC ties. This reference point is expressed as a reinforced concrete tension element of known reinforcing percentage (or otherwise ratio), bar diameter and most importantly, known value for the average distance between primary normal cracks. Such an element is further denoted as the reference element and the mentioned variables as the reference reinforcement ratio, reference bar diameter.

As the mean strain approach is deemed to provide reasonably accurate average deformation behaviour of an element, the statement is further projected to the mean behaviour of a short RC block divisioned by two primary cracks as being representative of the mean behaviour of the entire RC element. Therefore, the average crack spacing of an element would be the length of such an RC block. The developed technique additionally requires the knowledge of the reinforcement strains within the element, or in this case, the short RC block. As examined in the literature survey, the reinforcement and concrete strains were originally taken as expressed linearly (Scott & Gill 1987, Beeby & Scott 2005), conforming with the classical bond theories. While over time it was observed that the exact spatial distribution is more complex, an approximation of the reinforcement strains with a first-order polynomial can be sufficiently accurate at increased loading levels, representative of the stabilized cracking stage for which the proposed approach is intended. The techniques that discretely define cracks and include the strain distributions are often encountered as the stress transfer, partial interaction or discrete crack based approaches.

With the reinforcement strain distribution defined, the mean reinforcement strain estimation becomes possible. Equating this strain value to the mean strain value obtained by a mean deformation method (also known as the smeared crack or mean strain-based approaches), such as the Eurocode 2, ensures the mean strains of both approaches are compatible, hence the name of the proposed cracking analysis approach and concept as the Strain Compliance approach.

Through this equality, it becomes possible to express the distance between cracks of any RC tension element with varying combinations of reinforcement bar diameter and ratios.

The discussed major assumptions and concepts can be summarized as:

1. For a tensile reinforced concrete member, only the normal cracks that extend throughout the entirety of the section are considered. These cracks are called the primary cracks in this study, whereas cracks that are mostly localized to the areas surrounding the ribs of the reinforcement bar are referenced to as the secondary cracks.
2. The crack prediction method applies only in the stabilized cracking stage as defined by the Model Code 2010. Formation of new primary cracks is assumed to be limited in this phase.
3. The reinforcement strains are assumed to follow a simplified linear expression over the distance of the element.
4. The ability of concrete to transfer stresses in the cracks is omitted from the formulations. This effect is otherwise known as the tension softening effect.
5. A segment of a reinforced concrete tensile element between two adjacent primary cracks is considered to represent the average deformation behaviour of a crack concrete element. This segment is later referred to as a reinforced concrete block.
6. A data point defined by a known crack spacing value of a reinforced concrete tension element with a known embedded bar diameter and reinforcement ratio is required as the foundation for the proposed analysis of tensile members. This data point and its mentioned values are later described with the word *reference* before them.
7. The average strain of the reinforcement can be obtained by any mean deformation based technique.

2.2. The Strain Compliance Principle for Tensile Elements

A new framework has been developed for the analysis of the cracking behaviour of RC elements. This chapter presents the principles of applying this approach to predicting crack spacing of tensile elements. The technique of analysis is divided into two stages. In the first stage, the analysis carried out on a reference element that has the crack spacing value known or established with enough certainty for a specific embedded bar diameter and reinforcement percentage. The second part

takes the bond stress value obtained from the slope coefficient of the reference element to continue calculations of alternative configuration RC tension members. As the strain compliance approach necessitates a smeared crack method for mean strain estimation, two cases are represented further in this research. Namely, the free-of-shrinkage tension stiffening model proposed by Kaklauskas et al. (2018) and the Eurocode 2 approach. Comparison and validation are carried out to determine the accuracy, advantages and disadvantages of the suggested novel concept against experimental results and design code calculations.

2.2.1. Approximation of Reinforcement Strain Distribution

The behaviour of RC tensile members has been studied quite extensively, particularly the strain distribution within the element, between primary normal cracks. The techniques for measuring strains have been various, from installing strain gauges within the reinforcement bars (Houde 1974, Kankam 1997) to optical sensor installations (Juknys (2017), Davis et al. 2017). The available research has first focused on suggesting linear approximations of reinforcement strains (Scott & Gill 1987, Beeby & Scott 2005), with later studies proposing more complicated strain profiles, such as second order polynomials with the introduction of local effects near the normal cracks (Jakubovskis 2015). A comparative investigation of different strain measuring techniques has been carried out by the author in Kaklauskas et al. (2019), where the strains revealed the progression of the strain distribution from more parabolic to greatly linearized behaviour at high loading levels.

The experimental strain profiles have been collected from the aforementioned research programmes and are presented in Figure 2.1 for comparison and validation of simplified strain representation with linear expressions. The solid black lines overlaid the data points are the approximations. Two important observations can be made from Figure 2.1, the first is on the overall tendency of strains to become significantly steeper as the loading increases, the other concerns the altered experimental strain behaviour within proximity of the normal cracks, more visible at higher loading levels. Hypotheses on the matter have been postulated by Maekawa & Qureshi (1996) that referred to this bond behaviour as the bond deterioration zone, later similar observations were made by Ruiz et al. (2007). Recently, the phenomenon has been studied by Jakubovskis (2015), with the study culminating in the definition of a zone with the damaged bond between concrete and embedded bar, equating the length of this altered bond area to the diameter of the reinforcement and its strain level:

$$l_d = 1000\varepsilon_s \emptyset_s. \tag{2.1}$$

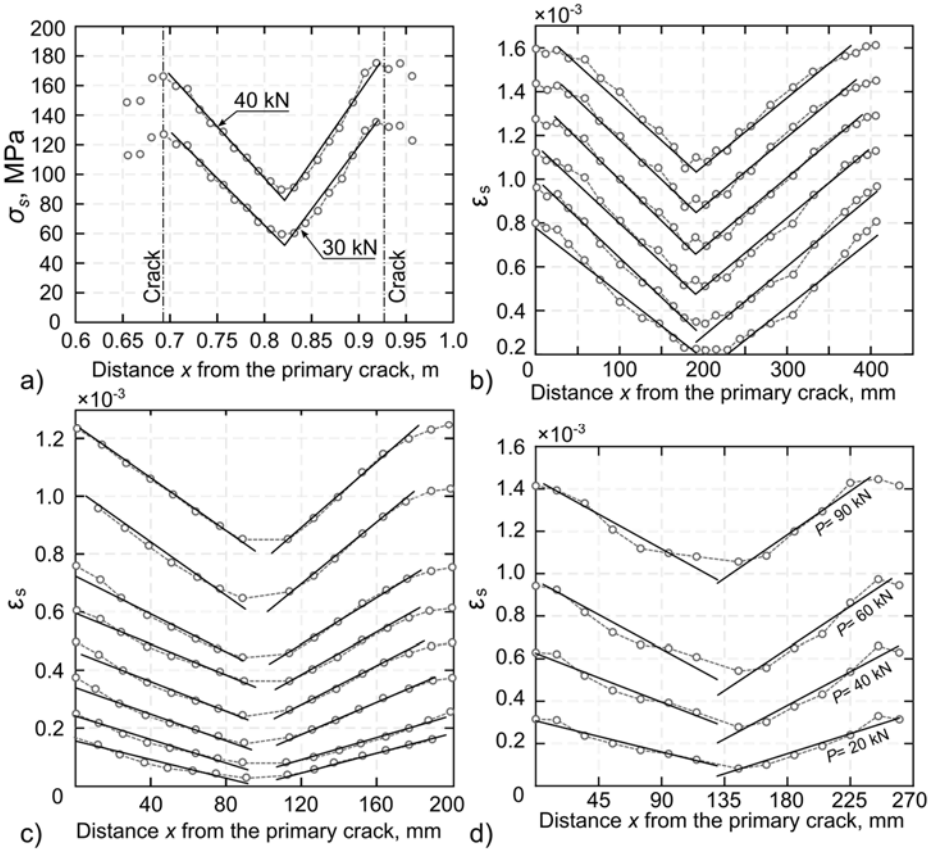

Fig. 2.1. Reinforcement experimental strain distributions of tensile reinforced concrete specimens: a) Beeby and Scott (2005); b) Houde (1974); c) Kankam (1997); d) Kaklauskas et. al. (2019) with linear strain approximation layered on top

The present research adopted the linear representation of strains, whereas the procedure for deriving the debonding length model (Equation 2.1) was based on the parabolic representation of strains. Jakubovskis (2015) approximated the strains with the parabolic equation and recorded the point where the approximated curve intersects the maximum reinforcement strain ε_s value of the experimental profile. The distance between this point and the end of the RC block was called the damage zone (in the present study referred to as the *debonding zone*). The remainder of the strain profile, where the change in strains occurs is controlled by the effective bond, hence the zone is referred to as the *effective zone*. An identical process is implemented in the present work, as a continuation, to redefine the

debonding expression. A representation of the process is provided in Figure 2.2 on results of Houde (1974), Kankam (1997) and Kaklauskas et al. (2019).

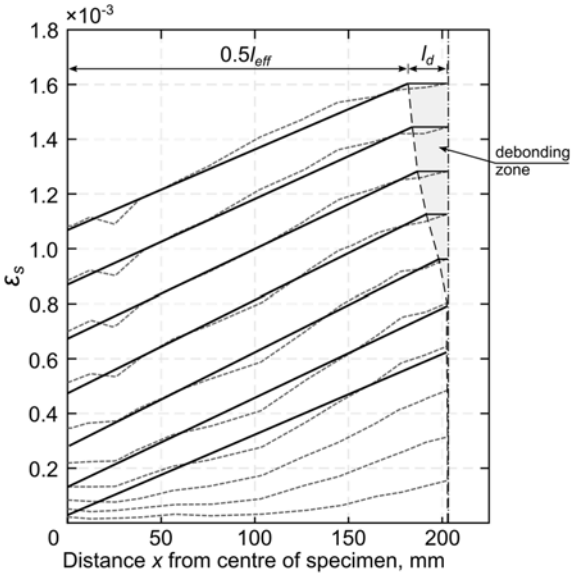

Fig. 2.2. Example of debonding zone definition through linear approximation for strain data by Houde (1974)

The remaining specimens of Houde (1974), Kankam (1997) and author's research (Kaklaukas et al. 2019) were processed in the same manner and the obtained data points from all specimens are presented in Figure 2.3. The distance between the intersection of the strain profile with the maximum reported strains and the end of the element is denoted by l_d, however, in Figure 2.3 they are normalized by the bar diameter and presented against the reinforcement strains. The data signified the previously expressed observation that the debonding zone tends to increase at higher loading levels. Though the data is scattered, a line was used to approximate the results, with the dashed line in Figure 2.3 representing the actual obtained fit and the solid line – the altered fit to intersect 0. The difference is marginal and with the aim of simplicity, the solid line expression is accepted for the debonding model to be further employed in the present research. The resulting equation is very similar to Equation (2.1) of Jakubovskis (2015), however, the length of the debonding zone was estimated shorter, hence the same formulation was maintained with a modifying division factor:

$$l_d = \frac{1000\varepsilon_s \emptyset_s}{3} = 0.00167\sigma_s \emptyset_s, \tag{2.2}$$

where σ_s is the stress of the reinforcement (obtained by including consideration for the reported elastic modulus of steel bars).

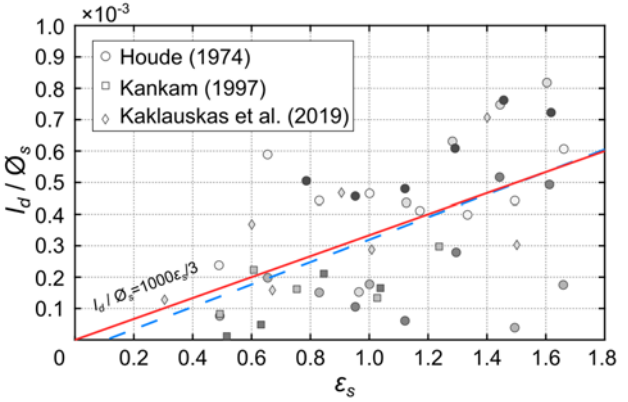

Fig. 2.3. Debonding zone length l_d model, normalized by bar diameter $Ø_s$ against loading level, expressed by reinforcement strains ε_s

In general, the linear approximations appear to be in good agreement with the experimental strains, specifically for higher loading cases representative of the stabilized cracking stage. The linear approximation is employed for the remainder of the current research on predicting crack spacing of tensile and flexural RC elements. Nevertheless, modifications are incorporated for the flexural case to account for the slightly different experimental strain behaviour. Detailed discussion on the matter is provided in Chapter 3. The area of damaged bond action is referred to as the debonding zone within the present research due to the name being more descriptive of the causality of the strain behaviour within it.

2.2.2. Crack Spacing Analysis Procedure With Stiffening Model for Mean Strain Estimation

As discussed under assumptions and concepts in Section 2.1 the proposed technique relies on the knowledge of the mean crack spacing of a particular RC tensile member for which the diameter of bar and ratio of reinforcement are known as well. The element and values are ascribed as the reference data point. The present subsection describes the process of strain compliance principle implementation for the analysis of crack spacing with emphasis on incorporating a stiffening model developed by the author (Kaklauskas et al. 2018) which also accounts for shrinkage. With consideration for the localised debonding effect between concrete and reinforcement bar within the proximity of the normal cracks.

As shown in the previous section, the strain distribution of tensile members appears to be well approximated by a first order polynomial, specifically at higher loading conditions. In other words, the conditions that mimic the stabilized cracking stage per Model Code 2010 characterisation. The approximated deformation behaviour for an RC block defined by two neighbouring normal cracks is shown in Figure 2.4. The shown strain levels are representative of the reference element, with the loading conditions taken as equal to an equivalent inducing 300 MPa stresses within the steel bar at the position of the normal crack. Taking a 200 GPa as the modulus of elasticity this equates to ε_s=0.0015 reinforcement strain.

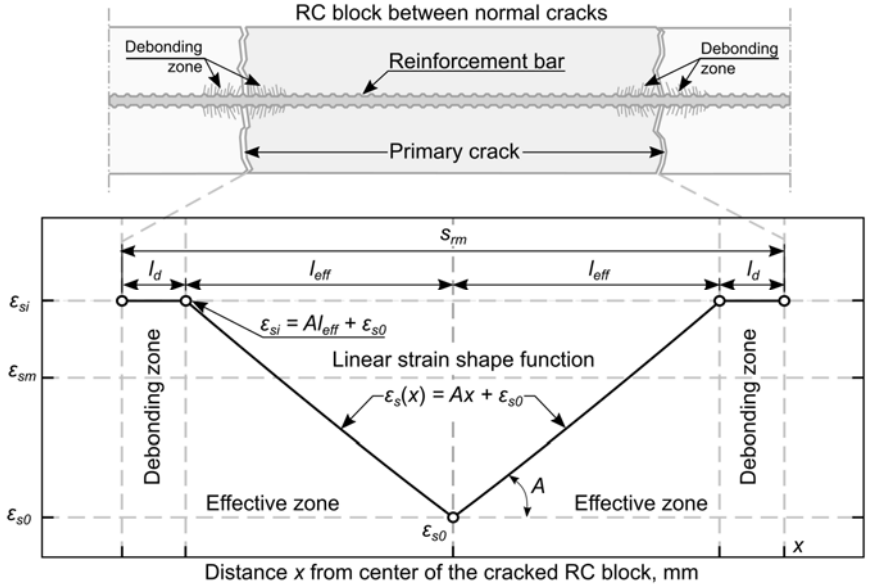

Fig. 2.4. Assumed reinforcement strain distribution of a reinforced concrete block defined by two neighbouring primary cracks

The debonding effect is a topic of debate, the present research does not provide enough evidence to substantiate the provided model (Equation 2.1) with enough certainty and, consequently, in terms of accuracy. Therefore, both cases considering and omitting debonding from the formulations are presented herein, as the key objective of this research is to develop an alternative cracking analysis methodology to existing methods discussed in Chapter 1. With the exact quantitative model not deemed as significant under present circumstances as the concept itself.

The approach is comprised of two distinct stages, the analysis of the reference element and subsequent investigation of alternative elements with varying configurations of reinforcement percentage and bar diameter. The strain compliance technique for tensile element analysis entails the estimation of the slope coefficient A of the linear strain distribution function for the reference element, which in turn provides the bond stress τ value for the chosen configuration.

The general strain compliance approach for the reference element is presented for one half of the investigated RC block, as the strain profile is symmetric. Therefore, the final crack spacing values are double the estimated ones from the procedure, and for one half would comprise of the debonding zone and effective zone lengths:

$$0.5s_{rm} = l_d + l_{eff}. \tag{2.3}$$

Describing the effective zone length by a linear reinforcement strain shape function yields the following expression:

$$\varepsilon_{s0} + Al_{eff} = \varepsilon_{si}, \tag{2.4}$$

where ε_{si} defines the reinforcement strains in the normal crack, in the present case equal to 0.0015 to induce ~300 MPa stresses or 60% of the yield strength of an ordinary S500 grade steel bar. A is the slope coefficient which plays a vital role as it enables bond stress estimation as will be shown later. The author would like to remark the notion of A without any subscripts, which indicates the slope coefficient throughout this research, as to not mistake with the areas of concrete or reinforcement that will always have a subscript indicated its intention.

The developed methodology is called the strain compliance approach due to the nature of integrating two separate techniques, namely the mean strain and the stress transfer approaches in a manner that equates the mean reinforcement strains as calculated from the aforementioned techniques. In general, this is represented as:

$$\varepsilon_{sm,discrete\ crack} = \varepsilon_{sm,smeared\ crack}. \tag{2.5}$$

Expressing this concept for the case presented in Figure 2.4 with a simplified linear strain profile provides the expression:

$$\frac{0.5A\left(l_{eff}\right)^2 + \varepsilon_{s0}l_{eff} + \varepsilon_{si}l_d}{0.5s_{rm}} = \varepsilon_{sm}. \tag{2.6}$$

As highlighted in the concepts and assumptions, the mean deformation can be obtained by a number of techniques, with careful consideration even numerical methods like FE methods. For the present study, the focus was on two methods, namely a free-of-shrinkage tension stiffening model developed by Kaklauskas et al. (2018) and the Eurocode 2. With the former being the focus of this

subsection and the latter discussed in subsection 2.2.3. The model herein was shown to be significantly more accurate when compared to the ones presented in Eurocode 2, furthermore, consistency and reduced spread of results was also greatly improved. The general tension stiffening model is presented through the tensile concrete stresses σ_{ct}, related to the mean concrete compressive strength and mean strains as follows:

$$\sigma_{ct} = 0.025 f_{cm} - \frac{0.85(\varepsilon_s \times 10^3)^{0.8} - 1.5}{0.25(\varepsilon_s \times 10^3)^{0.3} + 0.8}. \tag{2.7}$$

Implementing the above model necessitates shrinkage to be accounted for as tension stiffening is greatly impacted by shrinkage of concrete prior to applying to load. Comparisons are presented further in this work of both cases when shrinkage strains were considered ($\varepsilon_{sh} \neq 0$) and taken as zero ($\varepsilon_{sh} = 0$). An approach presented by Kaklauskas et al. (2009) that accounts for shrinkage by way of a pseudo force $N_{sh}(t)$ is adopted. The process is summarised as follows:

$$\varepsilon_s(t) = \frac{N_{sh}(t) + P}{E_{c.sec}(t)A_c + E_s A_s}, \tag{2.8}$$

where P is the externally applied load, $E_{c,sec}(t)$ is the secant modulus of concrete at time t and $N_{sh}(t)$ is the pseudo force that is defined by:

$$N_{sh}(t) = \overline{\varepsilon_{sh}}(t) E_{c.sec}(t) A_c, \tag{2.9}$$

where $\overline{\varepsilon_{sh}}(t)$ is the effective shrinkage strains, that is used to account for the creep effect. It is supposed that shrinkage strain progresses instantly and the resulting effect on the reinforcement strain is identical to as if shrinkage was increasing progressively from 0 to the free shrinkage strain value ε_{sh} inclusive of creep and ageing effects. The force $N_{sh}(t)$ is foreseen as a short-term action. The analysis involves an iterative process (Kaklauskas et al. 2009), whereby the secant concrete modulus is obtained from Equation (2.7). The effective shrinkage strain can be evaluated by:

$$\overline{\varepsilon_{sh}}(t) = \varepsilon_{sh}(t,\tau) \frac{1 + \left[\frac{E_s}{E_c(t)}\right]\rho}{1 + \left[\frac{E_s}{E_{ca}(t,\tau)}\right]\rho}, \tag{2.10}$$

where $E_c(t)$ is the elastic modulus of concrete at time t, $\varepsilon_{sh}(t,\tau)$ is the average free shrinkage strain value of concrete (taken with negative sign) and $E_{ca}(t,\tau)$ is the effective modulus of concrete adjusted for age and estimated by:

$$E_{ca}(t) = \frac{E_c(t)}{1 + \varphi(t,\tau)\chi(t,\tau)}, \tag{2.11}$$

where $\varphi(t,\tau)$ is the concrete creep factor and $\chi(t,\tau)$ is the coefficient of ageing.

Shrinkage induces a negative displacement on the element, that results in a shifted load-strain diagram (Fig. 2.5).

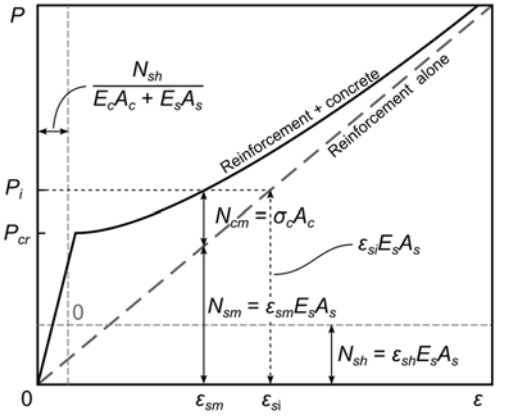

Fig. 2.5. Shifted load-strain diagram due to shrinkage effect

After estimating the mean strains of the reference element, Equation (2.2) and (2.3) can be substituted into Equation (2.5) and it can further be rearranged in terms of slope coefficient *A* as follows:

$$A = \frac{\varepsilon_{si} l_{eff} + \varepsilon_{si} l_d - 0.5\varepsilon_{sm} s_{rm}}{0.5 l_{eff}^2}, \tag{2.12}$$

where average crack spacing is replaced with the crack spacing value of the reference configuration $s_{rm} = s_{rm,ref}$. With the debonding model known from Equation (2.1) and the effective length of the reference element expressed from Equation (2.2) with an average distance between cracks as $l_{eff} = 0.5 s_{rm,ref} - l_d$, the slope coefficient A can be calculated. The linear equation of strain distribution in the effective zone can yield the bond stress expression by differentiating it. The resulting equation is a constant bond stress expression, dependent on the diameter of the reinforcing steel bar:

$$\tau(x) = \frac{E_s \emptyset_s}{4} \frac{d\varepsilon_s}{dx} = A \frac{E_s \emptyset_s}{4}. \tag{2.13}$$

The first stage of analysing the reference element with the proposed strain compliance approach is complete after estimation of the bond stress value. Bond stresses τ are taken as uniform for the approach, i.e. constant value $\tau = const.$ for any other subsequent element, therefore the slope coefficient can be obtained for the analysis of alternative element configurations, varying ratios of reinforcement and bar diameters. The value of *A* for other configurations is expressed from Equation (2.12) as:

$$A = \frac{4\tau}{E_s \emptyset_s}. \tag{2.14}$$

Furthermore, the strain value at the middle of the analysed RC block are considered to be fixed throughout all configurations $\varepsilon_{s0} = \varepsilon_{s0,ref}$. This statement remains intact for any reinforcement percentage or bar diameter value. Flowing from the strain compliance principle in Equation (2.5), the strain compatibility, i.e. strain equality can be ensured by having the loading level and resultant maximum reinforcement strain value at the crack ε_{si} as the key variable. On the condition that the mean strain approach used for average strain estimation is the stiffening model presented herein, manipulating the strain value ε_{si} will require a relatively complex numerical iterative process for the Equation (2.5) equilibrium conditions to be satisfied. With simpler smeared crack techniques this could potentially be overcome, thus resulting in greater ease of application. Though the iterative procedure was not bypassed in case of using the method presented in Eurocode 2, it greatly reduced the overall complexity as will be shown in the next subsection.

Satisfying the strain compliance condition (Equation 2.5) provides the length of the effective zone from the strain shape function (Equation 2.3) and crack spacing definition in terms of governing zones (Equation 2.2), resulting in the final crack spacing value estimated of any investigated element by:

$$s_{rm} = 2\left(\frac{\varepsilon_{si} - \varepsilon_0}{0.5A} + l_d\right), \tag{2.15}$$

where the effective zone length l_{eff} is expressed in terms of strains.

Prediction from the herein described approach with the tension stiffening relation is provided in Section 2.3, where the findings are compared for cases with considered $l_c \neq 0$ and neglected debonding $l_c = 0$, with shrinkage strains accounted for $\varepsilon_{sh} = 2\times10^{-4}$ and without considering them $\varepsilon_{sh} = 0$. In addition, a comparison against the common design code prediction is carried out.

2.2.3. Crack Spacing Analysis Procedure With Eurocode 2 for Mean Strain Estimation

The estimation of mean reinforcement strains by the stiffening model (Equation 2.6) in theory should provide more accurate results, to test that theory the approach was also tested with Eurocode 2 as the basis for ε_{sm}. The larger part of the strain compliance approach remains identical to the one defined previously, with the changes located to the estimation of ε_{sm} which, from an observation by the author, lead to a more easily applicable method, with fewer steps and simpler numerical schemes for the second stage, involving estimation of crack spacing of alternative elements.

The procedure for estimating the mean strains by the Eurocode 2 relies on interpolating between the uncracked and fully cracked states of the element:

$$\varepsilon_{sm} = (1 - \xi)\varepsilon_{el} + \xi\varepsilon_{si}, \tag{2.16}$$

where ξ is the interpolation (stiffening) coefficient, and ε_{el} is the elastic strain of the uncracked section. ξ is determined by:

$$\xi = 1 - \left(\frac{P_{cr}}{P}\right)^2, \tag{2.17}$$

where P_{cr} is the cracking load of the tensile element. The elastic strains are estimated for the same loading level P, however by assuming that the element remains uncracked:

$$\varepsilon_{el} = \frac{P}{E_c A_c + E_s A_s}. \tag{2.18}$$

Hence the process is more straightforward than applying the stiffening model from the previous subsection, without requiring iterative procedures for the estimation of the secant concrete modulus of deformation.

2.2.4. General Strain Compliance Flowchart for Crack Spacing of Tensile Elements

The entire strain compliance process with the analysis of the reference element to the investigation of alternative configurations is simplified graphically in a flowchart presented in Figure 2.6. The flowchart highlights the key input parameters that are then used to establish the linear reinforcement strain shape ε_{si}, the debonding zone l_d and the mean reinforcement strain value ε_{sm} as obtained from a selected mean deformation approach. While the present investigation analysed the implementation of Eurocode 2 provisions, any technique can be applied, hence the flowchart does expand this step with more details. After the mentioned parameters are determined and are inserted into the mean strain compatibility Equation (2.6), the minimum reinforcement strain value ε_{s0} and the bond stress τ values can be determined for the reference element. With the bond stress known, it is possible to estimate the mean spacing between primary cracks of alternative reinforcement ratio ρ and embedded bar diameter $Ø_s$ configurations.

A *Matlab* script written with the presented flowchart in mind is provided in Annex B, that covers the analyses carried out within the present Chapter and can be used for investigation of alternative variables. Moreover, the script can be employed in future works and extensions of the proposed concepts.

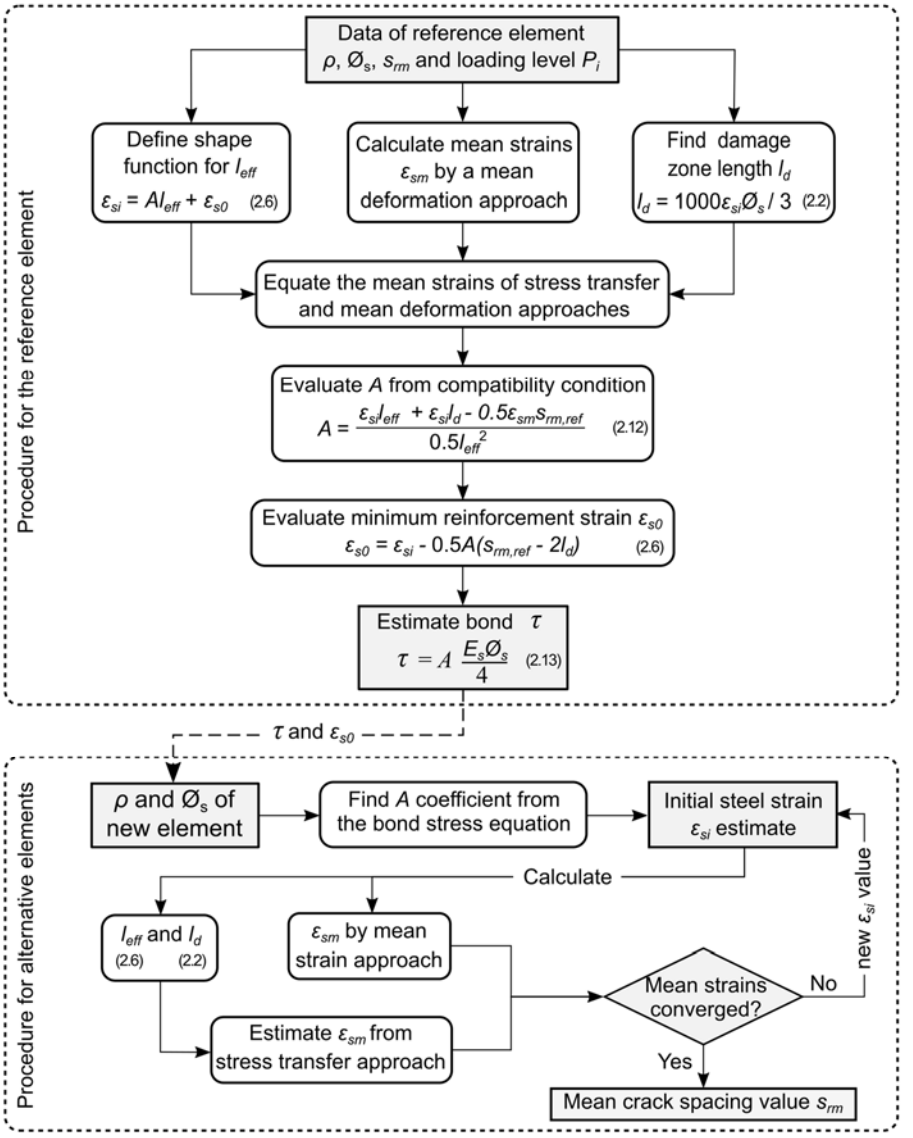

Fig. 2.6. Generalized flowchart for the implementation of the strain compliance concept for mean crack spacing prediction of tensile reinforced concrete elements

2.3. Validation and Evaluation of Adequacy of the Strain Compliance Approach for Tensile Elements

The outcomes obtained from the strain compliance approach introduced in previous sections are presented in this section. The predicted spacing values are compared against the different mean strain estimation techniques implemented in the strain compliance concept, moreover, the estimations are compared to Model Code 2010 and Eurocode 2 predictions. A number of published tensile RC element test results are gathered from literature, with focus on those sources containing crack spacing values either in numerical format or as images. The purpose of the data is twofold, to serve as the reference mean crack spacing value and to serve as data for comparisons against predicted values. A total of 170 test results of 100×100 mm tensile specimens, reinforced with a single bar were collected from experimental studies of Bischoff & MacLaggan (2006), Choi & Maekawa (2003), Danielius (2014), Farra & Jaccoud (1992), Lorrain et al. (1998), Scott (1987), Wu & Gilbert (2008). The tested elements were between 1 and 2 meters in length. The results are summarised in Table 2.1 per bar diameter, with mean, minimum and maximum crack spacing values as well as other statistical data, where the full dataset can be found in Annex A.

Table 2.1. Crack spacing and statistical data of reinforced concrete tension elements

$Ø_s$	No. of samples, n	$s_{rm,mean}$	median	min	max	std. dev. σ
mm		*mm*	mm	mm	mm	mm
10	48	217.6	216	162	319	31.3
12	11	182.5	173	143	300	42.0
14	43	162.4	160	122	193	18.0
16	20	149.9	142.5	125	210	21.9
20	48	137.6	135	117	187.5	16.0

The results are presented graphically in Figure 2.7a with statistics summarised in Figure 2.7b. Where the spread of results can be observed more clearly. The box representing the 25% and 75% quartiles. One of the possible reasons could be attributed to the different lengths of the elements, as the shorter 1 meter long RC ties are more likely to have fewer cracks per specific distance as a 2 m long member. Mostly due to the distance necessary to transmit the stresses from the reinforcement to the surrounding concrete layer. Another aspect relates to subjectivity in identifying normal cracks from secondary cracks, that can represent a challenge in tensile element cases.

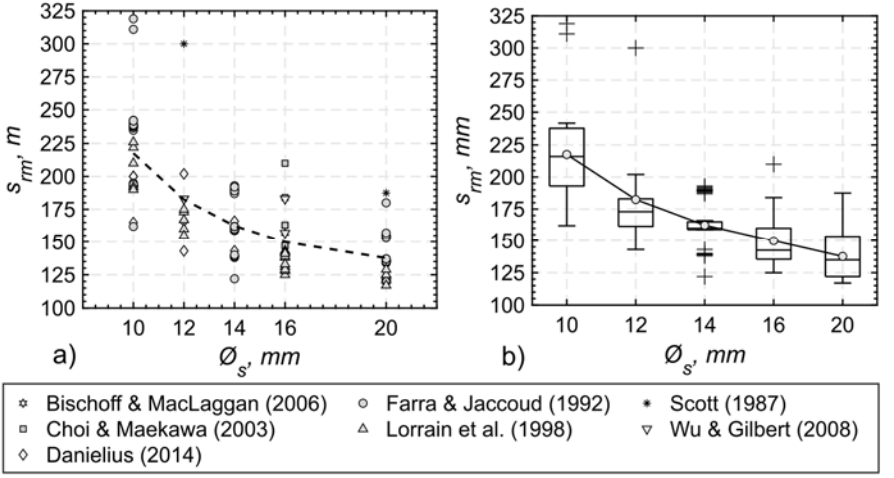

Fig. 2.7. The average spacing between primary cracks: a) experimentally tested reinforced concrete tension elements; b) statistical distribution of specimens

It was previously observed by Danielius (2014) and later Kaklauskas et al. (2017), the spacing values do not correlate with the mean concrete compressive strength of the collected samples. The spacing values are charted individually for every different bar diameter in Figure 2.8. The level of scatter and the horizontal tendency suggests that concrete strength f_{cm} has a negligible impact on the spacing outcome. Lack of a clear relationship between the aforementioned variables is taken into consideration when selecting standard material characteristics for the reference and successive elements. The following parameters define the reference element and values for the remaining elements:

- Ø14 mm diameter steel bar,
- Mean crack spacing s_{rm} = 162.4,
- Reinforcement ratio ρ = 1.54%,
- The crack spacing value is taken from Table 2.1 where the average spacing of all Ø14 mm bar specimens was taken. Since the elements tested were of a square section of 100 mm dimensions for each side, the resulting reinforcement ratio was 1.54% for the Ø14 mm bar. The diameter was chosen due to it representing the middle of the experimental spectrum. Other variables are kept constant in this study for comparison purposes:
- The mean compressive strength of concrete f_{cm} = 30 MPa,
- The elasticity modulus of steel reinforcement E_s = 200 GPa,
- Shrinkage strains $\varepsilon_{sh} = 2.0\times10^{-4}$.

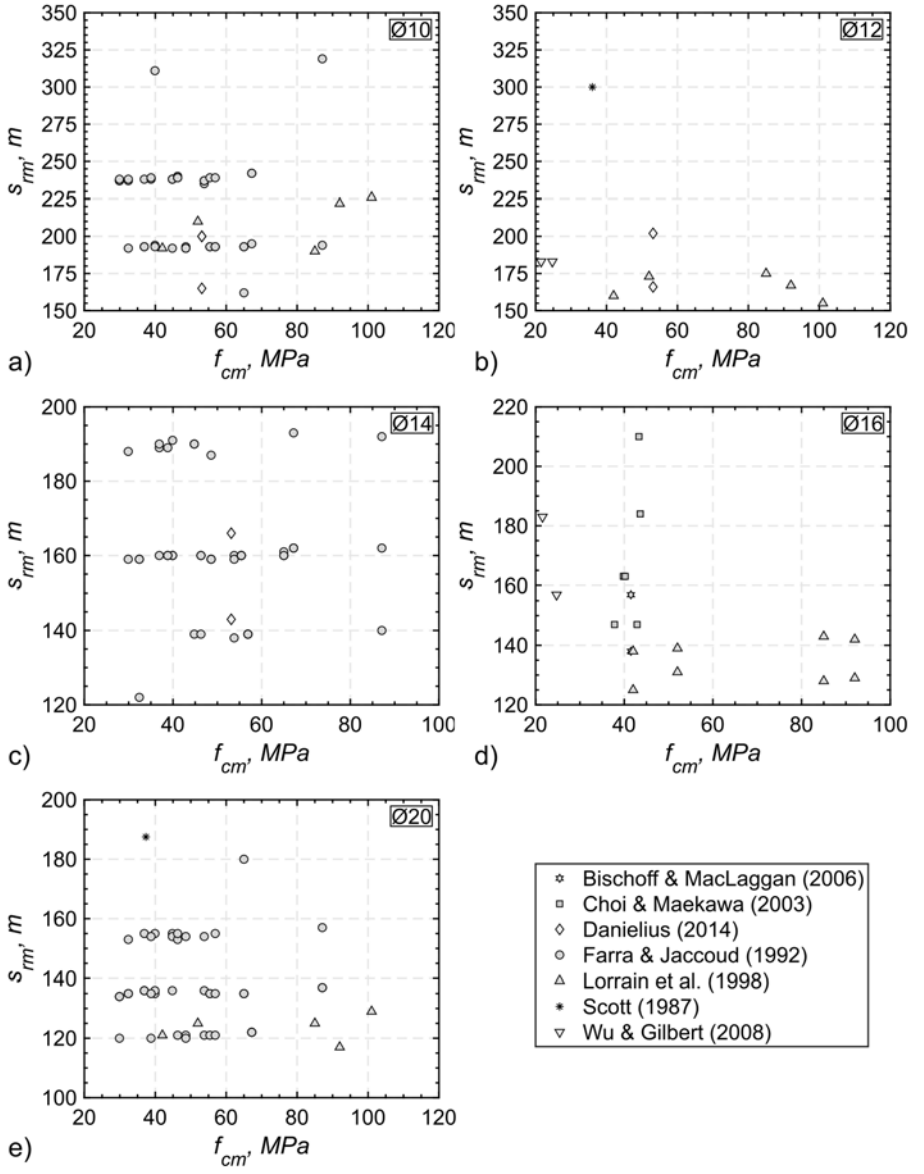

Fig. 2.8. Average distance between normal cracks of experimental ties against the mean compressive strength of concrete: a) Ø10 mm bar reinforcement; b) Ø12 mm; c) Ø14 mm; d) Ø16 mm; e) Ø20 mm.

Remaining characteristics like elasticity modulus of concrete and concrete compressive strength are determined from Model Code 2010 as:

$$E_c = 21500 \cdot \sqrt[3]{\frac{f_{cm}}{10MPa}}. \tag{2.19}$$

The tensile strength of concrete is obtained from:

$$f_{ctm} = \begin{cases} 0.3{f_{cm}}^{2/3} & , f_{cm} \leq 50\ MPa \\ 2.12\log\left(1 + 0.1(f_{cm} + 8)\right) & , f_{cm} > 50\ MPa \end{cases}, \tag{2.20}$$

hence, the material characteristics were estimated as:

- Mean compressive strength of concrete E_c = 31 GPa ,
- Elasticity modulus of steel reinforcement f_{ctm} = 2.9 MPa,

The analysis was carried out for a range of configurations of reinforcement ratio and bar diameter values:

- ρ = 0.78, 1.0, 1.13, 1.25, 1.54, 2.0, 2.5, 3.0, 3.14 and 3.5%
- $Ø_s$ = 10, 12, 14, 16, 20 and 25 mm

2.3.1. Crack Spacing Predictions With Stiffening Model

The strain compliance approach has been employed to analyse a number of RC tie configurations. Among these configurations are the experimental specimens, representing Ø10, Ø12, Ø14, Ø16 and Ø20 mm diameter bars, that for a 100×100 mm section RC element, equate to reinforcement ratios of 0.78%, 1.13%, 1.54%, 2% and 3.14%, respectively. Estimations calculated using the free-of-shrinkage stiffening model (Equation 2.7) as the mean strain technique for the strain compliance principle (Equation 2.6). The results are summarised in Table 2.2 for the cases when shrinkage strains were accounted for ($\varepsilon_{sh} = 10^{-4}$) and when shrinkage strains were taken as $\varepsilon_{sh} = 0$. Additionally, the impact of the debonding effect has been investigated on the resulting mean spacing.

The greyed out row represents the reference element, therefore accuracy is not given for the row. The remaining configurations reveal a tendency for the proposed concept to underperform when it comes to lightly reinforced elements. Of the tested variations, the ones including the debonding effect show slightly higher accuracy. Including shrinkage strains into consideration further increases the accuracy of all bar diameters except Ø10 mm, which has displays decreased performance. However, the improvements over the no shrinkage strain case are marginal. One aspect to be remarked is the fact the study is based on shrunk members, which is also used as the reference element. The observations cannot

be extended universally, as future studies should explore the impact more robustly.

Table 2.2. Crack spacing predictions (with stiffening model as the mean deformation apprroach) of 100×100 mm reinforced concrete section

$Ø_s$	ρ_s	$s_{rm,exp}$	$\varepsilon_{sh} = 2\times10^{-4}$				$\varepsilon_{sh} = 0$			
			$l_d \neq 0$		$l_d = 0$		$l_d \neq 0$		$l_d = 0$	
			s_{rm}	$s_{rm} / s_{rm,exp}$	s_{rm}	$s_{rm} / s_{rm,exp}$	s_{rm}	$s_{rm} / s_{rm,exp}$	s_{rm}	$s_{rm} / s_{rm,exp}$
mm	%	mm	mm		mm		mm		mm	
10	0.78	217.6	187.7	0.87	197.5	0.91	188.5	0.87	196.0	0.91
12	1.13	182.5	174.4	0.96	178.9	0.98	174.9	0.96	178.3	0.98
14	1.54	162.4	162.4	–	162.4	–	162.4	–	162.4	–
16	2.00	149.9	152.7	1.02	148.8	0.99	152.0	1.01	149.1	1.00
20	3.14	137.6	135.7	0.99	124.8	0.91	133.5	0.97	125.6	0.91

The approach can be considered as validated against experimental mean crack spacings due to generally good agreement, nevertheless, a comparison against other popular approaches is compulsory to provide closure on the strain compliance methodology's adequacy. For this purpose, the techniques described in Model Code 2010 (Equation 1.23) and Eurocode 2 (Equation 1.22) are used to determine the mean spacing between cracks of the configurations in Table 2.2. The calculated values are represented graphically in Figure 2.9. The stiffening model case with shrinkage strains considered is presented for the strain compliance technique. For comparison purposes, the individual data points are displayed. The first observation is the Eurocode 2 estimations which deviate the most from the rest of the approaches and experimental data. One aspect to keep in mind is the lack of direct estimation of the mean spacing value by Eurocode 2 (2008), which is currently expressed as the maximum spacing value. In order to compare the results with the rest of the data, the values obtained for divided by 1.7 to obtain the mean value (Barre et al. 2016). The large discrepancy can be partially attributed to the cover of the concrete present in Equation (1.22) and the effective area in tension, which for an RC tensile element with a single centrally located bar can reach unrealistic values. The Eurocode 2 method in principle is more suited to flexural elements because of the aforementioned reasons. The comparison shown in Figure 2.9 highlights this observation, where inclusion of the kc term in the equations of crack spacing resulted in greatly overestimated crack spacing values. Model Code 2010 predictions, on the other hand, are significantly more accurate, though the estimated value was reduced by a factor

of 2/1.5 (Barre et al. 2016). Overall the accuracy is very high, yet the predictions tend to overestimate the spacing for Ø10 mm and Ø12 mm, as opposed to the proposed approach by the author, where both cases tend to underestimate the spacing at smaller bar diameters. The Model Code 2010 predictions for 20 mm bar starts to clearly underestimate the experimental value, whereas the proposed technique, particularly with considered debonding zones, is very close to the experimental data point. In general, the proposed technique can be declared to be performing adequately in terms of accuracy and the general behaviour against bar diameters and reinforcement ratios, nevertheless, more experimental data should be collected in the future to increase the confidence in the present technique and the tension stiffening model by Kaklauskas et al. (2018).

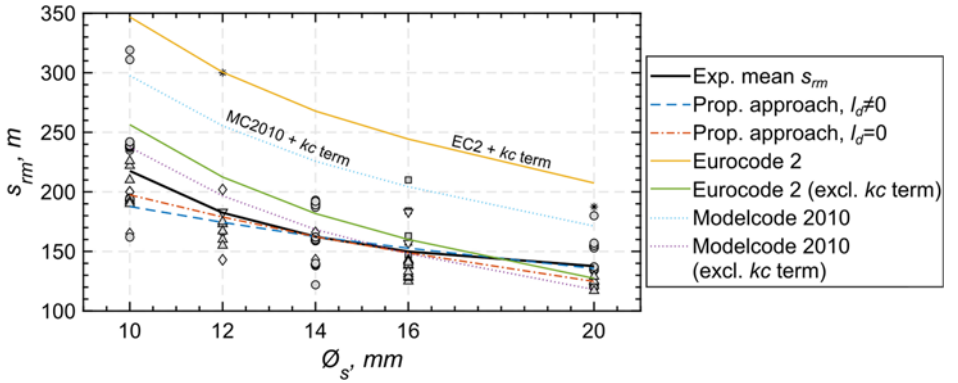

Fig. 2.9. Comparison of predicted and experimental mean crack spacing values

The entire outcome of the analysis is conveyed in the tabular format against the array of bar diameters and reinforcement ratios discussed at the end of the previous subsection (see Table 2.3). The reference configuration is shown with a greyed-out table cell.

Examining the predictions in terms of bond stresses, reveals the values are very close, though exceeding the commonly encountered $\tau = 1.8f_{ct}$ (Model Code 2010) or $\tau = 2.0f_{ct}$ (Bischoff & MacLaggan 2006). In the case of shrinkage ε_{sh} considered, the bond stresses are $2.24f_{ct}$ and $2.74f_{ct}$, when debonding zone is neglected and considered, respectively. Correspondingly, when shrinkage strains are taken as 0, bond stress becomes $2.55f_{ct}$ and $3.06f_{ct}$. The discrepancy is deemed to be reasonable at the present stage of the strain compliance concept development and the investigated experimental data. The decrease of accuracy when shrinkage strains are ignored leads to conclude the necessity of shrinkage strains with the implemented tension stiffening model. Debonding zones should be investigated further in the future, addressing the scarce data for the derivation of the l_d model.

Table 2.3. Predictions for a range of reinforcement ratios and diameters

ρ	Ø10 mm	Ø12 mm	Ø14 mm	Ø16 mm	Ø20 mm	Ø25 mm
0.78%	187.7	225.8	263.7	301.7	377.5	472.2
1.00%	158.1	190.2	222.3	254.4	318.4	398.3
1.13%	144.8	174.4	203.8	233.2	292.0	365.3
1.25%	134.6	162.0	189.4	216.8	271.5	339.7
1.54%	115.2	138.8	162.4	185.9	232.9	291.4
2.00%	94.4	113.9	133.3	152.7	191.3	239.5
2.50%	79.4	95.9	112.4	128.8	161.4	202.2
3.00%	68.9	83.4	97.7	112.0	140.5	176.0
3.14%	66.5	80.5	94.3	108.1	135.7	170.0
3.50%	61.2	74.0	86.8	99.5	124.9	156.5
4.00%	55.2	66.8	78.4	89.9	112.9	141.5

Some of the profiles representing the reinforcement strains are shown in Figure 2.10. The impact of the ratio of reinforcement and diameter of the bar can be clearly observed, with larger diameters the crack spacing value increases, whereas with increased reinforcement ratio, the spacing decreases. As mentioned before, the influence of the debonding zone on the overall distance between cracks is relatively minor and for simplicity could be neglected. Though it is important to point out that the removal of the debonding zone will shift the mean strain value down.

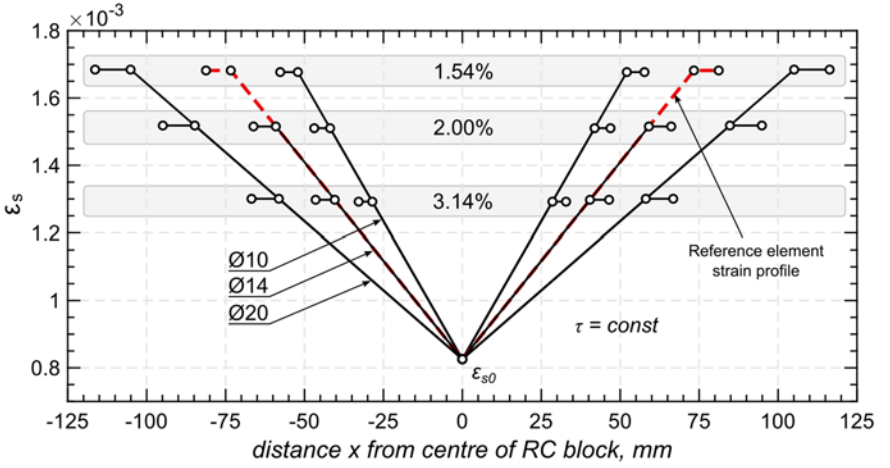

Fig. 2.10. Reinforcement strain profiles of the strain compliance approach with mean strains calculated by the tension stiffening model

2.3.2. Crack Spacing Predictions With Eurocode 2

An identical analysis was executed with the mean strain approach of Eurocode 2 as an alternative to the stiffening model implemented in the previous subsection. Identical configurations were tested, with the exception of shrinkage which was not considered, only the debonding zone impact was investigated. The main outcomes are summarised in Table 2.4. The rows representing the reference element is shown in grey. In general, the spacing predictions are in good agreement with the experimental mean value. However, the behaviour distincts itself from the tension stiffening model mean strain calculation method, with the higher reinforcement ratio case (or the larger diameter in this instance), reveals the proposed concept is underestimating the results. Ø10 and Ø12 mm are overestimating slightly. Another aspect concerns the impact of debonding zone l_d on the spacing value, similar to the tension stiffening model case, employing Eurocode 2 approach and neglecting the debonding behaviour, leads to slightly worse results compared to the results when debonding was included. Nevertheless, the differences are subtle and leave the question open of whether the debonding effect, in general, has a significant enough impact to be proposed strain compliance concept. Future studies should investigate the influence more thoroughly, otherwise, with the aim of simplicity and ease of application for general use, the concept could rely only on the effective zone to describe the strain distribution between neighbouring normal cracks.

Table 2.4. Crack spacing predictions (with Eurocode 2) of 100×100 mm RC section

$Ø_s$	ρ_s	$s_{rm,exp}$	$l_d \neq 0$		$l_d = 0$	
			s_{rm}	$s_{rm} / s_{rm,exp}$	s_{rm}	$s_{rm} / s_{rm,exp}$
mm	%	mm	mm		mm	
10	0.78	217.6	226.1	1.05	231.9	1.07
12	1.13	182.5	188.4	1.03	191.0	1.05
14	1.54	162.4	162.4	–	162.4	–
16	2.00	149.9	144.0	0.96	141.9	0.95
20	3.14	137.6	116.7	0.85	111.1	0.81

The values from Table 2.4 are presented graphically in Figure 2.11 against experimental averaged and scattered data, with Eurocode 2 and Model Code 2010 predictions included as well. The general observations remain the same as for Figure 2.9, with the exception of the proposed approach, which now resembles the general Eurocode 2 crack spacing model result. The predictions for smaller bar diameter are overestimated, whereas the larger bar diameters are underestimated. This behaviour is expected due to the compatibility of Eurocode 2

techniques. Compared to the tension stiffening model case, the resulting adequacy is nominally worse when Eurocode 2 mean strain approach is employed for the strain compliance concept. Thought the variation in absolute errors is marginal. This aspect provides substantiation for the strain compliance approach, as the prediction accuracy holds up with alternative smeared crack techniques. Moreover, the adequacy validation gives credibility to the classical approaches that rely on constant bond.

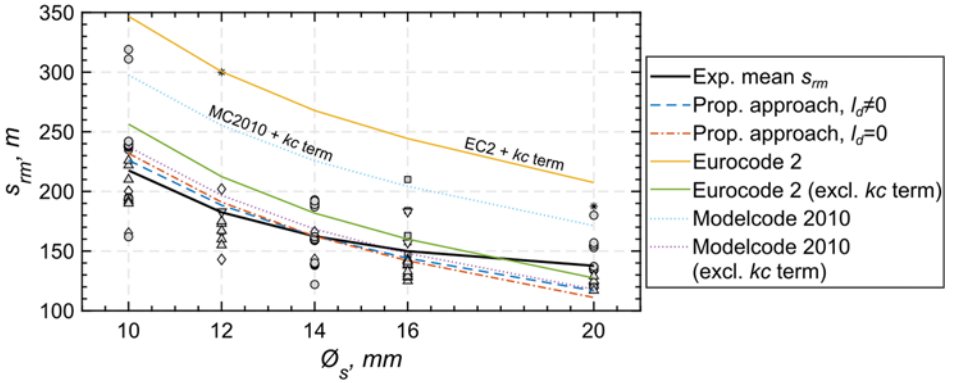

Fig. 2.11. Comparison of predicted and experimental mean crack spacing values

Results for all the calculated alternative element configurations are given in Table 2.5. The grey cell represents the reference element configuration, hence perfect accuracy.

Table 2.5. Predictions for a range of reinforcement ratios and diameters

ρ	Ø10 mm	Ø12 mm	Ø14 mm	Ø16 mm	Ø20 mm	Ø25 mm
0.78%	226.1	271.3	316.6	361.8	452.2	565.3
1.00%	177.0	212.4	247.8	283.2	354.1	442.6
1.13%	157.0	188.4	219.8	251.2	314.0	392.5
1.25%	142.2	170.7	199.1	227.6	284.4	355.6
1.54%	116.0	139.2	162.4	185.6	232.0	290.0
2.00%	90.0	108.0	126.0	144.0	180.0	225.0
2.50%	72.6	87.1	101.6	116.1	145.1	181.4
3.00%	61.0	73.1	85.3.0	97.5	121.9	152.4
3.14%	58.4	70.0	81.7	93.4	116.7	145.9
3.50%	52.6	63.2	73.7	84.2	105.3	131.6
4.00%	46.4	55.7	65.0	74.3	92.8	116.0

The bond stresses are significantly higher of the proposed approach with Eurocode 2 mean strain method when compared to the tension stiffening implementation, with $\tau = 3.86f_{ct}$ and $4.62f_{ct}$ when debonding zone is excluded and included, respectively. Which signifies considerably worse performance and adequacy to the commonly accepted bond stress τ ranges. Hence, this aspect leads to summarise that the tension stiffening model is the better performing and the more adequate one, representing the crack spacing predictions and the general behaviour of tensile RC elements with a higher degree of accuracy.

2.3.3. General Recommendations for Future Research

The intent of the present research is the introduction and validation of the general behaviour of the novel strain compliance concept for predicting crack spacings. Numerous aspects were not given priority, like establishing the strain shape functions with increased certainty through a larger experimental data array or for the part establishing a more reliable debonding zone length model. Hence, various aspects remain to be explored and solidified in future studies, to confirm and further justify the robustness and flexibility of the technique. Among the potential objectives are the following:

1. An extended database of experimental results would further increase the confidence in the proposed concept. Emphasis should be given to strain distribution experiments, as the adopted linear simplification of the strain profile is a subject of debate. The preliminary research carried out within has revealed that while at higher loading stages the linear function provides a relatively good agreement with the experimental shape, numerous local effects are highlighted as well. These include the debonding zone l_d, the length of which was shown to be sensitive to the strain approximation. The other aspect concerns the central area, that is not as well approximated with a line as with a parabola, due to its flatness. Future experiments could potentially give higher priority to distributed optical sensing techniques (Barrias et al. 2016) to acquire data more robust in both the quantity and quality of data points.
2. The collected experimental data contains RC elements reinforced with a single bar. Future studies should explore alternative material options, such as FRP or basalt bars. Additionally, cases, when multiple tensile bars are present in the RC tie such as tested by Rimkus & Gribniak (2017), should be investigated. Fibre reinforced concrete is of interest as well. In theory, the strain compliance approach should be able to account for different materials, but that statement remains to be verified. The strain profile would be shifted downwards for the strain increment $A_c f_{res}/A_s E_s$, where f_{res} is the residual concrete stress.

3. Modification of the strain compliance method in such a way as to remove the necessity of the reference element, greatly reducing the empiricism of the concept for tensile members. Furthermore, investigations should be carried out to address the need for iterative calculations when establishing the mean strain of alternative reinforcement ratio ρ and bar diameter $Ø_s$ configurations. Currently, the maximum reinforcement strain ε_{si} or in other words the loading level must be iterated until the mean strain compatibility is ensured, with the minimum strain value ε_{s0} and bond stress τ being fixed for all analysed elements. Potential solutions could be explored by maintaining the maximum strain ε_{si} fixed and the mean strain calculations would not have to be iterated, however, the ε_{s0}.value cannot be fixed and would need to be obtained to satisfy the strain compatibility.
4. Development of the crack width estimation approach based on the strain compliance concept. The approach should encompass both short- and long-term loading scenarios (Strauss et al. 2017).

2.4. Conclusions of Chapter 2

The conclusions from the research carried out within the current chapter can be summarised as:

1. The linear strain shape function, adopted for the description of the effective zone, governing the transfer of stresses from the reinforcement to the concrete through bond action, has been shown to be adequate for predicting the mean crack spacing by the strain compliance approach.
2. The proposed concept, while still relying on empirical notions such as the reference element with a reference bar diameter $Ø_s$ and reinforcement ratio ρ, is mostly theoretical in nature, with a sound mechanical background. In general, the strain compliance principle is not tied to the reference element implementation, the framework is highly flexible with a wide array of permissible modifications provided the mean strain compatibility between smeared crack and stress transfer approaches is ensured.
3. The core of the proposed technique relies on equating the mean strains of two distinct methods, the mean strain and the discrete crack based one. The former is necessary for the description of the average strain behaviour of the investigated reinforced concrete element, whereas the latter enables the estimation of the spacing between primary cracks from the known strain distribution between two normal cracks, defining a block of length equal to the mean spacing value. The adequacy of predictions was revealed to be greater with the implementation of a stiffening model as

opposed to the mean strain method provided by Eurocode 2. Moreover, the assessed bond stress value is more reasonable at $\tau = 2.24f_{ct}$ for the implemented tension stiffening model versus $\tau = 3.86f_{ct}$ for the Eurocode 2 case.

4. The inclusion of the debonding effect has not altered the results considerably. Nevertheless, taking the effect into consideration has an improvement effect, yet marginal, on the spacing predictions.
5. The observed robustness of the strain compliance concept is very high, with the ability to provide consistently accurate results, specifically when comparing against experimental data points and design code predictions. With Eurocode 2 mean crack spacing predictions by themselves significantly overestimating the spacing of tensile elements. Another feature is the flexibility of the approach, enabling inclusions of varying strain distribution functions, localised effects such as debonding, alternative mean strain techniques for mean strain calculations.

3

Strain Compliance Concept for Predicting Crack Spacing of Flexural Reinforced Concrete Structures

The innovative concept for a theoretically and mechanically sound technique to predicting the average distance between consecutive cracks of RC tension members, called the Strain Compliance approach, has been extended to accommodate RC elements subjected to bending loading. The main changes in assumptions and concepts have been highlighted and substantiated for the different flexural behaviour as opposed to simple uniform tension. Opposed to the method presented in chapter 2, the current modified approach does not rely on any reference reinforcement ratio and reference reinforcement diameter notions and does not necessitate the use of any iterative procedures. This was in part enabled by the introduction of the simplified *central zone* model used to describe the reinforcement strain profiles of beams and slabs. Various published experimental results have been collected and investigated to carry out the derivation of the modelling methodology.

Detailed procedure steps have been outlined from the establishment of the central zone length model to the application of the strain compliance principles for the analysis of any flexural RC member. Accuracy has been compared with values estimated by major design codes and experimental data of a wide range of

key parameters like reinforcement ratios, bar diameters, section heights and so on. Material published in journal papers Kaklauskas et al. (2017a, 2019a, 2019b) and conference proceedings Kaklauskas & Ramanauskas (2016a) is included in this chapter.

3.1. Methodology and Assumptions of the Flexural Element Primary Crack Spacing Prediction Approach

In order to extend the method presented in the previous chapter, some changes were necessary to the fundamentals, as the cracking behaviour of RC elements subjected to bending differ from the cracking behaviour of those subjected to tension. One of the key concepts in this study relates to dividing the cracks of a beam or slab into either primary or secondary cracks. The other major consideration is the investigation within the stabilized cracking phase. The statements are related to the investigations and conclusions by Beeby (1970) and Gilbert & Nejadi (2004). After the applied load reaches a certain threshold, as defined by the material mechanical properties, cracks begin to form that immediately extend in height approximately close to the neutral axis. Other cracks begin to form right after between these primary cracks and are usually but not limited to the concrete cover. These cracks are identified as the secondary cracks, typically appearing next to the ribs of the reinforcement bars (Goto 1971).

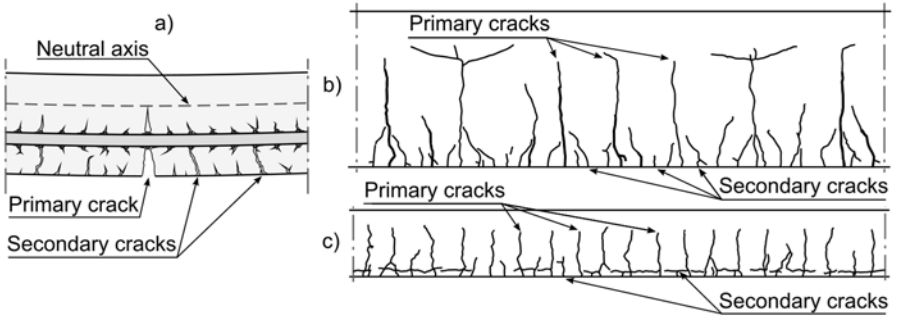

Fig. 3.1. Primary and secondary crack pattern: a) schematic view; b) Beam R103 (Rüsch & Rehm 1964); c) Beam 8 (Calderón Bello 2008)

After a sufficient increase in the applied load, these cracks expand and become visible on the surface of the concrete cover (Broms 1965). Higher section and higher reinforcement percentage RC elements generally display these effects most intensely. In the circumstance that a secondary crack would extend to the neutral axis even at later loading stages, these secondary cracks would be

considered as primary cracks, as they satisfy the main criteria for having a height equivalent to the position of the neutral axis.

The described cracking related and other major assumptions paving the groundwork for this study can be summarized as follows:

1. The behaviour is analysed and the method is derived for the stabilized cracking phase as defined by the *Fédération Internationale du béton* in the Model Code 2010. Formation of primary cracks that extend up to the neutral axis of a beam or slab is considered to have stopped and only existing cracks continue increasing in height and width.
2. The proposed approach for predicting crack spacing accounts for the primary crack formations only. The secondary cracks are omitted, that do not extend up to the neutral axis are omitted.
3. The ability of concrete to transfer stresses within a crack also known as the tension softening effect is neglected.
4. The mean deformation behaviour of a cracked reinforced concrete element can be represented by a shorter member defined as an RC block between two adjacent primary cracks.
5. The mean strain value of the reinforcement under the tension of the RC element can be estimated, either by experimental, numerical or analytical approaches.

Further discussion and inclusion of other concepts such as the central zone definition are presented in successive sections.

3.2. Strain Compliance Approach for Flexural Elements

The foundation for estimating the mean crack spacing of flexural elements is identical to the one presented for RC ties. By ensuring compatibility between the average reinforcement bar strain value of the mean deformation and stress transfer methods through equality of said variables, the estimation of the actual distance between cracks can be obtained from the reinforced strain distribution profiles of the investigated RC block. The general principles have been presented graphically in Chapter 2, Figure 2.4 and 2.6. The key difference lies in the deformation behaviour of flexural and tensile reinforced concrete elements. The reinforced strain distribution of RC ties was shown to be relatively accurately definable by a linear equation for higher loadings cases that are within the stabilized cracking stage. Beams and slabs that are subjected to bending reveal additional complexity in the middle parts between neighbouring primary cracks. The flexural case is inherently more complex due to the appearance of compressive and tensile zones,

neutral axis, multiple bar configurations and other aspects, therefore the strain behaviour simplification from Chapter 2 necessitates additional modifications and rationalisation.

3.2.1. Simplification of the Reinforcement Strain Profile

In order to provide more insight into the reinforcement strains of RC elements subjected to bending loads, an investigation of available data, strain profiles in published literature was carried out. Early results of strain distributions are available for mostly short RC tensile elements (Houde 1974, Scott & Gill 1987, Kankam 1997), that conform with the assumption No. 4 of this chapter. Up to this day, there are still relatively few experimental programmes that have covered the strain distribution within beams or slabs. Nevertheless, the few studies that exist (Kenel et al. 2005, Henault et al. 2012, Davis et al. 2017, Monsberger et al. 2018) have provided great insight on the intricate strain and bond characteristics. The cornerstone of these studies is the adoption of innovative strain sensing techniques such as Fibre Bragg Grating or Optical Frequency Domain Reflectometry, also known as distributed sensing.

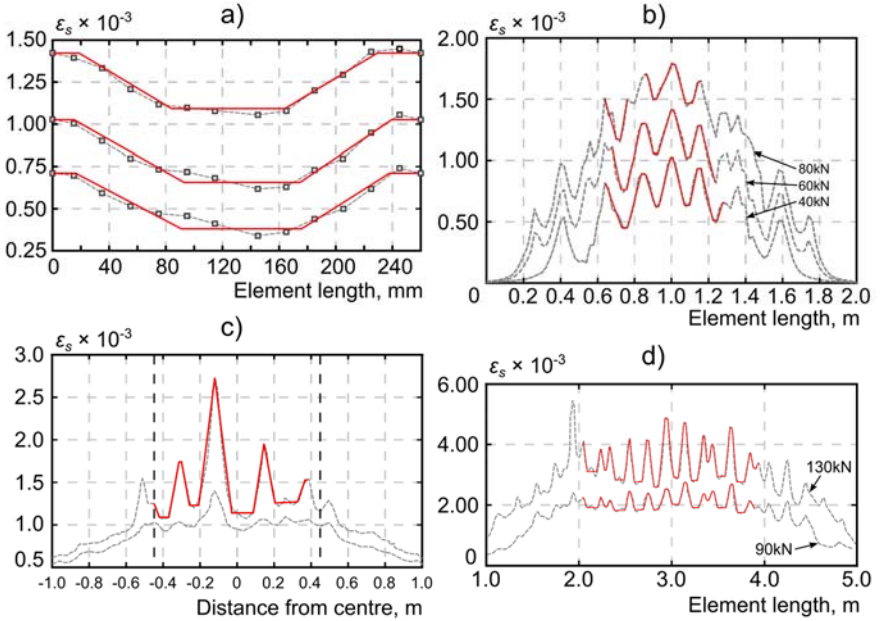

Fig. 3.2. Experimental reinforcement strain distributions with overlayed simplified representations: a) Kaklauskas et al. 2019; b) Davis et al. 2017; c) Henault et al 2012; d) Monsberger et al. 2018

The published strain profiles from the aforementioned studies have been analysed and are presented in Figure 3.2 with overlayed simplified strain shapes. The general character of the experimental strain profiles is quite similar. A steep descent is visible of the strain value in the vicinity of the cracks, flattening out as we approach the middle between neighbouring cracks.

Another important observation that can be maid relates to the debonding zones established in Chapter 2. Due to the limited data points, it is uncertain whether the phenomena have a profound effect on flexural RC members. Hence, both implications will be considered in this research and the approach expressed for both cases. Retaining the goals of adequacy and simplicity, a pattern comprised of linear expressions is adopted to describe approximate the general strain shape. This representation follows the idea of zone division, where a flat horizontal line near the cracks represent the debonding zone, the descending line equates to the effective zone and the new *central zone*, which averages the complex strain action in the middle. This simplification is presented graphically in Figure 3.3, where the dashed line represents the normally encountered experimental shape and the solid line is the assumed simplified shape.

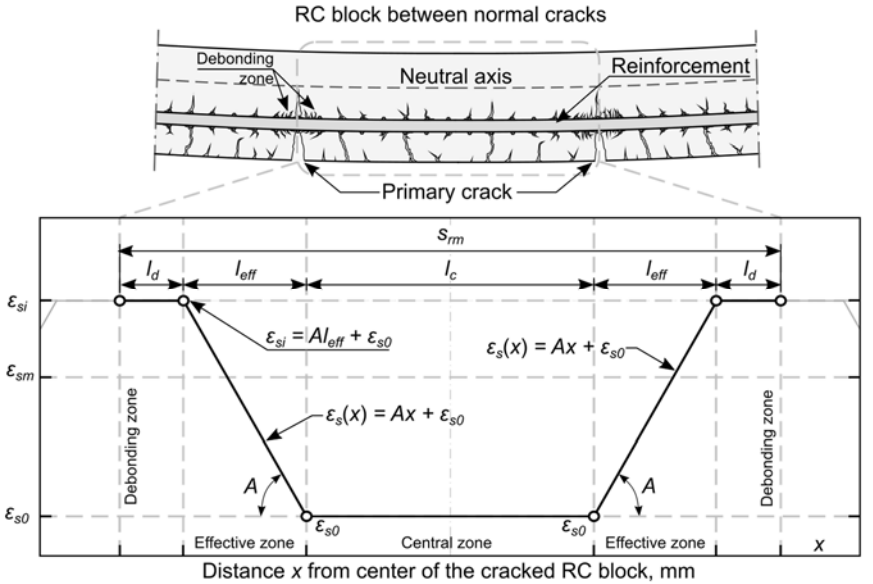

Fig. 3.3. Simplification of the reinforcement strain profile between neighbouring cracks

The areas neighbouring the cracks display the negligible change in reinforcement strains when compared to the steeply descending strains that proceed them. This effect is explained by bond theory. Since the concrete

surrounding the reinforcement bar at the location of the crack is damaged, it is not able to transmit any stresses to reinforcing bars. This effect is highly localized within a short segment from the location of the crack. The source of damaged concrete normally concentrates around the bar ribs. Concerning the lack of this characteristic in some investigated results, further exploration of the crack spacing prediction approach will accommodate cases when debonding is considered and omitted. The debonding effect has been studied in detail by Jakubovskis (2015) with a model suggested on how to estimate the length of this zone. Ruiz et al. (2007) and Model Code 2010 (2013) have the length related to the bar diameter.

A model derived for investigatory purposes in Chapter 2 is retained in this extension of the *Strain Compliance* approach for consistency, as well as the notation l_d to describe the debonding zone length.

The length of the linearly descending strains is characterized as the effective zone, same as for tensile RC elements. The key trait is the ability to transfer bond stresses between the concrete and the steel bar. Due to the linear shape function, the bond stresses are constant within this zone. This partly reflects the classical approaches, where constant bond is considered throughout the entire segment. Marti et al. (1998) have suggested bond to be related to double the concrete tensile strength $\tau = 2f_{ct}$, which is the expression assumed in the present research. Alternatively, $\tau = 1.8f_{ct}$ is the expression provided in Model Code 2010. The length of this area, referred to as the effective zone, is given as l_{eff}.

The remaining area in the middle of the RC block is a new notion established as the central zone. The main feature is the omission of bond stresses, leading to a flat horizontal representation. The nature of these characteristics stems from the deformation behaviour between two primary cracks. Many secondary cracks that originate mainly around the ribs of the reinforcing bar continue to increase in both width and size in the stabilized cracking phase. The result is the spikes in reinforcement strain as observed in Figure 3.2. All the primary cracks are assumed to have been formed and already exist in the stabilized cracking stage, however the remaining cracks, while still growing, are limited in their ability to reach the size of the primary crack, partly due to the nature of localised damage spreading around the bars and limiting the bond stress transfer (Wu & Gilbert 2009). The constitutive expression will be provided in further sections with l_c used as the notation for the length of the central zone.

3.2.2. Finite Element Investigation of Reinforcement Strains in Reinforced Concrete Beams

In order to further explore and substantiate the central zone concept as a mean representation of reinforcement strains, FE analysis has been carried out on a RC beams. For this purpose, elements were selected from Rüsch & Rehm (1964)

experiments that would be modelled in ATENA FE analysis software using nonlinear concrete mechanics. The specimens were chosen because of very detailed information provided within the report of Rüsch & Rehm (1964), and most importantly due to the available detailed cracking pattern which can be used for comparison and adequacy evaluations. The beams chosen to be analysed were R102 and T31, where the former is a rectangular section tall beam and the former is T shape beam. The section of R102 beam is 120 cm in height and 45 cm in width, whereas the T31 beam has a height of 62.5 cm, the width of 20 cm and flange width of 60 cm. The length of the pure bending zones is 4 m and 2 m, respectively. Full material and physical characteristics are presented in Annex C.

In order to capture the intricate effects of the reinforcement layouts of the chosen beams, 3D FE models were created, using 8 node solid brick and 4 node tetrahedral elements. Reinforcement bars were modelled as embedded bar elements in ATENA for longitudinal and shear reinforcement (Fig. 3.4). Symmetry conditions were employed to reduce computational time.

Loading was applied by controlled displacement iteratively in ~235 steps to reach an average induced strain of $\varepsilon_{si} = 1.5\times10^{-3}$ within the reinforcement bars. Loads were applied to steel plates that in turn transfer the loading to the RC beam, hence no unrealistic stress concentrations are present in the areas of applied loading and supports. The sizes of these plates were modelled to mimic the actual experiments as described by Rüsch & Rehm (1964). Steel reinforcement material properties were defined by an elastic-plastic relationship, while concrete material was modelled by the default ATENA definition for the appropriate concrete strength. The model is based on Model Code 2010 implementation; hence it allows for bond-slip to occur between the concrete and the embedded reinforcement bars. Furthermore, it allows for smeared cracking representation. Nonrotating, fixed cracking was selected for the smeared crack model, which inhibits the change of cracking direction after it has formed.

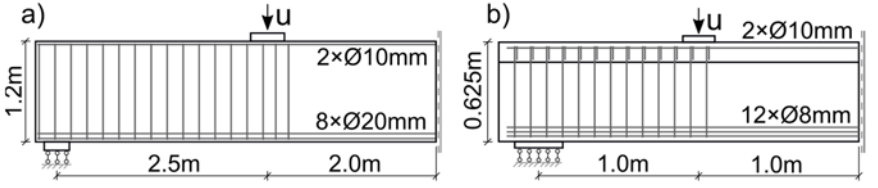

Fig. 3.4. Reinforcement bar layouts of the modelled Rüsch & Rehm (1964) beams: a) specimen R102; b) specimen T31

The size of the mesh was partially restricted by the limited processing power available and limited computer memory. The R102 beam due to its simple geometry was modelled with uniform finite elements throughout the element length, whereas the T31 beam due to its complex shape and the need for more

elements to represent the flange, were modelled with a denser mesh in the pure bending zone with greatly increased size of the mesh in the remaining part. While this has a negative effect on the detail level of the cracking, the aim is to investigate the area of pure bending and reinforcement strains within it.

The final crack patterns are shown in Figure 3.5 for R102 and T31 beams of Rüsch & Rehm (1964).

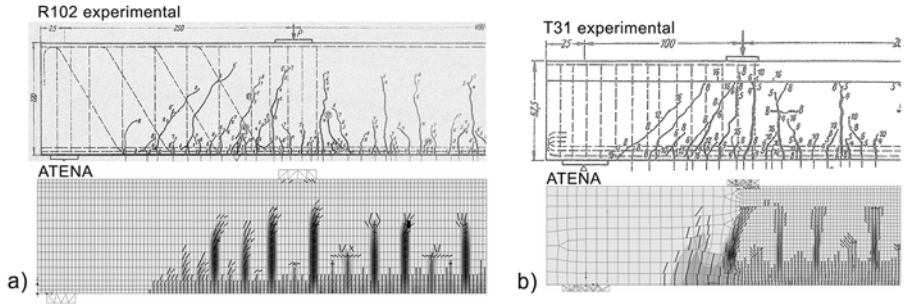

Fig. 3.5. Cracking patterns of experimental tests and FE numerical calculations of Rüsch & Rehm (1964): beams a) specimens R102; b) specimens T31

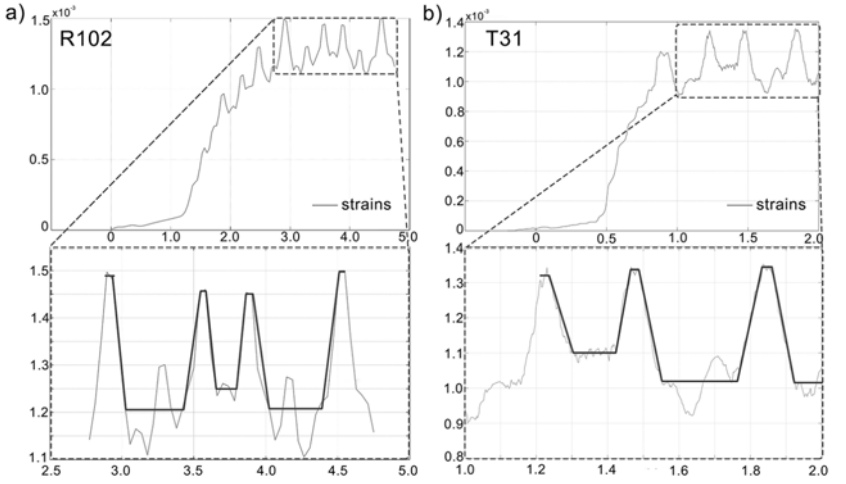

Fig. 3.6. Mean reinforcement strain value of all bars along the length of the element: a) specimen R102; b) specimen T31

FE analysis provided further substantiation for the simplified reinforcement strain representation employed in this work. In the pure bending zone, where it can be clearly seen how secondary cracking affects the strain profiles, overlays are provided of the debonding, effective and central zones. This representation is

shown in Figure 3.6, where all tensile reinforcement mean strains are shown distributed over the length of the pure bending zone. The principle concept of the central zone as an average reinforcement strain representation within the secondary cracking affected area can be clearly inferred. Inherently, the exact representation of the minimum reinforcement strain value is lost with the proposed representation, as the central zone strains will always be slightly above it.

With advances in distributed sensing techniques, a detailed experimental investigation of an actual RC beam should be carried out in the future. At present, FE analysis remains among the best, though still relatively complicated, tools to obtain the necessary insight for the present research.

3.2.3. General Crack Spacing Analysis Procedure with Debonding Effect Included

The general procedure is detailed and discussed in this section with the inclusion of local debonding effects near the formed primary cracks. The expressions are provided with the presumption that debonding zone length and central zone length models are known. The derivation of the central zone length model is presented in Section 3.3.

The method takes the sum of all introduced zone lengths from the stress transfer approach. The strain distribution of tensile reinforcement, as given in Figure 3.3, forms the basis for expressing the average crack spacing value:

$$s_{rm} = 2l_d + 2l_{eff} + l_c. \tag{3.1}$$

A unified loading condition represented by the reinforcement strain value $\varepsilon_{si} = 0.0015$ within the location of the crack is adopted. This value characterizes approximately 60% of the yield strength of the common S500 grade reinforcement bars, that have a yield value equal to $f_y = 500$ MPa. The general bending moment for a cracked section can be evaluated by:

$$M = \varepsilon_{si} \frac{EI_{tr}}{d - y_0}, \tag{3.2}$$

where I_{tr} is the second moment of area of the transformed section, reduced due to cracking, EI_{tr} together is the flexural stiffness of the cracked section.

Depending on the reinforcement percentage of the investigated element, it is possible the fixed reinforcement strain of 0.0015 might conflict with core assumption No. 1, regarding the necessity for the stabilized cracking stage to be ensured. The following condition must be verified, else the strain value needs to be recalculated:

$$M \geq cM_{cr}, \tag{3.3}$$

where c is taken as 2.5 in order to ensure that the stabilized cracking stage is reached and M_{cr} is the cracking moment, which according to Eurocode 2, is obtained as:

$$M_{cr} = f_{ct}\frac{bh^2}{6}. \tag{3.4}$$

If the condition given in Equation (3.3) is not satisfied, the strain value is recalculated assuming $M = cM_{cr}$. For exploratory purposes, future research could study the exact value of the c parameter and its influence on the results.

Expressing the mean reinforcement strain value from the chart provided in Figure 3.3 in terms of given coordinates, the following equation is obtained:

$$\frac{2\varepsilon_{si}l_d + 2\left(\varepsilon_{si} - 0.5Al_{eff}\right)l_{eff} + \varepsilon_{s0}l_c}{2l_d + 2l_{eff} + l_c} = \varepsilon_{sm}, \tag{3.5}$$

where ε_{s0} is the minimum reinforcement strain value, encountered in the central zone, A is the slope of the effective zone strain line, l_c is the central zone length.

The strain compliance approach dictates the mean strains of the smeared crack method and stress transfer approaches to be equated together, hence ε_{sm} in Equation (3.5) is substituted with the Eurocode 2 estimation as used in the present study:

$$\varepsilon_{sm} = (1 - \xi)\varepsilon_{el} + \xi\varepsilon_{si}, \tag{3.6}$$

where ξ is the tension stiffening coefficient from Eurocode 2, ε_{el} is the elastic strain the section in uncracked condition at the centroid of the tensile reinforcement.

The elastic strain can be estimated by:

$$\varepsilon_{el} = M\frac{d - 0.5h}{EI}, \tag{3.7}$$

where EI is the flexural stiffness of the uncracked cross-section.

The tension stiffening factor is determined from the Eurocode 2 as:

$$\xi = 1 - \left(\frac{M_{cr}}{M}\right)^2. \tag{3.8}$$

After equating expressions (3.5) and (3.6) are equated, the resulting equation can be further simplified by expressing the minimum reinforcement strain ε_{s0} and the debonding length l_d through the maximum strain found at the crack ε_{si} using Equations (2.2) and (2.4). Further rearranging the formulation in a quadratic manner gives the outcome:

$$\begin{aligned} &Al_{eff}^2 + (2\varepsilon_{sm} + l_cA - 2\varepsilon_{si})l_{eff} \\ &+ (l_c\varepsilon_{sm} + 2l_d\varepsilon_{sm} - l_c\varepsilon_{si} - 2l_d\varepsilon_{si}) = 0. \end{aligned} \tag{3.9}$$

The main unknown variable is the l_{eff}, as the debonding length l_d and the central zone length l_c models are presumed to be known for the explanation presented in the current section. Hence, the subsequent simplification is made:

$$Al_{eff}^2 + Bl_{eff} + C = 0, \tag{3.10}$$

where the term B is expressed as:

$$B = l_c A - 2(\varepsilon_{si} - \varepsilon_{sm}), \tag{3.11}$$

and the term C provided as:

$$C = -(\varepsilon_{si} - \varepsilon_{sm})(l_c + 2l_d). \tag{3.12}$$

The coefficient A has been expressed in terms of bond stress and bar diameter as given in Equation (2.13). Thus, the outcome is an ordinary quadratic equation with the general solution discarding the negative root given by:

$$l_{eff} = \frac{-B + \sqrt{B^2 - 4AC}}{2A}. \tag{3.13}$$

With the length of the effective zone established, the aggregate of all zone lengths, symbolizing the average distance between two primary cracks, can be estimated from Equation (3.1). The general resulting characteristics of this approach are supplied in Figure 3.7. The influence of varying sections heights, reinforcement ratios and bar diameter combinations on the reinforcement strain distribution chart are exemplified. The generalisations conform with the knowledge that smaller reinforcement ratios and larger bar diameters increase the distance between cracks. In the proposed technique, the section height has a profound effect on the length of the central zone and, as a consequence, the mean crack spacing, whereas longer effective zones, or alternatively, the delta difference $\Delta\varepsilon_s = \varepsilon_{si} - \varepsilon_{s0}$ of the maximum and minimum steel bar strains are greater for elements with less reinforcement percentage.

3.2.4. General Crack Spacing Analysis Procedure Without the Debonding Effect

Due to the lesser impact of debonding zones on the primary crack spacing value, as will be demonstrated in later sections, an alternative procedure of the strain compliance approach is derived without considering the debonding effect. Although this method does not represent the generalized concept, it serves an investigatory purpose, helping understand and highlight the robustness of the innovative crack modelling concept. Removing the debonding zone component, the aggregate crack spacing value is defined by:

$$s_{rm} = 2l_{eff} + l_c. \tag{3.14}$$

Therefore, the strain chart will become different (see Fig. 3.7) and the subsequent mean strain Expression (3.5) will be transformed into:

$$\frac{2\left(\varepsilon_{si} - 0.5Al_{eff}\right)l_{eff} + \varepsilon_{s0}l_c}{2l_{eff} + l_c} = \varepsilon_{sm}. \tag{3.15}$$

The quadratic Equation (3.9) now becomes:

$$Al_{eff}^2 + (2\varepsilon_{sm} + l_cA - 2\varepsilon_{si})l_{eff} + (l_c\varepsilon_{sm} - l_c\varepsilon_{si}) = 0. \tag{3.16}$$

Simplifying further into the form as given in Equation (3.10), the coefficient C to that formula would equate to:

$$C = -(\varepsilon_{si} - \varepsilon_{sm})l_c. \tag{3.17}$$

The final solution, nor do the other coefficients, change from the one given by Equation (3.13).

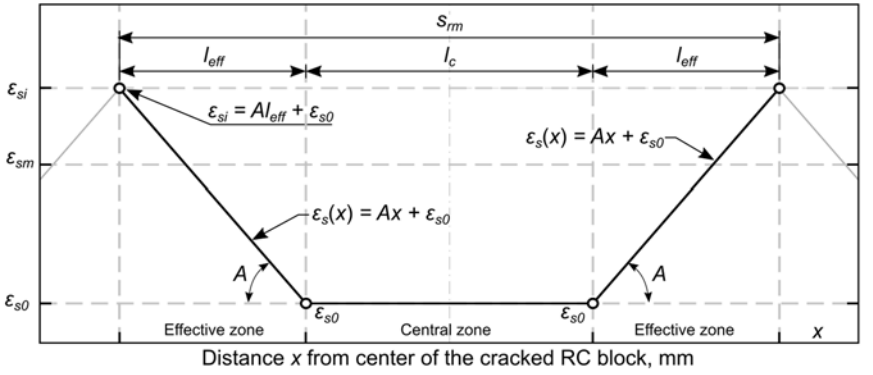

Fig. 3.7. Simplified reinforcement strain graph without debonding zones

3.3. Formulation of the Central zone Constitutive Length Model

In order to derive a central zone length l_c constitutive model, the collection of experimental data was necessary. For this purpose, data representing a wide range of configurations in reinforcement bar diameters and ratios were necessary. Results featuring detailed descriptions of geometrical, mechanical properties and cracking outcomes, have been reported by Calderón Bello (2008). In total, 14 RC beam samples of identical section height and width were tested, maintaining the same concrete cover and concrete strength. The variables were picked as a number of bars and their diameters, ranging from 2 bars to 30 bars and from Ø10 mm to Ø25 mm, respectively. Consequently, the reinforcement ranged between 0.86%

and 2.3%. The samples were tested under constant bending condition, the four-point scheme was defined by the distance of 4.0 m between supports. The results, such as crack spacing, crack widths and patterns, were documented over the entire pure bending zone.

Table 3.1. Geometrical and material characteristics of reinforced concrete beams

Source	Id	h	b	d	c	$No.\times Ø_1$	$No.\times Ø_2$	E_{s1}	f_{cm}	s_{rm}
		mm	mm	mm	mm	×mm	×mm	GPa	MPa	mm
Calderón Bello (2008)	1	500	250	452	36	4×25	2×8	204	24.1	176
	2			434	40	10×16	2×8	204	22.6	173
	3			413	37	24×10	2×8	203	24.4	151
	4			453	35	2×25	2×8	203	26.1	196
	5			452	40	5×16	2×8	202	24.4	187
	6			445	35	12×10	2×8	203	24.6	185
	7			457	35	2×16	2×8	205	21.9	382
	8			460	35	5×10	2×8	204	24.1	217
	9			436	34	5×25	3×16	204	26.0	116
	10			416	40	12×16	3×16	202	28.2	143
	11			402	33	30×10	3×16	204	24.2	105
	12			436	34	5×25	4×20	205	27.1	137
	13			416	40	12×16	4×20	202	26.3	128
	14			402	33	30×10	4×20	203	24.1	114
Gribniak (2016)	S1-2	300	284	273	20	5×14	2×6	211	49.4	100
	S1-4	300	280	267	22	2×22	2×6	199	49.4	133
	S2-3	300	282	272	21	3×14	2×6	211	48.1	133
	S1-1	299	282	248	23	9×10	2×6	210	49.7	124
	S1-6	303	271	217	19	12×8	2×6	210	43.0	91
Rüsch & Rehm (1964)	R58	625	300	589	28	4×16	2×19	200	13.8	257
	R66			587	26	2×26	2×19		14.8	243
	R68			584	28	3×26	2×19		14.3	213
	R72			582	30	4×26	2×10		26.8	231

The initial investigation was carried out on the Calderón Bello (2008) data (given in Table 3.1), as the uniformity of sections and variety of reinforcement options enabled to obtain more consistent and reliable insight, with the mitigated risk of crack spacing being affected by unforeseen variables. Subsequent analysis of the central zone features involved additional experimental data points for

regression of the central zone length l_c model and confirmation of its size dependency as discussed in the following subsections.

The expanded data included an additional four specimens from Rüsch & Rehm (1964) and five from Gribniak et al. (2016), that covered sections heights of 625 mm and 320 mm, respectively. All the key values can be found in Table 3.1. The author would like to remark that the proposed cracking analysis concept relies on assumption No. 2, only primary cracks, extending up to the neutral axis of the RC beam is considered. Identification was predominantly straightforward, however for some elements, particularly with lower section heights, the process demanded a degree of subjectivity. Hence, the developed strain compliance approach was validated with more experimental data, outside the scope of the current l_c parameter investigation, as shown further in this chapter.

3.3.1. Central Zone Length Definition With Included Debonding Zones

Determining the constitutive relation of l_c with other physical parameters follows the process described in Section 3.2 for establishing the mean crack spacing s_{rm}. The current aim is to determine the central zone length l_c employing the strain compliance approach with the substitution $s_{rm} = s_{rm,exp}$ of mean crack spacing value with the experimentally obtained ones from Table 3.1.

Redefining Equation (3.1) with l_c as the unknown:

$$l_c = s_{rm,exp} - 2l_d - 2l_{eff}. \tag{3.18}$$

The general strain compliance Equation (3.8) now features the experimental spacing s_{rm}:

$$\frac{2\varepsilon_{si}\, l_d + 2\left(\varepsilon_{si} l_{eff} - 0.5A l_{eff}^2\right) + l_c \varepsilon_{s0}}{s_{rm,exp}} = \varepsilon_{sm}. \tag{3.19}$$

Maintaining the same structure and the substitution of ε_{s0} as in the previous section, a quadratic expression is expanded as:

$$\begin{gathered} l_c\left[\varepsilon_{si} - A\left(0.5s_{rm,exp} - 0.5l_c - l_d\right)\right] \\ +2\left[\varepsilon_{si}\left(0.5s_{rm,exp} - 0.5l_c - l_d\right)\right]\left[-0.5A\left(s_{rm,exp} - 0.5l_c - l_d\right)^2\right] \\ +2\varepsilon_{si}\, l_d = \varepsilon_{sm} s_{rm,exp}, \end{gathered} \tag{3.20}$$

hence, the resulting equation can be further simplified into:

$$\begin{gathered} 0.25Al_c^2 - Al_d^2 + As_{rm,exp} l_d + \varepsilon_{si} s_{rm,exp} - 0.25As_{rm,exp}^2 \\ = \varepsilon_{sm} s_{rm,exp}. \end{gathered} \tag{3.21}$$

A direct solution for l_c is found by rearranging the above formula into:

$$l_c = 2 \times \sqrt{\frac{\varepsilon_{sm} s_{rm,exp} - \varepsilon_{si} s_{rm,exp} + A l_d^2 + 0.25 A s_{rm,exp}^2 - A s_{rm,exp} l_d}{A}}. \quad (3.22)$$

The results obtained from the implementation of the procedure are summarised in Table 3.2 with lengths of each defining zone and the maximum, mean and minimum reinforcement strain values.

Table 3.2. The calculated central zone, debonding and effective zone lengths

Source	Id	$s_{rm,exp}$	l_c	l_{eff}	l_d	ε_{si}	ε_{sm}	ε_{s0}
		mm	mm	mm	mm	$\times 10^{-3}$	$\times 10^{-3}$	$\times 10^{-3}$
Calderón Bello (2008)	1	176	145.6	2.7	12.5	1.5	1.493	1.492
	2	173	153.7	1.7	8.0	1.5	1.493	1.493
	3	151	138.0	1.5	5.0	1.5	1.489	1.489
	4	196	142.3	14.4	12.5	1.5	1.462	1.453
	5	187	156.1	7.5	8.0	1.5	1.469	1.464
	6	185	164.2	5.4	5.0	1.5	1.462	1.458
	7	382	276.3	44.9	8.0	1.5	1.341	1.310
	8	217	139.3	33.9	5.0	1.5	1.297	1.245
	9	116	86.6	2.2	12.5	1.5	1.495	1.493
	10	143	123.7	1.7	8.0	1.5	1.492	1.491
	11	105	93.0	1.0	5.0	1.5	1.493	1.492
	12	137	107.6	2.2	12.5	1.5	1.494	1.493
	13	128	108.9	1.6	8.0	1.5	1.493	1.492
	14	114	102.0	1.0	5.0	1.5	1.493	1.492
Gribniak (2016)	S1-2	100	65.1	10.4	7.0	1.5	1.423	1.398
	S1-4	133	68.9	21.1	11.0	1.5	1.407	1.362
	S2-3	133	48.4	35.3	7.0	1.512	1.3	1.175
	S1-1	124	92.4	10.8	5.0	1.5	1.377	1.352
	S1-6	91	51.2	15.9	4.0	1.5	1.321	1.257
Rüsch & Rehm (1964)	R58	257	216.2	12.4	8.0	1.5	1.473	1.470
	R66	243	190.1	13.4	13.0	1.5	1.481	1.478
	R68	213	176.4	5.3	13.0	1.5	1.493	1.492
	R72	231	192.9	6.1	13.0	1.5	1.483	1.480

One of the main observations from the formulation of the constitutive l_c parameter is the presence of an expressive central zone within all investigated specimens. Selected elements representing distinct reinforcement ratios from low to high have their reinforcement strain charts shown in Figure 3.8. Charts for all 23 investigated specimens are presented in Annex C. Figure 3.8 suggests there could be a correlation between the delta difference between the maximum and minimum reinforcement strains $\Delta\varepsilon_s = \varepsilon_{si}–\varepsilon_{s0}$ and the reinforcement ratio, as beams 8 and 4 that are weakly reinforced elements display very marginal $\Delta\varepsilon_s$ values compared to highly reinforced beams 1 and 12 with a larger gap between strains. This, in turn, could suggest that the tension-softening effect is marginal, the stress-strain state is close to the fully cracked state.

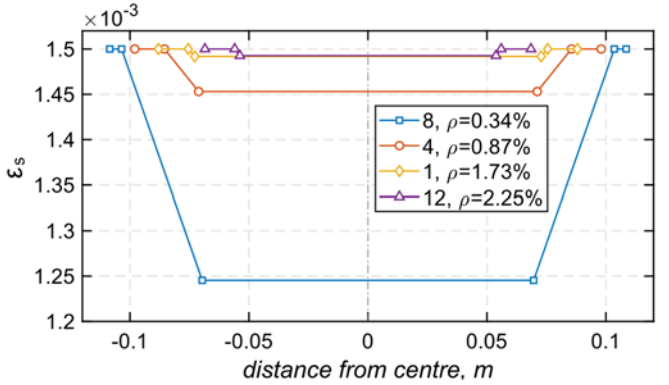

Fig. 3.8. Strain distribution profiles of reinforcing steel bars of selected specimens 8, 4, 1, 12 from Calderón Bello (2008) data, in ascending order from smallest to highest reinforcement ratio of the element

A separate plot of the $\Delta\varepsilon_s$ against the reinforcement ratios (Fig. 3.9) further highlights the likelihood of a correlation. Even though the spread is clearly higher for small reinforcement percentages, it must be taken in relation to different experimental programmes, only Calderón Bello (2008) providing a consistent variation of specimens under uniform conditions. Hence, external factors could have some effect on this scatter. The correlation seems to be non-linear in nature, which is partly highlighted in Figure 3.8, where specimen 8 has a significantly smaller minimum strain than specimen 4. A linear correlation check was done in *Matlab* and yielded a significance level of $0.0029 < \alpha=0.05$ which proves there is a strong correlation between the data.

As shown in Equations (2.4) and (2.14), the effective zone length is related to the diameter of the bar. Nevertheless, the distance between cracks and the effective zone length are more dependent on the combined influence of the ratio of reinforcement and bar diameter rather than diameter alone. Figure 3.10 displays

the strains computed for beams no. 7 and 8 from Calderón Bello (2008) data. Minimum strains have slightly deviated for both beams with very little reinforcement but different bar diameters. The same is true for the central zone lengths and the sum crack spacing. When highly reinforced specimens are investigated, the marginal $\Delta\varepsilon_s$ values lead to a greatly reduced length of the effective zone. Hence, it becomes complicated to establish the actual influence of bar diameter in such cases and may lead to believe the influence is marginal.

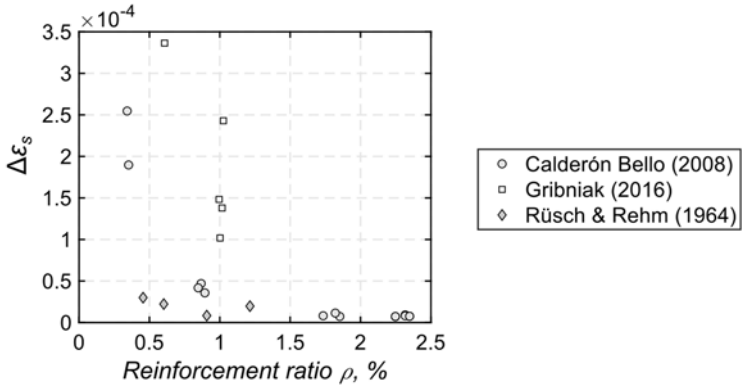

Fig. 3.9. Difference between maximum and minimum strain plotted against the reinforcement ratio of specimens from Table 3.1

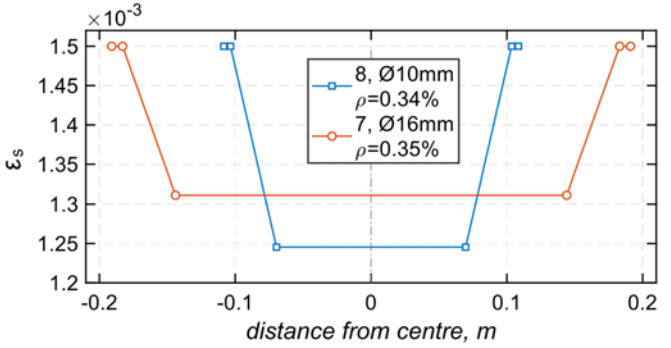

Fig. 3.10. Strain distribution profiles of beam 7 and 8 from Calderón Bello (2008) data

Regarding the debonding model, the study reveals that it does not play a significant role in the aggregate crack spacing, as the fraction of made up by the debonding zone is on average from the 23 specimens just 10.7%, with only a single case when it exceeds 20%, yet multiple specimens when it dips below 5%.

Future studies should focus on integrating a more robust debonding zone model, derived from the larger experimental data cache.

The insight of the Table 3.1 data exposes parameter combinations that can be considered outliers. The constitutive parameter l_c, defining the central zone, values are mostly clustered together with beam No. 7 being the outlier. It has the lowest ratio of reinforcement, but unlike beam No. 8, the bar diameter is greater in the former than the latter. The large difference in the crack spacing conveys the need to investigate the bond stress τ relation, potentially relating it to the diameter of the reinforcement bar in future research, similarly as has been investigated by Ichinose et al. 2004.

In order to establish the relationship between the length of the central zone model, the lc parameter has been plotted against the distance between the neutral axis and the centroid of the tensile reinforcement $d - y_0$, against the concrete compressive strength f_{cm}, tensile reinforcing bar diameter $Øs_1$ and ratio of reinforcement ρ_{s1} (Fig. 3.11a–c). The dependence of the l_c parameter on the diameter of the embedded bar is not profound on its own, as shown in Figure 3.11c, as the scatter is relatively high as shown by the 95% confidence interval lines. Comparing the findings against the reinforcement percentage does (Fig. 3.11d) exhibit a degree of downward correlation, decreasing l_c with higher reinforcement ratios, however, the data is inconclusive. In addition, with the reduction of the central zone length l_c of beams 9–14 from Table 3.1, that have great amounts of compressive reinforcement and the most tensile reinforcement spread over several layers, it can be postulated that the parameter l_c can be size dependent, as the listed specimens had the shortest height from the neutral axis to the tensile bars. In fact, the statement is proven to be accurate by Figure 3.11a, where l_c is shown to be linearly related to the $d - y_0$ parameter, with the best fit regression shown as the dashed line. The 95% confidence prediction interval is so tight, it is not shown as to not obscure the main prediction line. A similar check was carried out for f_{cm} parameter (Fig. 3.11b), where the influence of compressive concrete strength on the central zone is visible, thought scattered. With higher strength, the length of the l_c gets shorter. The observation contrasts the findings from the tensile RC element analysis, where charting the concrete compressive strength f_{cm} against spacing s_{rm} of experimental RC ties did not provide any visible correlation between the variables, the scattered was spread out uniformly. It could be partially attributed to the inherently different behaviour of the RC beams, which experience both tension and compression that are distincted by the neutral axis. However, the presently analysed central zone length l_c derived from the 14 specimens of Calderón Bello (2008) only encompasses a segment of the aggregate crack spacing, and as will be shown in the next subsection, the relation is not clear due to the scatter being uniformly spread out over the entire range of f_{cm} values.

In future research, the database of specimens should be extended to encompass more variety in, namely, the bar diameter, reinforcement ratio, section height and material properties. As the relation between the l_c and the compressive concrete strength remains in question, further studies could potentially pave the way for a multivariate relationship of l_c, $d - y_0$ and f_{cm}.

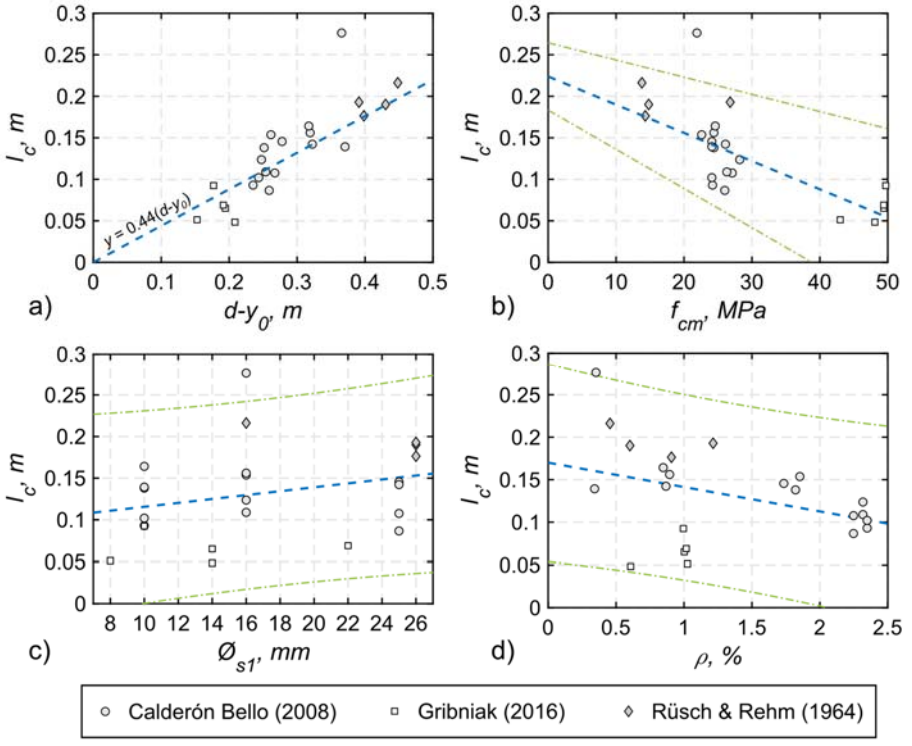

Fig. 3.11. Central zone relationship with key physical parameters: a) size-dependent $d - y_0$ parameter; b) compressive concrete strength f_{cm}; c) tensile reinforcement diameter $Ø_{s1}$; d) tensile reinforcement ratio ρ

From the comparative analysis of regressed curves, the strongest correlation was obtained for the formula governing the l_c parameter dependence on the $d - y_0$ parameter, with coefficient of determination $R^2 = 0.9874$ as opposed to the relationship against compressive strength f_{cm}, with $R^2 = 0.7516$. Therefore, the constitutive model presented in Equation (3.23) is proposed:

$$l_c = 0.44(d - y_0). \tag{3.23}$$

Gilbert and Nejadi (2004) expressed that the height of the crack h_0 controls the distance between primary cracks and has argued the spacing to fall between

$h_0 < s_{rm} < 2h_0$. The notion is partly substantiated by the derived Equation (3.23), that also strongly resembles the crack spacing model developed by Reineck (1991):

$$s_{rm} = 0.7(d - y_0). \tag{3.24}$$

An additional model as derived from both relations of $d - y_0$ and concrete strength f_{cm}. The fit model is shown in Figure 3.12a with the residuals of that fit given in Figure 3.12b. The derived model is presented in Equation 3.25. The obtained regression is relatively satisfactory at $R^2 = 0.8$ with a root mean squared error (RMSE) of 0.02565 in terms of meters. However, the residuals chart reveals a number of data points that had significant deviations. Recalling the observation from Chapter 2, where concrete strength f_{cm} had no discernable impact on the mean crack spacing, caution should be exercised with the derived relationship. With that in mind and the superior behaviour of the model proposed in Equation (3.23) over the model in (3.25), the former is adopted for the remainder of the present research. Future research should investigate this relation more extensively, with a greater number of samples to derive the central zone from.

$$l_c = 0.24(d - y_0)^{(f_{cm}/55)}. \tag{3.25}$$

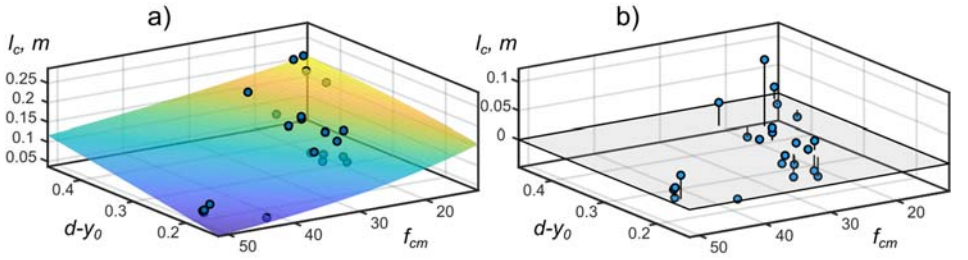

Fig. 3.12. Central zone length relationship with parameters: a) $d - y_0$ and concrete compressive strength f_{cm}; b) residuals of the fit

Contemplating the existence of the central zone, Murray et al. (2016) discussed localized damage of the concrete surrounding the bar due to secondary cracks originating from the influence of the shrinkage effect existing prior to loading. The effect is expected to increase toward the middle of the block defined by two cracks. Gribniak et al. 2016 asserted the effect to be greater in elements subjected to flexure, as beams normally contain higher ratios of reinforcement in the tensile zone than tensile reinforced concrete members.

3.3.2. Central Zone Length Definition Without Debonding

Data in Table 3.1 reveals the limited influence of the parameter ld on the total crack spacing, therefore this section investigates an alternative case for when the parameter l_d of the debonding zone is neglected, taking 0 as its value. The overall procedure remains the same and will not be discussed again, only the key outcomes are presented in Table 3.3 for when the debonding zone is not considered. Comparing the data between the previous subsection and the current, the differences are marginal and consist of an increase in the central zone as expected due to the lack of the debonding zone strains lowering the general mean strain value.

Table 3.3. The calculated central zone, debonding and effective zone lengths

Source	Id	$s_{rm,exp}$	l_c	l_{eff}	ε_{si}	ε_{sm}	ε_{s0}
		mm	mm	mm	$\times 10^{-3}$	$\times 10^{-3}$	$\times 10^{-3}$
Calderón Bello (2008)	1	176	171.4	2.3	1.5	1.493	1.493
	2	173	167.0	1.5	1.5	1.493	1.493
	3	151	148.2	1.4	1.5	1.489	1.489
	4	196	171.5	12.2	1.5	1.462	1.460
	5	187	173.5	6.8	1.5	1.469	1.468
	6	185	174.8	5.1	1.5	1.462	1.461
	7	382	297.2	42.4	1.5	1.341	1.321
	8	217	153.7	31.6	1.5	1.297	1.262
	9	116	112.6	1.7	1.5	1.495	1.494
	10	143	140.1	1.5	1.5	1.492	1.492
	11	105	103.2	0.9	1.5	1.493	1.493
	12	137	133.4	1.8	1.5	1.494	1.494
	13	128	125.3	1.4	1.5	1.493	1.493
	14	114	112.2	0.9	1.5	1.493	1.493
Gribniak et al. (2016)	S1-2	100	82.7	8.6	1.5	1.423	1.416
	S1-4	133	100.6	16.2	1.5	1.407	1.394
	S2-3	133	76.8	28.1	1.512	1.300	1.243
	S1-1	124	104.5	9.7	1.5	1.377	1.366
	S1-6	91	63.4	13.8	1.5	1.321	1.289
Rüsch & Rehm (1964)	R58	257	233.9	11.5	1.5	1.473	1.472
	R66	243	219.9	11.8	1.5	1.481	1.480
	R68	213	203.8	4.6	1.5	1.493	1.493
	R72	231	220.3	5.3	1.5	1.483	1.483

Regression of the central zone parameter l_c against $d - y_0$, provides a slightly modified model, with $R^2 > 0.98$ as before (Figure 3.13).

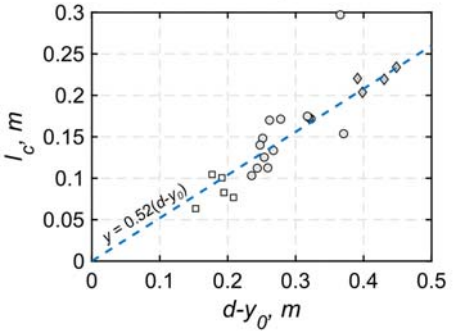

Fig. 3.13. Central zone relationship with size dependent $d - y_0$ parameter without considering the debonding effect

The central zone length model without accounting for the debonding effect is expressed as:

$$l_c = 0.52(d - y_0). \tag{3.26}$$

Additionally, a model was derived for comparison with Equation 3.25, as to what influence the debonding zone has on the model. The removal of the l_d term and relating the $d - y_0$ and f_{cm} parameters have improved the performance of the fit, producing Equation (3.27) with $R^2 = 0.95$ and RMSE = 0.011 m. While the fit is significantly better, for consistency in the present study, Equation 3.26 is adopted for cases when debonding is not considered.

$$l_c = 0.27(d - y_0)^{(f_{cm}/60)}. \tag{3.27}$$

3.3.3. Strain Compliance Application Flowchart for Crack Spacing of Flexural Elements

A dedicated flowchart summarising the application of the strain compliance principles on flexural RC members for mean crack spacing estimation is presented in Figure 3.14. It highlights the sequence of operations in a generalized way for alternative mean strain approach integration. Annex D contains the *Matlab* script for the development of the constitutive l_c model and the analysis of crack spacing of reinforced concrete members subjected to bending. The algorithm is written to follow the procedure shown in the flowchart.

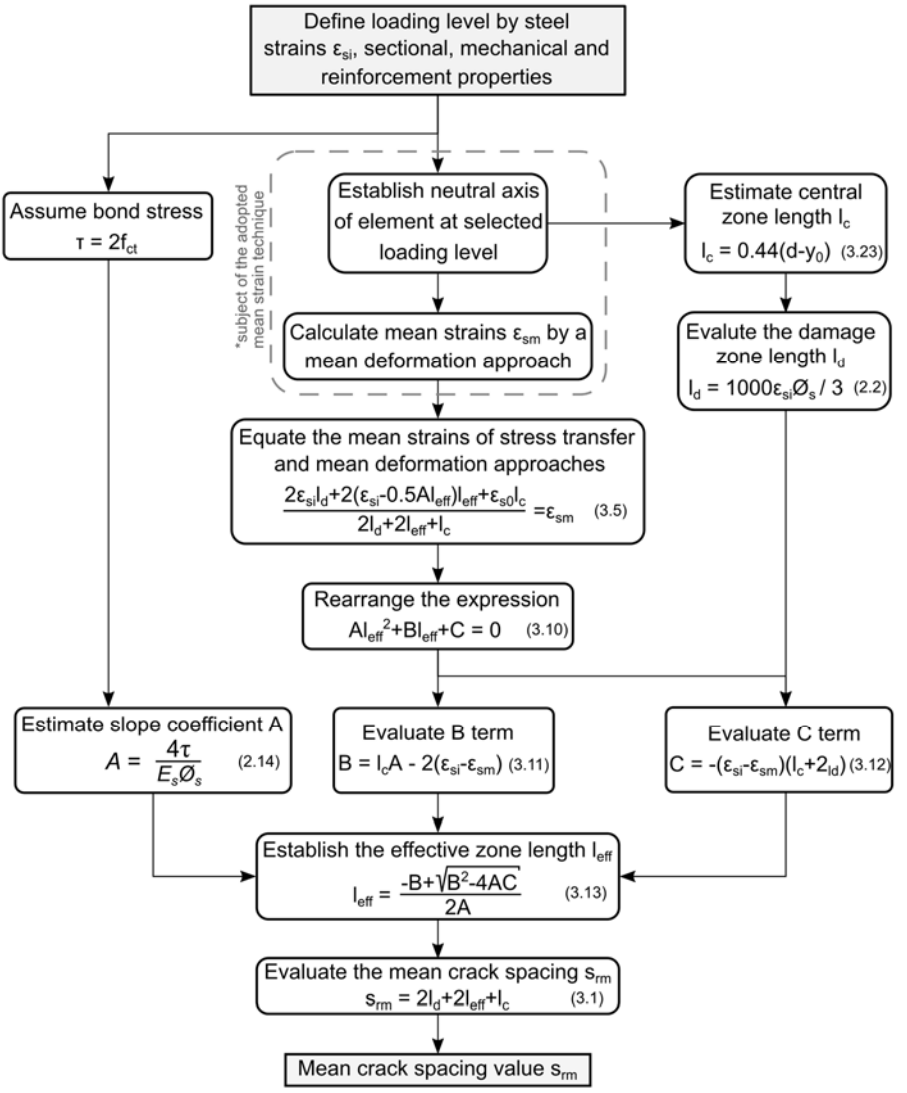

Fig. 3.14. Flowchart for the implementation of the strain compliance conceptfor mean crack spacing prediction of flexural reinforced concrete elements assuming linear strains

3.4. Validation and Evaluation of Adequacy of the Strain Compliance Approach for Flexural Elements

The developed approach with the derived central zone length l_c constitutive model has been implemented on a separate the experimental data set, that does not include the previously employed results for the derivation of the l_c relationship, i.e. it excludes entries listed in Table 3.1. A distinct larger collection of experimental results of beams and slabs was employed for the evaluation of the adequacy in terms of accuracy, investigation of the general observed the behaviour and most importantly – the validation of the strain compliance approach as a robust and flexible alternative to existing crack spacing estimating techniques. Rectangular RC beams and slabs tested by Beeby (1971), Frosch et al. (2003), Gilbert & Nejadi (2004), Plizzari et al (1996), Hognestad (1962), Liao & Fang (2011), Rafi et al. (2007), Rüsch & Rehm (1964), Vanderwalle (2000), Wu M.H.Q (2010), Yang et al. (2018) and Zhao et al. (2008) are provided in Table 3.4. Some results were omitted from these authors as they lacked key reported variables, had too complex cracking patterns to differentiate between secondary or primary cracks or had alternative section geometries. Data, that was excessively redundant was omitted as well, this applies to the results by Beeby (1971), as all the beams were of identical geometrical properties and identical reinforcement. Small variation was present in compressive concrete strength fcm, hence only 4 specimens were employed in the present study to cover the range and represent the mean crack spacing of all specimens. Table 3.4 only provides key characteristics necessary for the present analysis, the entirety of the data is given in Annex C.

Generally, a straightforward comparison cannot be carried out with the current Eurocode 2 versions, as the formulations for mean crack spacing s_{rm} have been replaced with maximum crack spacing s_{rmax} prediction which can be directly employed in crack width analysis. Furthermore, it is important to note that the present study focuses on primary crack spacing, whereas design codes are not explicitly defined whether they are intended for the primary crack spacing or the spacing of both primary and secondary cracks, inclusively. Therefore, an older version of EC2 (CEN 1992) was chosen for comparison, as it was explicitly related to the mean value through the following expression:

$$s_{rm} = 50 + 0.25 k_1 k_2 \frac{\emptyset_s}{\rho_{eff}}, \tag{3.27}$$

where k_1 and k_2 are coefficients for bond and loading conditions, respectively, ρeff is the reinforcement ratio of the effective area in tension, which depends on the effective height when determining the sectional area and is estimated by:

$$h_{eff} = min\begin{cases}2.5(h-d)\\(h-y_0)/3.\\0.5h\end{cases} \tag{3.28}$$

Model Code 2010 features multiple ways of determining the crack spacing. Though in general, it relies on the bond stress value and the bond concept between reinforcement and concrete. The crack spacing will be estimated from the maximum transfer length as defined by:

$$l_{s,max} = kc + \frac{1}{4}\frac{f_{ctm}}{\tau_{bm}}\frac{\emptyset_s}{\rho_{eff}}, \tag{3.29}$$

where k is an empirical factor, normally taken as 1.0, c is the cover of concrete and τ_{bm} is the bond stress with the exact expression of it dependent on the cracking stage and load conditions as per table 7.6-2 of the Model Code 2010. For the present research, that demands the presence of the stabilized cracking stage for the strain compliance concept to be valid, yields the expression $\tau_{bm} = 1.8f_{ctm}$.

Model Code 2010 states that maximum spacing $s_{r,max} = 2l_{s,max}$ and that the average s_{rm} value is less or equal to 2/3 of the maximum. The same deduction is argued by Barre et al. (2016), with a further declaration of 1.7 as the factor used for relating Eurocode 2 maximum and mean spacing values.

Table 3.4. Geometrical and material characteristics of reinforced concrete tests employed for the strain compliance method validation

Source	Id	h	b	d	c	$No.\times\emptyset_1$	$No.\times\emptyset_2$	E_{s1}	f_{cm}	s_{rm}
		mm	mm	mm	mm	×mm	×mm	GPa	MPa	mm
Beeby (1971)	M1P2	391	178	346	35	2×19	2×10	200	25.1	132
	M3D2								22.7	129
	M6P2								27.1	144
	N4								22.3	101
Frosch et al. (2003)	B-6	203	914	157	38	6×16	–	200	47.0	175
	B-9					4×16			44.0	229
	B-12					3×16			44.0	249
	B-18					2×16			47.0	310
	E12-6					6×16			47.0	170
	E12-9					4×16			46.0	226
	E12-12					3×16			46.0	257
	E12-18					2×16			47.0	338
	E12-12					4×16			46.0	203
	E12-18					4×16			46.0	188

Table 3.4 continued

Source	Id	h	b	d	c	$No.\times Ø_1$	$No.\times Ø_2$	E_{s1}	f_{cm}	s_{rm}
		mm	mm	mm	mm	×mm	×mm	GPa	MPa	mm
Gilbert & Nejadi (2004)	B1-a	348	250	300	40	2×16	–	200	3606	192
	B1-b	348	250	300	40	2×16			3700	186
	B2-a	333	250	300	25	2×16			3605	164
	B2-b	333	250	300	25	2×16			3605	187
	S2a	161	400	130	25	3×12			3808	125
	S2b	161	400	130	25	3×12			38.8	131
A	B1	400	350	160	40	4×20	–	200	47.2	120
Hognestad (1962)	B1	406	203	358	35	2×25	–	200	25.2	140
	B7			345	55	8×13			17.9	157
	B15			345	55	8×13			39.0	114
	B19			345	55	8×13			27.6	160
	B32			284	111	2×22			20.1	234
B	RCB1	400	376	200	24	3×12	2×6	200	24.2	171
	RCB2	400	376	200	24	2×12	2×6	200	22.9	150
C	BRS1	200	175	120	20	2×10	2×8	201	47	96
	BRS2	200	175	120	20	2×10	2×8	201	45	100
Rüsch & Rehm (1964)	R1	625	300	587	30	4×16	–	200	43.0	244
	R33			584	33	4×16	–		13.6	225
	R29			582	35	4×16	–		17.5	222
	R34			590	27	4×16	–		19.4	261
	R35			587	30	4×16	–		20.8	271
	R54			578	34	2×26	–		13.1	253
	R61			583	29	2×26	–		13.3	210
	R70			587	25	2×26	–		14.2	217
	R67			585	28	2×26	–		14.8	239
	R65			587	26	2×26	–		17.3	269
	R8			579	30	2×32	–		31.4	253
	R9			579	30	2×32	–		32.1	304
	R69			586	26	3×26	–		13.5	211
	R5			587	30	4×16	–		19.7	234
	R4			587	30	4×16	–		31.6	236
	R14			587	30	4×16	–		13.8	251
	R25			582	35	4×16	2×10		14.4	192

End of the Table 3.4

Source	Id	h	b	d	c	$No.\times Ø_1$	$No.\times Ø_2$	E_{s1}	f_{cm}	s_{rm}
		mm	mm	mm	mm	×mm	×mm	GPa	MPa	mm
	R26			582	35	4×16	–		14.3	202
	R49			584	33	4×16	2×10		13.1	249
	R50			580	37	4×16	2×10		35.1	271
	R17[1]			552	30	8×16	–		23.0	176
	R18[1]			569	28	7×12.3	–		22.6	212
	R19	625	300	553	33	10×10	–	200	20.2	186
	R21[1]			554	35	5×21.3	–		20.0	180
	R102[1]	1200	450	1141	30	8×20	–	200	22.3	500
	R103			1157	30	5×26	–		19.2	503
D	B1	350	305	200	35	2×20	2×10	200	34.1	135
Wu M.H.Q (2010)	SSTN4	140	800	114	20	4×12	–	200	30	128
	SSTS4			114	20	4×12			30	133
	BSTN2	400	200	342	50	2×16	–	200	26	172
	BSTS2			342	50	2×16			40	181
	BSTS3			342	50	3×16			40	184
E	H120R2	250	202	200	40	3×16	2×16	200	98.9	100
Zhao et al. (2008)	DP-11	410	358	170	40	2×25	–	194	36.6	200
	DP-21	390	340	170	40	2×20		188	31.6	171
	DP-32	450	403	170	40	2×14		192	31.8	240
	DP-41	450	404	170	40	2×12		186	31.6	300
	BC20-2	445	418	135	20	2×14		192	36.6	240
	BC30-1	455	418	135	30	2×14		192	36.6	240
	BC40-1	465	416	170	40	2×18		190	31.8	240
	BC50-1	475	415	185	50	2×20		188	31.8	171
	BC60-2	485	414	200	60	2×22		201	37.9	200
	BC70-2	500	418	220	70	2×25		194	36.6	200

1 – element with multiple tension bar diameters, standardised as a uniform diameter
a – results from the proposed approach with considered debonding effect
b – results from the proposed approach without the debonding effect
A – Plizzari et al (1996)
B – Liao & Fang (2011)
C – Rafi et al. (2007)
D – Vanderwalle (2000)
E – Yang et al. (2018)

3.4.1. Validation of Predicted Mean Crack Spacing Results

The crack spacing values were estimated by the procedure described in Section 3.2 with the central zone models developed for both cases of considered and neglected debonding effect, Equations (3.23) and (3.26), respectively. The general statistical evaluation of the performance of the proposed approach and its comparison against the estimations by major design codes and the size-dependent crack spacing equation proposed by Reineck (1991) is presented in Figure 3.15. Separate cases of design codes with the exclusion of the cover of concrete term *kc* are presented as well, to align with the comparisons carried out in Chapter 2 of this research. The estimated primary crack spacing values were normalized by the experimental ones $s_{rm,calc}$ / $s_{rm,exp}$. Therefore, a general overview of the adequacy of accuracy and consistency of scatter levels canbe deducted.

The top and bottom of the rectangular box represent the 25% and 75% quartiles, with the horizontal line inside the rectangle referring to the median spacing value. The top and bottom most handles represent the range of normally distributed data with +/– 2.7σ or 99.3% coverage with any values outside the extents considered outliers and shown with a cross symbol. The connected circles represent the mean values of 1.04, 1.02, 0.91, 0.65, 0.62, 0.74, 0.35 and 1.02 of all analysed specimens by the strain compliance approach with debonding accounted for, strain compliance approach without considering local debonding, Model Code 2010 predictions by Equation (3.29), Model Code 2010 without the *kc* term, Eurocode 2 predictions by Equation (3.27), Eurocode 2 predictions by Equation (1.22), Eurocode 2 predictions by Equation (1.22) with the *kc* term excluded and Reineck (1991) model as given by Equation (3.24), respectively.

From Figure 3.14, it can be inferred that the suggested methods are significantly more consistent than the design code results with less scattered values and greater overall accuracy. While the accuracy of the Reineck (1991) model in terms of the general average performance is higher than the design codes, it significantly falls behind in terms of consistency, with minimum prediction accuracy approaching just 20% and in cases reaching over 160% of the experimental values.

Another observation relates to the general tendency to overestimate the mean crack spacing, whereas design codes lean strongly towards underestimating the primary crack spacing in flexural members. This observation aligns with the research of Barre et al. (2016). Although the minimal number of outliers further solidifies the robustness and versatility of the proposed technique, it is important to note that other methods did not yield any outliers. An increase in the number of experimental specimens should bring more clarity whether outliers will persist.

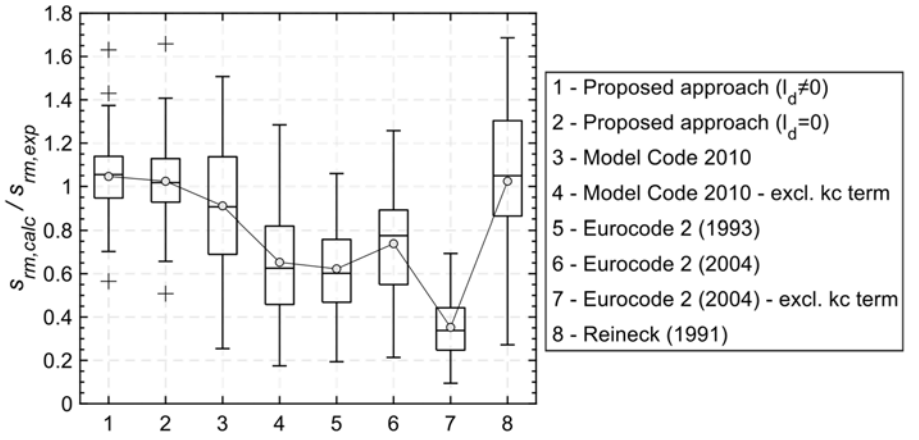

Fig. 3.15. Comparison of key statistics of normalized crack spacing srm results of the proposed approach, design codes and Reineck (1991) model

Unravelling the normalized performance values for each specimen, a more thorough analysis can be made in terms of tendencies. Figure 3.16 compares the spread of prediction accuracies of specimens when the calculated spacing values are plotted against experimental ones. Results above the solid black line indicate overestimations, while results below the solid line indicate underestimations. Design codes are compared in full, with the *kc* term included where applicable.

For the proposed technique (Fig. 3.16a), the specimens are mostly uniformly distributed and follow the path well, with few values displaying higher than expected under- or overestimations. The same is true for the case when the debonding effect was not included (Fig. 3.16b). In contrast, both design codes exhibit (Fig. 3.16c and d) tendencies to decrease in performance when experimental crack spacing values are increasing, significantly underestimating the actual crack spacing value. In other words, the spread appears to increase for larger spacing values. However, without separating the data and relating to distinct physical variables it is early to say with certainty.

The last analysed model (Fig. 3.16e) does not display clear tendencies, notwithstanding the clustered behaviour which is expected due to the simplicity and limited nature of the Equation (3.24), which accounts only for the distance between the centre of the tension bars and the neutral axis, excluding all other physical parameters. Comparing Fig. 3.16e chart with the Fig. 3.16a and Fig. 3.16b charts it is clear that including other physical parameters is necessary from the better controlled scatter of results.

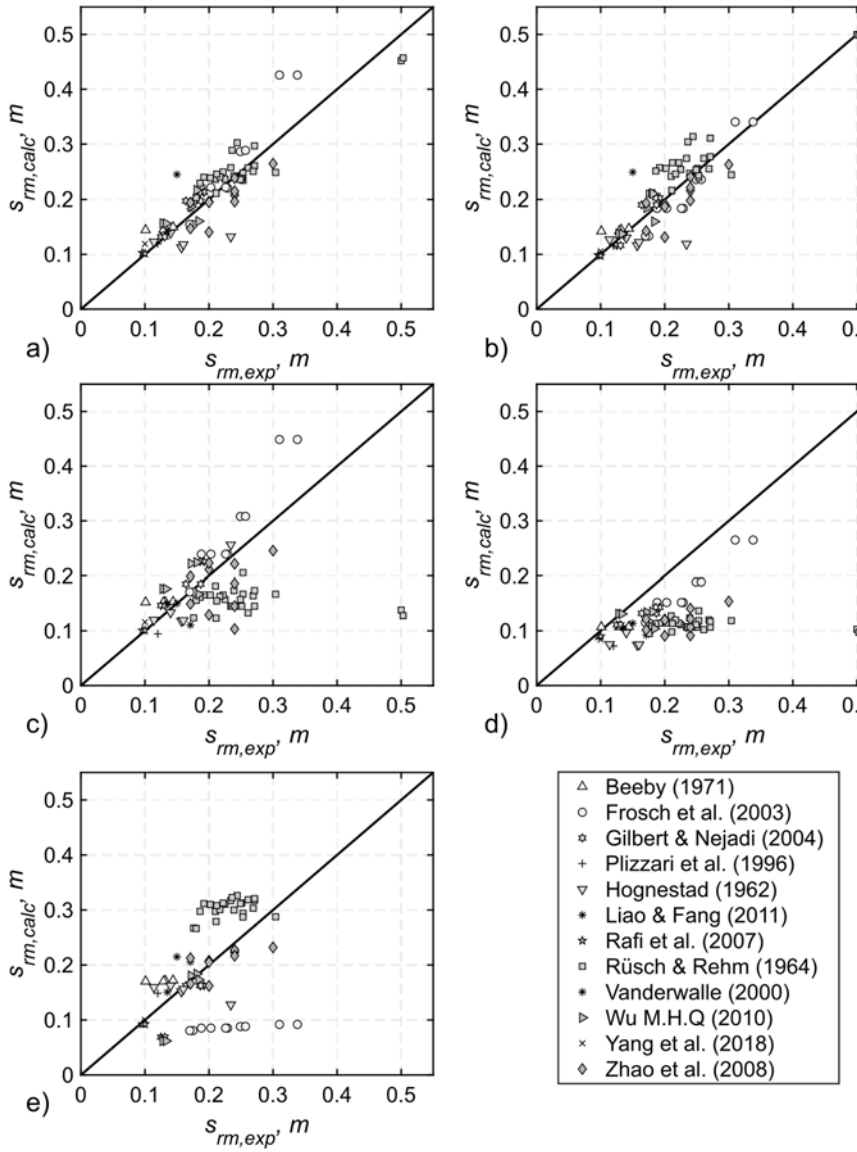

Fig. 3.16. Predicted primary crack spacing against experimental values: a) strain compliance approach with debonding effects; b) strain compliance approach excluding debonding; c) Model Code 2010; d) Eurocode 2 (1992); e) Reineck (1991)

3.4.2. Analysis of Individual Parameter Impact on Predicted Crack Spacing Values

For more insight on the behaviour of the proposed crack spacing estimation method, the normalized crack spacings are presented against the $d - y_0$ parameter, ratio of reinforcement ρ, concrete compressive strength f_{cm}, tensile bar diameter $\emptyset_{s1}$ and concrete cover c (Figs. 3.17a–e). Simplified linear trend lines (represented as dashed lines) are overlaid for easier identificatio0n of any tendencies in data. Relating $s_{rm,calc}$ / $s_{rm,exp}$ to the $d - y_0$ size dependent parameter (Fig. 3.17a) reveals that scatter of normalized results is rather significant, however most data is clustered together, with a tendency to approach the horizontal line, representing 100% accuracy of predictions, as it gets closer to 0.8–0.9 $d - y_0$ range. The trend line shows that for $d - y_0$ values exceeding approximately 0.9, spacing values would become underestimated, however, this observation is extrapolated. Only a few data points exist for higher values of $d - y_0$, particularly above 0.5.

Investigating the accuracy of predictions against the ratio of reinforcement (Fig. 3.17b) reveals that the accuracy of the approach appears to increase up to a reinforcement ratio value of ρ = 1%, afterwards, the trendline intersects the solid line indicating the ideal accuracy and begins to underestimate results. It would appear that for very large reinforcement ratios the accuracy would be highly inadequate, however, this deduction is not conclusive due to the minimal number of variables at larger reinforcement ratio values and the potentially skewed trend line. In contrast to the narrow range of parameter values for $d - y_0$ and ρ, a wide spectrum of f_{cm} values was represented from the collected experimental results, covering the range from approximately 13 MPa to 48 MPa. The generally high levels of data scatter reveal that the accuracy of the predictions is not sensitive to the aforementioned parameter (Fig. 3.17c). While more variety is needed for bar diameter sensitivity comparison (Fig. 3.17d), the trend appears to hold true, as data approaches the horizontal line with increasing bar diameters. Another questionable trend for accuracy is the concrete cover c parameter (Fig. 3.17e). The single value representing a very large cover of ~11cm distorts the trendline, furthermore, very large concrete cover sizes of over 75mm are not commonly encountered in actual structural elements.

Ideally, the proposed approach should not exhibit any clear tendencies to increase or decrease in terms of accuracy but maintain uniform accuracy throughout the range. That would indicate a well-performing technique that can be easily generalised for other variable combinations. Presently, such behaviour is observed only for the $d - y_0$ parameter and compressive strength f_{cm}. More data woulds ware needed for other parameters, particularly larger values.

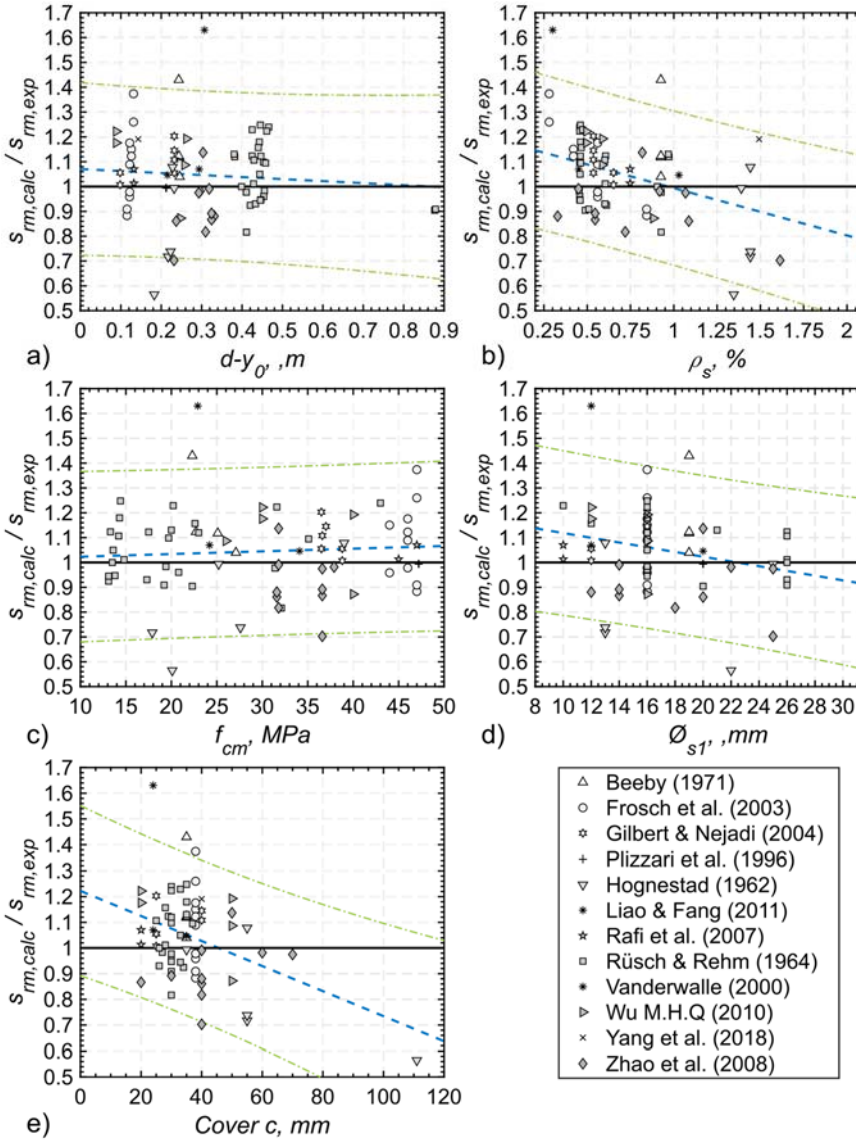

Fig. 3.17. Mean crack spacing values of the proposed approach normalized by experimental values against parameters: a) $d - y_0$ parameter; b) ratio of reinforcement ρ; c) concrete compressive strength f_{cm}; d) tensile bar diameter $Ø_{s1}$; e) concrete cover c

Analysing the absolute crack spacing values of the experimental and predicted values against the $d - y_0$ parameter (Fig. 3.18), a few observations can be made. The results of Frosch et al. (2003) are the ones that deviate most from

experimental results. These specimens represent slabs, that were of ~20 cm height and ~91 cm width, whereas the majority of the remaining specimens are beams. The growth of crack spacing with increasing $d - y_0$ values is as expected since the constitutive central zone length model is dependent on the $d - y_0$ parameter and the central zone was shown to make up the largest fraction of the aggregate crack spacing (Table 3.3 and Figure 3.8).

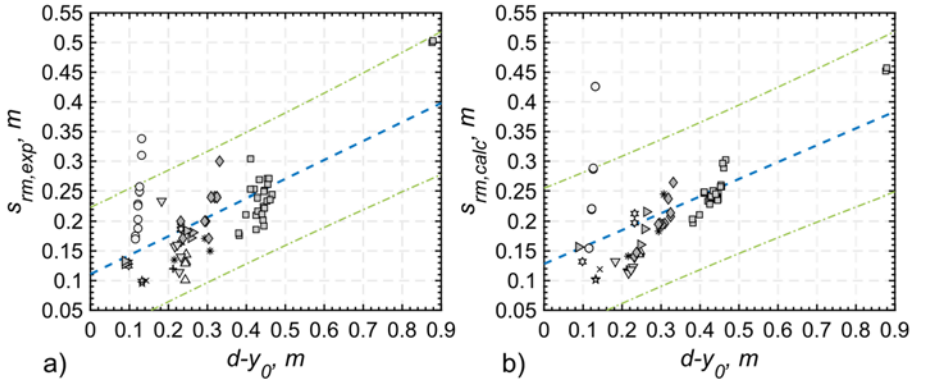

Fig. 3.18. Experimental and predicted spacing comparison against $d - y_0$ parameter: a) experimental mean crack spacing values; b) predicted mean crack spacing values

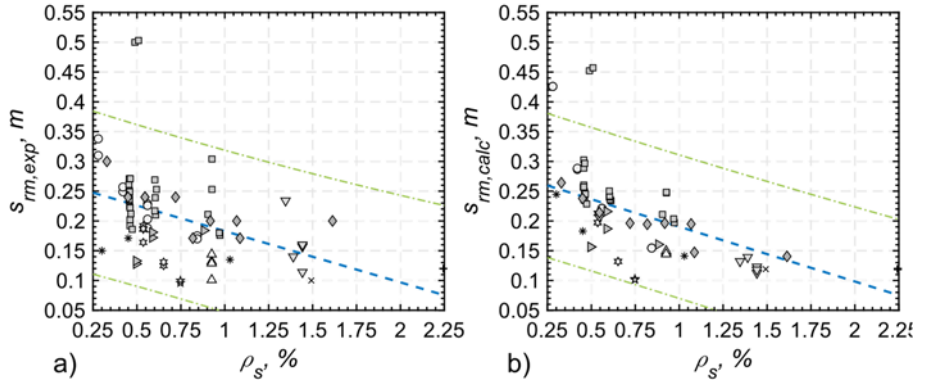

Fig. 3.19. Experimental and predicted spacing comparison against ratio of reinforcement ρ: a) experimental mean crack spacing values; b) predicted mean crack spacing values

Comparing the crack spacing of experimental results and predictions against reinforcement percentage ρ (Fig. 3.19) displays the tendency to remain intact, with shorter distanced between cracks as the ratio increases. Furthermore, the data can be seen to become more clustered together with less scatter than before. This is

particularly clear for data reported by Beeby (1971), that are all of 0.93% reinforcement ratio.

Figure 3.20 presents the experimental and estimated spacing values by the compressive concrete strength f_{cm}. The characteristic is very similar, with the expected outcome of more clustered results for elements of similar variables. The same observations apply to Figure 3.21, where the spacings are compared by the tensile reinforcement bar diameter.

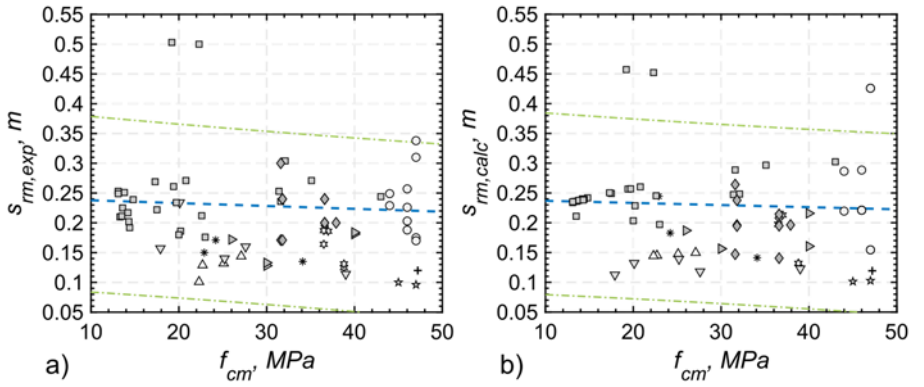

Fig. 3.20. Experimental and predicted spacing comparison against concrete compressive strength f_{cm}: a) experimental mean crack spacing values; b) predicted mean crack spacing values

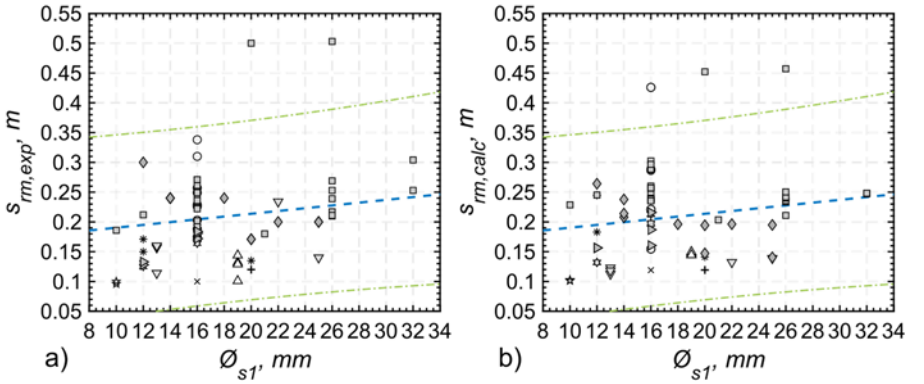

Fig. 3.21. Experimental and predicted spacing comparison against tensile bar diameter $Ø_{s1}$: a) experimental mean crack spacing values; b) predicted mean crack spacing values

Lastly, correlating the data against the cover of concrete c (Figure 3.22) does reveal the reduced scatter of predicted values over experimental ones. The

provided trendline does display a decrease in the predicted outcome with greater cover values, although the data remains too scattered and limited in range (mostly between 20 and 40 mm) to conclude this with certainty.

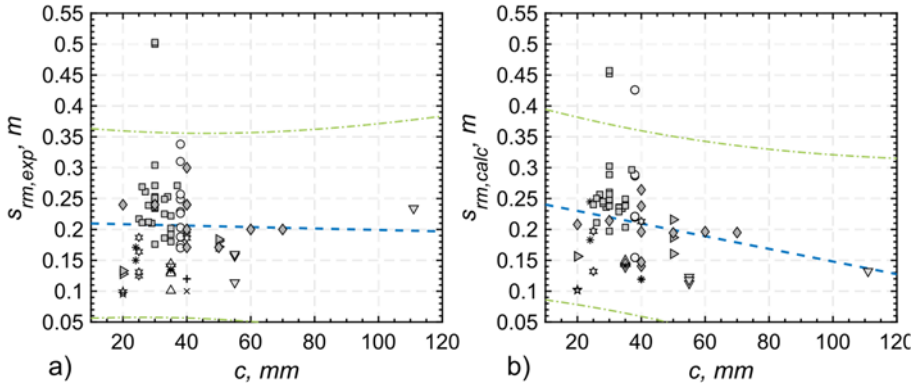

Fig. 3.22. Experimental and predicted spacing comparison against cover of concrete *c*: a) experimental mean crack spacing values; b) predicted mean crack spacing values

3.4.3. Predicted Crack Spacing Values of Individual Samples

Selected results are presented in Table 3.5, that provide detailed insight on each individual specimen performance for the proposed strain compliance approach (both including and excluding debonding), the Model Code 2010 predictions and Reineck (1991) model results. Full results for all approaches including the missing Eurocode 2 values can be found in Annex C. The Results of Table 3.5 should be analysed together with Table 3.4.

Table 3.5. Mean crack spacing analysis results, absolute and normalized values

Experimental			Strain compliance approach				MC 2010		Reineck (1991)	
Source	Id	$s_{rm,exp}$	$s_{rm,calc}$	$\frac{s_{rm,calc}}{s_{rm,exp}}$	$s_{rm,calc}$	$\frac{s_{rm,calc}}{s_{rm,exp}}$	$s_{rm,calc}$	$\frac{s_{rm,calc}}{s_{rm,exp}}$	$s_{rm,calc}$	$\frac{s_{rm,calc}}{s_{rm,exp}}$
		mm	mm[a]	$l_d \neq 0$[a]	mm[b]	$l_d = 0$[b]	mm		mm	
Beeby (1971)	M1P2	132	147.6	0.89	145.1	0.91	152.8	0.64	194.5	1.11
	M3D2	129	144.9	0.89	142.6	0.90	152.3	0.54	183.1	1.06
	M6P2	144	149.7	0.96	147.0	0.98	153.1	0.51	176.0	1.17
	N4	101	144.4	0.70	142.2	0.71	152.3	0.94	225.7	1.15

Table 3.5 continued

Experimental			Strain compliance approach				MC 2010		Reineck (1991)	
Source	Id	$s_{rm,exp}$	$s_{rm,calc}$	$\frac{s_{rm,calc}}{s_{rm,exp}}$	$s_{rm,calc}$	$\frac{s_{rm,calc}}{s_{rm,exp}}$	$s_{rm,calc}$	$\frac{s_{rm,calc}}{s_{rm,exp}}$	$s_{rm,calc}$	$\frac{s_{rm,calc}}{s_{rm,exp}}$
		mm	mm[a]	$l_d \neq 0$[a]	mm[b]	$l_d = 0$[b]	mm		mm	
Frosch et al. (2003)	B-6	175	154.5	1.13	133.3	1.31	171.0	0.76	223.4	1.19
	B-9	229	219.5	1.04	183.8	1.25	238.9	0.58	222.0	1.20
	B-12	249	286.5	0.87	235.4	1.06	308.0	0.64	255.9	0.67
	B-18	310	425.9	0.73	340.4	0.91	448.8	0.76	259.4	1.20
	E12-6	170	154.5	1.10	133.3	1.28	171.0	0.83	181.2	1.56
	E12-9	226	221.0	1.02	184.0	1.23	239.2	0.61	173.3	1.21
	E12-12	257	288.5	0.89	235.5	1.09	308.3	0.63	164.6	1.57
	E12-18	338	425.9	0.79	340.4	0.99	448.8	0.71	187.0	1.37
	E12-12	203	221.0	0.92	184.0	1.10	239.2	0.69	177.6	1.39
	E12-18	188	221.0	0.85	184.0	1.02	239.2	0.58	170.4	1.49
Gilbert & Nejadi (2004)	B1-a	192	212.7	0.90	202.9	0.95	225.4	0.91	136.0	1.36
	B1-b	186	213.0	0.87	203.0	0.92	225.5	1.06	134.0	1.01
	B2-a	164	197.3	0.83	190.3	0.86	185.4	1.04	145.9	1.10
	B2-b	187	197.3	0.95	190.3	0.98	185.4	0.71	123.8	1.00
	S2a	125	131.9	0.95	116.3	1.07	146.3	0.86	106.9	1.18
	S2b	131	131.9	0.99	116.3	1.13	146.3	0.53	313.7	1.22
A	B1	120	119.3	1.01	115.2	1.04	94.5	0.68	301.2	1.24
Hognestad (1962)	B1	140	139.1	1.01	130.3	1.07	133.5	0.61	278.8	1.31
	B7	157	112.6	1.39	116.4	1.35	118.1	0.49	273.7	1.18
	B15	114	122.9	0.93	127.0	0.90	119.9	1.16	171.3	1.30
	B19	160	118.1	1.35	122.1	1.31	119.1	1.18	170.5	1.32
	B32	234	132.2	1.77	118.9	1.97	256.2	1.06	171.9	1.19
B	RCB1	171	182.9	0.93	190.7	0.90	110.7	1.51	170.3	1.69
	RCB2	150	244.6	0.61	248.7	0.60	150.0	0.98	80.7	0.46
C	BRS1	96	102.7	0.93	98.7	0.97	100.9	1.04	85.2	0.37
	BRS2	100	101.3	0.99	97.4	1.03	100.8	1.24	88.1	0.35
Rüsch & Rehm (1964)	R1	244	302.4	0.81	313.7	0.78	145.0	1.45	91.9	0.30
	R33	225	236.2	0.95	253.7	0.89	157.3	1.01	80.7	0.47
	R29	222	249.2	0.89	266.0	0.83	165.5	1.06	85.3	0.38
	R34	261	256.6	1.02	273.9	0.95	132.7	1.20	88.2	0.34
	R35	271	260.2	1.04	277.0	0.98	145.0	1.33	91.9	0.27
	R54	253	233.9	1.08	238.7	1.06	205.4	1.18	85.3	0.42

Table 3.5 continued

Experimental			Strain compliance approach				MC 2010		Reineck (1991)	
Source	Id	$s_{rm,exp}$	$s_{rm,calc}$	$\frac{s_{rm,calc}}{s_{rm,exp}}$	$s_{rm,calc}$	$\frac{s_{rm,calc}}{s_{rm,exp}}$	$s_{rm,calc}$	$\frac{s_{rm,calc}}{s_{rm,exp}}$	$s_{rm,calc}$	$\frac{s_{rm,calc}}{s_{rm,exp}}$
		mm	mm[a]	$l_d \neq 0$[a]	mm[b]	$l_d = 0$[b]	mm		mm	
Rüsch & Rehm (1964)	R61	210	235.9	0.89	241.1	0.87	181.7	1.27	85.3	0.45
	R70	217	240.1	0.90	245.4	0.88	162.8	1.17	162.5	0.85
	R67	239	241.7	0.99	246.7	0.97	173.6	1.21	162.6	0.87
	R65	269	250.3	1.07	254.9	1.06	164.1	1.13	162.5	0.99
	R8	253	247.3	1.02	243.0	1.04	167.0	0.99	162.5	0.87
	R9	304	248.2	1.22	243.9	1.25	167.0	1.17	68.8	0.55
	R69	211	210.9	1.00	215.6	0.98	123.2	1.12	68.8	0.53
	R5	234	257.0	0.91	273.9	0.85	145.0	0.79	148.5	1.24
	R4	236	288.7	0.82	304.1	0.78	145.0	0.95	162.3	1.16
	R14	251	237.7	1.06	255.4	0.98	145.0	0.75	151.7	0.97
	R25	192	239.6	0.80	257.0	0.75	165.5	1.05	159.5	1.40
	R26	202	238.3	0.85	255.5	0.79	165.5	0.74	156.1	0.98
	R49	249	235.3	1.06	253.1	0.98	157.3	1.09	127.8	0.55
	R50	271	296.7	0.91	310.7	0.87	173.7	0.65	205.7	1.20
	R17[1]	176	197.1	0.89	210.5	0.84	123.7	1.00	214.8	1.43
	R18[1]	212	245.3	0.86	265.9	0.80	154.7	1.05	92.7	0.97
	R19	186	228.6	0.81	250.8	0.74	161.3	1.01	92.5	0.93
	R21[1]	180	203.5	0.88	211.2	0.85	155.7	0.59	326.2	1.34
	R102[1]	500	452.2	1.11	499.8	1.00	137.9	0.70	310.5	1.38
	R103	503	457.2	1.10	498.5	1.01	127.9	0.75	312.5	1.41
D	B1	135	141.2	0.96	134.0	1.01	149.0	0.51	318.6	1.22
Wu M.H.Q (2010)	SSTN4	128	156.4	0.82	137.4	0.93	176.7	0.54	317.6	1.17
	SSTS4	133	156.4	0.85	137.4	0.97	176.7	0.81	294.2	1.16
	BSTN2	172	186.9	0.92	184.7	0.93	221.9	0.87	297.3	1.42
	BSTS2	181	215.9	0.84	210.1	0.86	224.1	0.75	300.6	1.39
	BSTS3	184	160.5	1.15	159.8	1.15	166.7	0.73	300.0	1.26
E	H120R2	100	119.1	0.84	105.6	0.95	115.9	0.61	303.3	1.13

End of Table 3.5

Source	Id	Experimental	Strain compliance approach				MC 2010		Reineck (1991)	
		$s_{rm,exp}$	$s_{rm,calc}$	$\frac{s_{rm,calc}}{s_{rm,exp}}$	$s_{rm,calc}$	$\frac{s_{rm,calc}}{s_{rm,exp}}$	$s_{rm,calc}$	$\frac{s_{rm,calc}}{s_{rm,exp}}$	$s_{rm,calc}$	$\frac{s_{rm,calc}}{s_{rm,exp}}$
		mm	mm[a]	$l_d \neq 0$[a]	mm[b]	$l_d = 0$[b]	mm		mm	
Zhao et al. (2008)	DP-11	200	140.5	1.42	131.4	1.52	129.1	0.66	287.3	1.14
	DP-21	171	147.2	1.16	142.6	1.20	149.3	0.55	287.6	0.95
	DP-32	240	237.8	1.01	240.3	1.00	221.5	0.58	279.0	1.32
	DP-41	300	264.1	1.14	262.5	1.14	245.6	0.62	317.0	1.35
	BC20-2	240	208.0	1.15	215.2	1.12	103.4	0.61	322.6	1.37
	BC30-1	240	214.1	1.12	220.7	1.09	145.1	0.58	312.5	1.25
	BC40-1	240	196.2	1.22	198.1	1.21	186.4	0.86	311.6	1.62
	BC50-1	171	194.4	0.88	193.5	0.88	198.8	0.82	310.0	1.53
	BC60-2	200	196.3	1.02	192.0	1.04	211.3	0.63	311.7	1.25
	BC70-2	200	195.0	1.03	187.0	1.07	223.0	0.64	320.7	1.18

1 – element with multiple tension bar diameters, standardised as a uniform diameter
a – results from the proposed approach with considered debonding effect
b – results from the proposed approach without the debonding effect
A – Plizzari et al (1996)
B – Liao & Fang (2011)
C – Rafi et al. (2007)
D – Vanderwalle (2000)
E – Yang et al. (2018)

3.4.4. General Discussion of the Results

Besides the aspects related to developing a more accurate and consistent approach to crack spacing predictions, the general work carried out in the present research also touches on the topic of classical bond theory. Particularly by addressing the ongoing scientific debate on the validity of the classical bond theory as a means to reliable analysis of cracking (Perez et al. 2013), which significantly relies on the $Ø_s/\rho_{eff}$ ratio for the estimation of the distance between cracks. While the present study relies on the classical bond theory concepts to a limited extent, it did not provide a clear resolution to the issue mentioned above. When lightly reinforced elements (with small ρ values) are in question, the classical bond theory can provide accurate outcomes for short element depths, however, with the increase in any of the aforementioned variables, the accuracy of crack spacing tends to decrease. In the scope of the current research, it seems that the most significant parameters affecting the average spacing between cracks are geometrical in nature

and consist of the height of the section, ratio of reinforcement, diameter of the reinforcing bar and cover.

Although the diameter of the tension reinforcing bar does not display any significant influence on the spacing value, with the observed trend to be inconclusive due to the limited number of data points, the parameter appears to have more profound effect on the the distance between cracks when ratio of reinforcement is low compared to high ratios, where the diameter has little to no influence on the spacing.

The impact of reinforcement ratio was observed to be quite significant, as smaller reinforcement percentage results in clearly decreased spacing between neighbouring cracks. The finding agrees very well with the classical bond theory.

The general adequacy of the model is controlled by the strain shape function and the overall strain profile. Constitutive parameters l_c, l_d and τ have played a vital role in defining the outcome of the strain compliance approach, notwithstanding, caution should be exercised when employing the mean strain-based technique for Equation (3.5), as it will affect the adequacy of the approach and the formulations of the mentioned parameters. In order to express the constitutive parameters with more confidence, alternative shape functions and mean strain estimation equations should be analysed in the future. At present state, the suggested concepts provide very adequate performance in terms of accuracy and greatly reduced scatter in the results, however without further study on the aforementioned variables it cannot be determined if these characteristics hold up.

Nevertheless, the strain compliance principle features strong theoretical soundness, as opposed to existing techniques that contain numerous empirical aspects within them. This is true for even many theoretically postulated approaches, the classical bond theory, the methods presented in Eurocode 2 and Model Code 2010 rely on empirical factors or concepts like the effective area of concrete in tension. The area is controlled by empirical conditions from multiple limiting settings. The strain compliance concept developed in the present research does not involve the effective area. The inclusion of empirical notions is limited to just the length characteristics of the defined zones, such as the debonding zone and central zone, for which a relation to the $d - y_0$ parameter was introduced, and the effective zone, that is governed by the bond stress. The debonding zone l_d is a subject of debate, as removing it yields a simpler model, which in the end becomes slightly more accurate. The phenomena behind the central zone demand further clarification and testing, potentially with distributed sensing techniques (Kenel et al. 2005, Davis et al. 2017) in the future. At present the cause of the central zone is assumed to be lack of bond behaviour in the middle part of an RC block due to excessive secondary cracking, however, this statement is not conclusive. It does serve as part of the framework for this research, partly due to simplicity and partly due to the average deformation behaviour in this area. As numerous secondary

cracks form and increase in density, the reinforcement strain profile maximum and minimum values within this region remain very close to each other, giving substantiation for the horizontal representation of the strains as an average. The extent of this zone is a crucial question to be investigated further in future studies. The adopted model l_c=0.44($d - y_0$) should also be improved further because the correlation with concrete compressive strength f_{cm} was shown to be quite significant yet developing an inclusive model of all three parameters necessitates more experimental data than was included in the present investigation.

Besides the complexity behind the concepts of the strain profile governing zones, the approach is very practical in terms of ease of application. Furthermore, with the accuracy of predicted mean crack spacing shown to be significantly closer to the actual value, design conditions for maximum crack spacing could potentially be developed from increased specimen numbers and application of statistical analysis. The most attention and time is required for the estimation of the mean strains of reinforcement ε_{sm}, though it depends on the adopted technique. For increased versatility, any means can be implemented, including numerical methods for predicting the ε_{sm} value. The application of the suggested concept is not limited to a single geometry or structure type, as was shown in Chapter 2, the strain compliance concept serves as a novel framework upon which many external assumptions and conditions can be built to modify and extend the method.

3.5. Applicability for Crack Width Analysis

Although the aim of this research is focused on the investigation and advancement of crack spacing predictions, contemplating the implications of the proposed crack spacing approach on crack width predictions, even if for exploratory purposes, can lay down a path for future extensions of the concepts proposed herein. First, the assumptions No. 2 must be recalled, which states that the secondary cracks, by nature not extending as high as the neutral axis defining primary cracks, are neglected from this approach. A significant fraction of the total crack width comes from the sum of these omitted secondary cracks. Referring to the classical crack width Equation (1.16), we can see that the width is obtained from the difference between reinforcement and concrete strains between neighbouring primary cracks. Thus, this expression represents the total from one primary crack and all secondary cracks that are present in between. The resulting mean crack width will be greater than the experimental value by the aggregate width of the secondary cracks. With these aspects considered, the following expression for the average crack width can be given:

$$w_m = s_{rm}(\varepsilon_{sm} - \varepsilon_{cm}) - \sum w_{\text{sec}}, \tag{3.30}$$

where ε_{cm} is the mean concrete strain and $\sum w_{sec}$ is the aggregate width of secondary cracks. Stemming from the literature review in Chapter 1, the maximum crack width can be related to the average width through the introduction of factor $\overline{\beta}$:

$$w_{max} = \bar{\beta} w_m. \tag{3.31}$$

It is suggested, the factor $\overline{\beta}$ to be determined through experimental means. Calderón Bello (2008) reasoned the factor for large and small reinforcement ratio RC elements to be within the range of 1.1 and 1.35, respectively. More research could bring in additional certainty currently lacking in these ratios. Alternatively, the approach proposed herein could be extended to appreciate the crack width evaluation by relating the mean crack spacing value with the maximum crack spacing value in the same manner as in Equation (3.31).

The technique is detailed in Figure 3.23, where the behaviours of the strain profiles for the average and maximum crack spacing cases in relation to the different defining zones are presented. The outcome would hypothetically have the maximum spacing s_{rmax} be expressed by the multiplication of the mean spacing s_{rm} by the empirical factor β:

$$s_{rmax} = \beta s_{rm}. \tag{3.32}$$

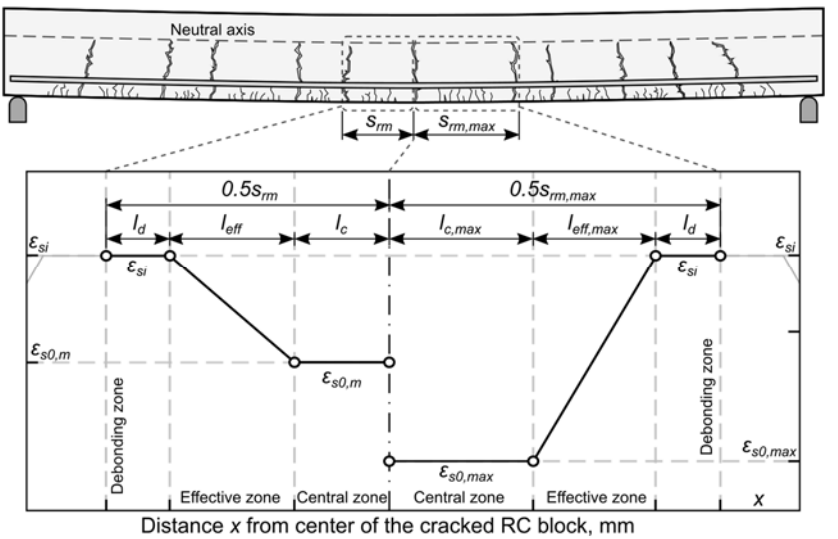

Fig. 3.23. The strain profiles of reinforcement for the mean (left) and maximum (right) crack spacing cases.

The long-term goal of the novel crack spacing modelling concepts presented in this research would be the harmonisation of tensile and flexural approaches and

direct application for predicting maximum crack widths, necessary for complete serviceability analysis of reinforced concrete structures.

As an example of the application of the above technique, selected Gilbert & Nejadi (2004) specimens with available crack width data were used for the calculations. The below equations are shown for B1a specimen. The sample results are given in Table 3.6, together with additional elements. The mean crack width, neglecting the secondary cracks, would, therefore, be equal to:

$$w_m = s_{rm}\varepsilon_{sm} = 212.7 \times 1.357 \times 10^{-3} = 0.289 \text{ mm}. \tag{3.33}$$

Taking the β factor equal to 1.3 as suggested by Calderón Bello (2008), the maximum crack spacing:

$$w_{max} = \bar{\beta} w_m = 1.3 \times 0.289 = 0.376 \text{ mm}. \tag{3.34}$$

The data can be compared to the real experimental values in Table 3.6 for the loading level, approximately representing $\varepsilon_{si} = 1.5{\times}10^{-3}$ steel strains at the location of the crack.

Table 3.6. Exploraroty crack width prediction comparison with experimental values

Source	Id.	$s_{rm,calc}$	$s_{rm,exp}$	$w_{m,calc}$	$w_{m,exp}$	$w_{max,calc}$	$w_{max,exp}$
Gilbert & Nejadi (2004)	B1-a	212.7	192	0.289	0.218	0.375	0.3
	B1-b	213.0	186	0.292	0.223	0.379	0.3
	B2-a	197.3	164	0.257	0.187	0.334	0.25
	B2-b	197.3	187	0.257	0.217	0.334	0.33

The author would like to note, that the value used for the β factor and the results are exploratory in nature and should not be taken as conclusive. Furthermore, the calculations presented above and in Table 3.6 are derived from primary crack spacing only, ignoring the secondary cracks and the concrete strain part, as mentioned above, the final crack width is conservative, i.e. on the safe side. Taking the aforementioned aspects into account could greatly reduce the crack width value, particularly for higher section RC elements or, in general, elements that have pronounced secondary cracking. The expansion of the approach for crack width analysis remains to be studied in the future, as the scope of the present research is aimed at the average primary crack spacing. As the β factor is empirical in nature, a recommendation would be to expand the herein proposed approach with mechanical soundness in terms of crack width analysis.

3.6. Conclusions of Chapter 3 and Recommendations for Future Research

Conclusions drawn from Chapter 3 can be summarized as follows:

1. Three distinctly characterised zones govern the strain behaviour between two neighbouring primary cracks. These are referred to as the debonding, effective and central zones, in sequence from the location of the crack towards the centre of the RC block. Debonding zone features no bond transfer between the bar and concrete, the effective zone facilitates the entire change in strains through constant bond. The central zone is represented as a flat strain line, the physical meaning relates to the averaged behaviour of strains originating secondary cracks. The aggregate length of these zones defines the average primary crack spacing.
2. The proposed concept has been shown to be theoretically robust and highly versatile. The strain compliance principle of equating the average strain value obtained by a discrete crack based approach to the value estimated by the mean strain focused approach takes advantage of both techniques and enables the estimation of crack spacing when strain compatibility is ensured.
3. A constitutive model has been proposed for the introduced central zone length l_c. It relates the length of the zone with the distance from the neutral axis to the axis of the tension reinforcement bars $d - y_0$.
4. Comparisons of the strain compliance approach with and without accounting for the local debonding effect near the cracks have revealed that it has minimal impact on the sum crack spacing. With a normalized prediction accuracy of 1.04 and 1.02 for when debonding was considered and omitted, respectively. Both cases produce significantly more consistent, less scattered results when compared to the Model Code 2010 and Eurocode 2. Furthermore, the proposed approach leans to the safe side, i.e. it slightly overestimates the crack spacing.
5. Predicted crack spacing values were observed to decrease with larger reinforcement ratios. This aspect agrees with the classical bond theory. The significance of reinforcement diameter $Ø_s$ on the crack spacing s_{rm} was found to be reduced for heavily reinforced elements with higher ratios of reinforcement ρ, whereas for lightly reinforced members the impact of bar diameter on the crack spacing increases. The influence of concrete cover c on the spacing is inconclusive. Concrete compressive strength f_{cm} was observed to have relatively little impact on the crack

spacing. The most significant parameters affecting the average spacing between cracks are geometrical in nature and consist of the height of the section, ratio of reinforcement, diameter of the reinforcing bar.

The current research has investigated the core concepts necessary for the substantiation of the strain compliance concept as a new framework for cracking analysis. However, many areas can be explored to increase the understanding of the approach, its potential and limitations. Key objectives for future research are:

1. Extension of the experimental database with more varied elements, particularly in terms of wider range of concrete compressive strength f_{cm}, reinforcement ratio ρ, bar diameter $Ø_{s1}$, effective section height d and cover of concrete c,
2. Further develop the approach to accommodate crack widths in a mechanically sound way, collect flexural elements with both crack spacing and crack width data for this purpose,
3. Establish the strain profile from experimental and numerical investigations with higher certainty, while maintaining simplicity and ease of application. The strain shape function can be theoretically of any expression, however, an overly complex one, could inhibit direct solution of the strain compliance equation without relying on numerical means, which is not desirable,
4. Investigation and analysis of other structural element types, different loading stages and alternative material options, such as FRP reinforcement, steel fibre reinforced concrete,
5. Improve the constitutive central zone model and adjust the model for alternative strain shape functions defining the introduced zones.

4

Artificial Neural Networks for Predicting Crack Spacing

Investigation of the cracking data collected from previous chapters has been employed for the development of an artificial neural network. The main intention of the neural network is to predict the mean distance between primary cracks. As observed in the previous chapter, the cracking data is highly scattered, hence crack spacing prediction is complicated, with many influencing parameters that have to be accounted for. Therefore, secondary aims were established related to the exploration of the interdependability of the various geometrical and material characteristics of the experimental specimens and impact on the final crack spacing prediction. A comparison of multiple trained neural networks is presented, with the intention of identifying the most reliable set of parameters both for future research of strain compatibility concept and better neural network models. The development of the neural network for a scarce data set has been analysed and partly substantiated. The accuracy of the neural network rivals the strain compliance approach as expected with good calibration. An observation was made regarding the prediction character of the neural network against the proposed method, whereby mean crack spacing predictions were identical or close to for several specimens. Material published in journal papers Kaklauskas et al. (2019a) and conference proceedings Kaklauskas & Ramanauskas (2016a) is included in this chapter.

4.1. Small Data Methodology

For a highly consistent and generalised neural network development, sufficient quality data is fundamental. With larger data sets, a more robust and accurate neural network can be trained. However, it is often the case, that data is limited and is costly to obtain. Such is the case for RC beam and slab test results. Each experiment is complex, demanding significant upfront costs in materials, expensive laboratory equipment, time and personnel. While larger scale experimental programmes have been carried out on RC structural elements, many are several decades old (Rüsch & Rehm 1964, Beeby 1971). Presently such large experimental programmes would be prohibitive in terms of costs. Moreover, concerning the existing data brings about the issues of non-uniformity, when alternative experimental studies focused on different aspects, leading to incompatible information, from missing material or geometrical properties to incomplete results. The present research has encountered this issue with some studies not providing enough information on the crack spacing nor in tabular or graphical formats.

The main focus of the present research has been the development of alternative crack spacing prediction techniques, culminating in the proposed strain compliance concept. The obtained results have been in good agreement with the experimental data and performed better than common design code methods. Nevertheless, the proposed approach suffers from scattered results, with 99.7% coverage of predictions within ~75% – 140% of the actual values. It is desirable for the spread to be as minimal as possible and with a guaranteed tendency to overestimate, i.e. produce safe approximations, for design purposes. Future studies could potentially significantly reduce the scatter of the strain compliance approach as the method is still in its early stages.

Alternative investigations of the cracking phenomena by numerical means, such as ANNs, can provide additional insight into the interrelations between the variables and general insight on the expected limits of accuracy and scatter. At present, available studies on ANN implementation for cracking phenomena are very scarce as discussed in Chapter 1. This can be attributed to the lack of large data sets as discussed above, however it has been recently shown that small and very small data sets can be employed to train a neural network with a very high degree of accuracy and generalization abilities, where the network avoids overfitting for individual values and is able to capture the overall behaviour of the underlying data. Some of the techniques revolve around the implementation of surrogate data sets (Timmer 1998), others encompass multiple runs to analyse the generalisation of the ANN. Ensemble methods (Dietterich 2000) rely on multiple independently trained neural networks that are combined in a sophisticated manner to generalise the predictions. The drawback of the ensemble method is

inconsistent and sometimes poor performance when the data set is very small, comprising of no more than a few dozen samples.

It is imperative that research on RC serviceability analysis is carried out in a well-rounded manner, therefore the present study aims to partially fill the gap in research on ANNs for RC crack spacing prediction. The techniques of multiple runs and surrogate data are combined to address the deficiencies in research such as Elshafey et al. (2013b), that had very limited data and carried out no subsequent assessment of the generalisation.

4.1.1. Multiple Run Approach

When a neural network is trained with little data, it is naturally susceptible to overfitting of the data. Such a neural network can predict the results with great accuracy on the original trained set of data and be validated, yet with the addition of new data, it can perform very poorly. Normally, in a well calibrated neural network, it is expected that the coefficient of correlation R will be higher for the training data than for the validation set. Small data neural networks can exhibit the opposite effect, which immediately signals problems of the developed ANN. This will be accounted for by removing the worst performing neural networks and assessing only the ones that are statistically significant.

The performance of a neural network is evaluated with statistical analysis. Provided the analysis shows that the network is performing consistently, the best performing neural network from the multiple runs is selected, based on its performance and regression coefficient. The number of runs of each neural network can range from 30 to a few thousand. Which is a subjective number, dependent on the number of inputs, samples, network configuration and processing power available. As a certain percentage is expected to fail, a higher number is preferable. The approach has been shown to yield reasonable accurate and reliable neural networks (Timmer 1998, Shaikhina & Khovanova 2017). The prerequisites for the implementation of this method are random initial weights and biases, the random split of the inputs between training, validation and test data. The present study has adopted 500–2000 runs for each ANN, for the network configuration and calibrated network development stages, respectively.

4.1.2. Surrogate Data

The use of surrogate data, replacing the original data set is another alternative to develop a neural network from a limited sample size. The purpose of surrogate data is to replicate the original in a statistically meaningful way, leading to maintained distributions and scatter characteristics but without the intricate relationship of the original values. Comparison of an ANN designed with original and surrogate data sets reveals if there actually are unique characteristics and

relationships within the selected data, or whether the data is not sufficient to design a well performing neural network. For a very large data set of concrete cube tests, it was shown (Shaikhina & Khovanova 2017) that surrogate data based ANN exhibited an order of magnitude worse behaviour in terms of regression coefficients, which were distributed very close to 0. Whereas the actual data provided R values above 0.9. When small data sets were concerned, the distribution of regression coefficients began to overlap. For very bad data, it is expected the overlap to be significant and minimally discernible between each other. The present study adopted a combined implementation of both multiple runs and surrogate data methods. The surrogate data was generated with the help of Kolmogorov-Smirnov test and employed in the present research, the data is presented in Annex E.

4.2. Selection of Best Neural Network Configuration

4.2.1. Investigated Parameters

Developing an optimal or close to the optimal neural network is not a trivial task. Different ANN configurations can yield better or worse performance, increased generalisation abilities or significantly overfit the data and lack the ability to perform well on new data. The present study does not cover the entirety of possibilities, however, focuses on exploring the configuration space for different training functions and a number of hidden layers and neurons within them. As these attributes can have the largest impact on a neural network (Hagan et al 1996).

In order to select the best performing training function, a multiple run approach was employed as described in Subsection 4.1.1. A *Matlab* script was written to automate the generation of 500 ANNs for each case of the training function, hidden layer and neuron count combination. With 4 investigated training functions, 35 combinations of a number of neurons and layers (ranging from 1 to 2 at most), the outcome was 70000 analysed ANN configurations or 17500 per training function. For the training functions, the following algorithms were tested: Levenberg-Marquardt, scaled conjugate gradient, BFGS quasi-Newton and Bayesian regularization backpropagation. The performance function was fixed for all as the mean square error (MSE) function. The summarised results of this investigation are presented in Subsection 4.2.1.

Selecting the number of layers and neurons is not straightforward. There is no single way to analytically determine the optimal configuration of layers and neurons per problem in a reliable way (Stathakis 2009). Many proposed equations for preliminary selection of the number of neurons are in the form of:

$$N_h = \frac{N_s}{(N_i + N_o)}, \tag{4.1}$$

where N_s is the number of samples in the training data set, N_i is the number of input neurons and *No* is the number of output neurons. The many derivations of this expression often involve certain scaling factors to reduce or increase neuron counts.

From the above equation, the resulting number of neurons in the hidden layer should be within the range of 9–10 for collected data (Table 3.1, 3.4, Annex C). That number usually serves as a starting guideline. There are numerous techniques to assist in selecting a competent number of neurons, as well as a multitude of rules-of-thumb, such as limiting the number to twice the number of input neurons or selecting half of the sum of input and output neuron count (Hagan et al 1996, Lawrence et al. 1998). Alternatively, other sources suggest focusing on an increased number of layers, although theoretically, a single hidden layer is sufficient to model any continuous function. A second layer would provide additional complexity, enable non-continuous function modelling. In the present study, a range of configurations is sampled for the development of the calibrated neural network. For this purpose, configurations ranging from 2 to 12 neurons per hidden layer to avoid severe overfitting. Furthermore, a scenario with a single hidden layer and two hidden layers is considered. The analysis is carried out after the best training function is established. Involving 2000 ANNs per configuration, of which there are 36, as shown in Subsection 4.2.2 and Figure 4.3. In the present case, 6 variables were chosen as the inputs for the neural network and the mean crack spacing as the outcome. The input variables include the reinforcement ratio ρ, reinforcement bar diameter $Ø_{s1}$, effective height d, concrete compressive strength f_{cm}, the position of the neutral axis y_0 and the concrete cover c, that mimic the key parameters governing the proposed strain compliance approach in Chapter 3. A comparison is carried out further in the chapter to assess the influence of combinations of these variables as input data for ANN training.

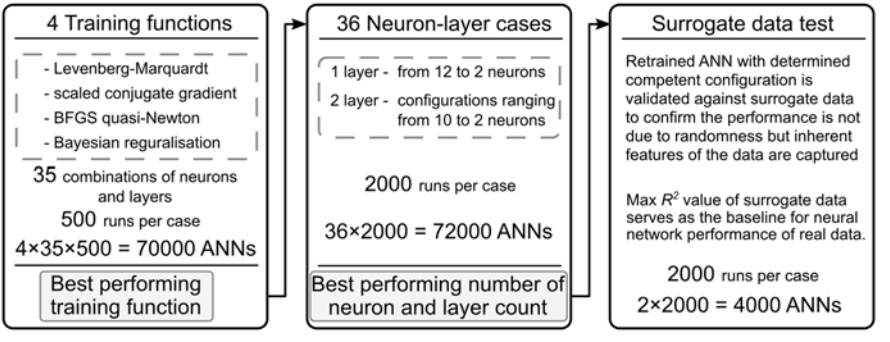

Fig. 4.1. Neural network calibration procedure

The best configuration is validated against the surrogate data set. The entire calibration process is shown in Figure 4.1.

Lastly, the 96 samples were divided into three groups of 70%, 15% and 15% for the training, validation and testing subsets, respectively. This resulted in 68 samples for training, 14 samples for validation and 14 samples for testing. In order to compare the neural networks produced by the multiple run approach, the testing data was randomly selected and fixed throughout the entire investigation, with only the training and validations subsets randomised at every run.

4.2.2. Effect of Training Functions

The 70 000 evaluated neural networks have been filtered to exclude cases where the coefficient of regression R is less than 0.6 and, subsequently, cases where $R_{train} < R_{val}$ were removed as well. The former check is to compare only statistically significant networks and the latter is to ensure appropriate behaviour of a well-tuned neural network, with the fit of predictions of training data being better than for the validation set. The summarised number of neural networks that satisfy the criteria along with the statistical representation is given in Figure 4.2.

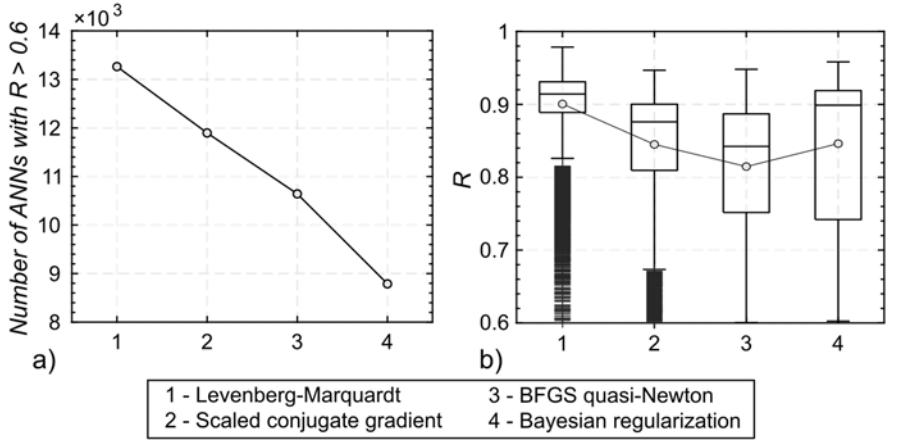

Fig. 4.2. Number of neural networks per selected training function: a) with coefficient R values exceeding 0.6 per investigated training function; b) statistics graph

Levenberg-Marquardt training algorithm has provided the largest number of valid neural networks. Further analysing in terms of statistics reveals the accuracy to be least scattered for the same algorithm. With 25 and 75% quartiles very close to each other. In terms of individual best performing networks, the aforementioned algorithms scored best. Therefore, the Levenberg-Marquardt training function has been employed for further stages.

4.2.3. Effect of Neuron and Layer Combinations

A total of 72 000 ANNs were trained, 2000 for each configuration. The evaluated neural networks have been filtered by the condition of considering only the ones that have the regression coefficient within statistically significant range $R > 0.6$. The remaining count of networks was further filtered by the condition $R_{train} > R_{val}$ to represent expected behaviour of training data being fit more accurately than validation data. The number of ANNs that satisfy both conditions is displayed in Figure 4.3. The connected line has been split to separate single hidden layer ANNs from two-layer ones. The first observation is that having two hidden layers actually reduces performance with fewer neural networks achieving statistical significance. A single hidden layer with 9 or 11 neurons has yielded the largest number of ANNs that satisfy the filtering criteria. Due to randomness in the initial weights and biases and the training/validation data split, a strict conclusion cannot be made, as highlighted by Figure 4.4.

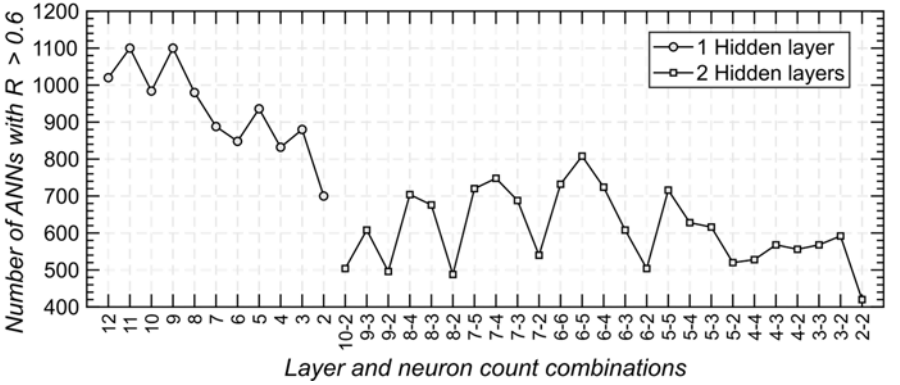

Fig. 4.3. Number of neural networks with coefficient R values exceeding 0.6 per investigated layer and neuron count configuration

Statistic distributions are presented for the single hidden layer combinations. The regression coefficients are shown to be relatively similar for neuron count of 12 to 8, with a slightly diminishing performance for a smaller number of neurons. Although the highest achieved regression coefficients for all data, including training, validation and testing are for the case of 9 neurons, the difference is marginal compared to other neuron numbers. Recalling the recommended number of neurons from Equation 4.1 was also around 9, therefore the final configuration of 9 neurons in a single hidden layer with the Levenberg-Marquardt training function will be adopted for the remainder of this study.

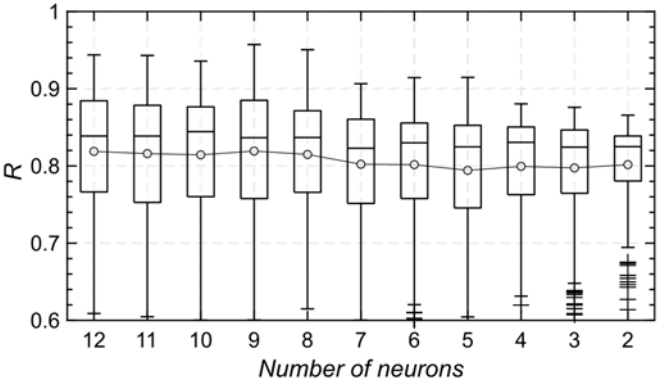

Fig. 4.4. Statistics of single hidden layer configuration per number of neurons

4.2.4. Comparison Against Surrogate Data

Due to the limited data set of experimental reinforced concrete beams and slabs, the impact of every sample can have an increased effect on the performance of the network. With only 96 specimens in the present study, the network has an increased risk of overfitting compared to a larger data set, regardless of calibration efforts, although that does mitigate it somewhat. After the neural network is tuned, an approach based on surrogate data comparison is chosen to validate the network's generalisation abilities and whether the performance is not due to randomness (Timmer 1998, Shaikhina & Khovanova 2017). The surrogate inputs are generated from the individual distribution profiles of the actual variables obtained from kernel density estimations. Hence, the substitute data is probable and maintains the statistic significance of real data. However, due to randomness, the intricate interrelations between the inputs should not be present in this data, as opposed to the real data. The collected data represents actual physical properties of reinforced concrete elements, with relationships between the chosen inputs well known or anticipated, the real data trained neural network performance is expected to significantly outperform the surrogate data. Figure 4.5 confirms the observation, the large gap between the data sets indicates the collected samples are minimally scattered and the chosen inputs have a large impact on the crack spacing predictions. A separate comparison of just the testing data sets, that did not participate in the development of the neural network (Fig 4.6) reveals a similar pattern, with the surrogate distribution slightly more spread out. In terms of the best performing individual network, the surrogate data yielded a network with $R = 0.31$ for cumulative training, validation and test samples. R of just the test samples was highest at 0.6389.

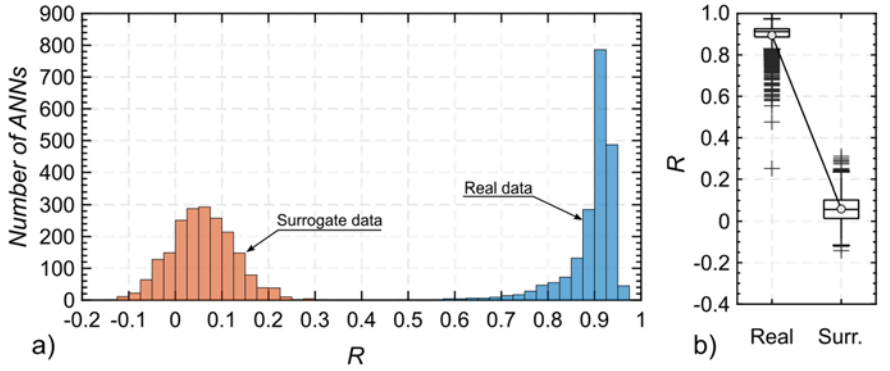

Fig. 4.5. Graphical prediction distribution representation of all data: a) the distribution of neural network regression coefficient *R* values for the full sets of real and surrogate data; b) statistics of data sets

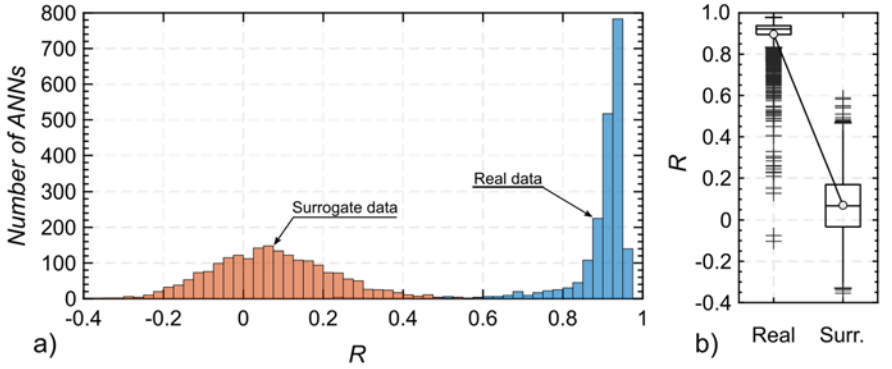

Fig. 4.6. Graphical prediction distribution representation of test data: a) the distribution of neural network regression coefficient *R* values for the test sets of real and surrogate data; b) statistics of data sets

4.3. Analysis of Crack Spacing Predictions

An analysis of the mean crack spacing s_{rm} predictions by the best performing individual neural network as presented in this section. The individual configuration is selected from the neural network (structure shown in Figure 4.7) configuration calibrated in the previous section. The network is an FFBP neural network, with a single hidden layer of 9 neurons. The transfer (also called the activation) function is the hyperbolic tangent. The input layer contains 6 variables, the output layer has a single neuron that linearly relates the incoming inputs to the outcome, the mean spacing s_{rm} value.

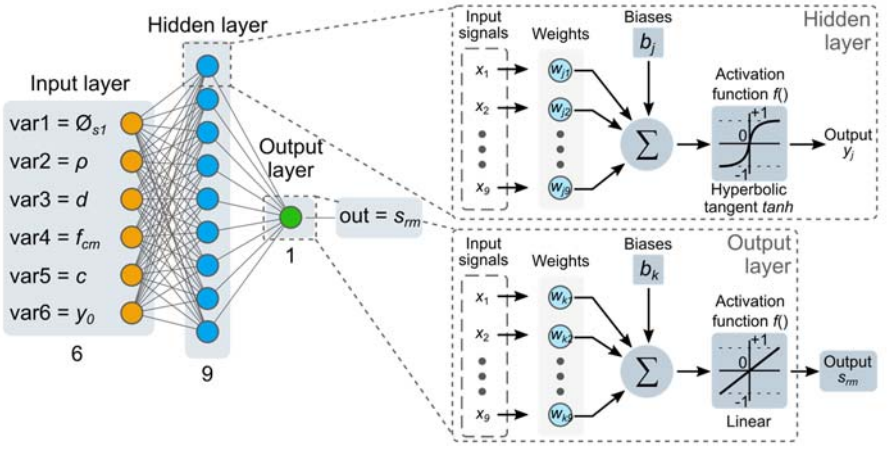

Fig. 4.7. Structure of the calibrated feed-forward backwards propagating neural network

The shown configuration has yielded an individual best performing FFNN with the coefficient of correlation R = 0.9738 for the full data set. The linear regressions of the full data set and the segmented training, validation and testing sample sets are displayed in Figure 4.8. The selected neural network exhibits proper behaviour in terms of $R_{training} > R_{validation} > R_{testing}$, with values of 0.9852 > 0.9581 > 0.9471, respectively. Generally, the training data is expected to be matched very well, as is the present case. Validation subset governs the convergence of the neural network training process. In the present study, the training process is stopped if the last 10 iterations failed to improve the performance for the validation subset. The testing sample group serves as an independent check, as these values did not participate in the development of the neural network. For a well generalised FFNN, the predictions should be consistently accurate for all cases and be able to predict the crack spacing of newly added samples.

The obtained very small discrepancies between the correlation coefficients of the training, validation and testing data is almost ideal. An observation should be made, that the testing data was chosen randomly and fixed for the entire neural network development process. While the performance is shown to be very high over the entire range, the amount of data to represent larger crack spacing value values s_{rm} >0.3 m is limited. Consequently, the degree of certainty is reduced for predictions in that region, exceeding 0.3 m values. The developed ANN should be tested with more data in the future, however, with sufficiently larger samples sizes, the network could be retrained as the performance is expected to increase. Particularly, with more robust and uniformly distributed variables covering the

gaps in the present study. Namely, more samples with larger concrete covers $c > 50$ mm, larger reinforcement ratios $\rho > 2.0\%$, taller sections $h > 500$ mm and samples with concrete mean compressive strength $f_{cm} > 50$ MPa.

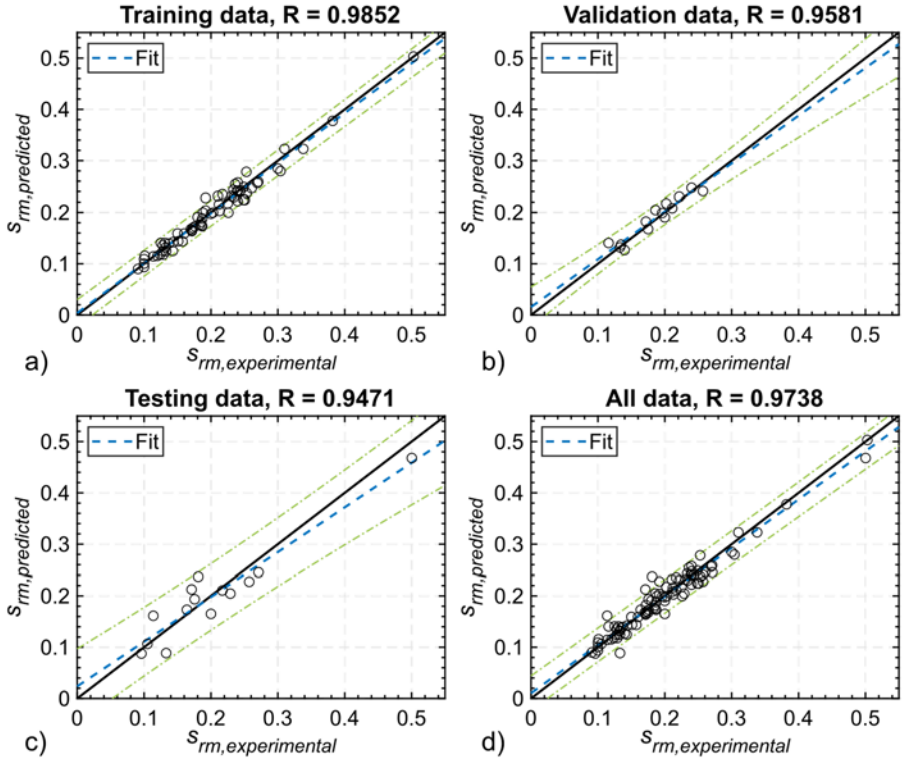

Fig. 4.8. Linear regression between the predicted crack spacing and the target crack spacing values of the best performing neural network configuration for input set No. 1 – [$Ø_{s1}$, ρ, d, f_{cm}, c, y_0]; a) of training data subset; b) validation data subset; c) testing data subset; d) all data set

4.3.1. Impact of Alternative Physical Input Variables

While the present study focuses on the 6 variable ($Ø_{s1}$, ρ, d, f_{cm}, c, y_0) inputs for the ANN, a comparison was carried out with alternative input data sets, with different sequences of variables. 12 sets were chosen for this comparison, with the ratio of reinforcement and bar diameter present in all cases. The procedure described in Section 4.2 for tuning the neural network was repeated. With 2000 runs per employed input variation, hence 24 000 ANNs were trained in total. The resulting comparison is presented in Figure 4.9.

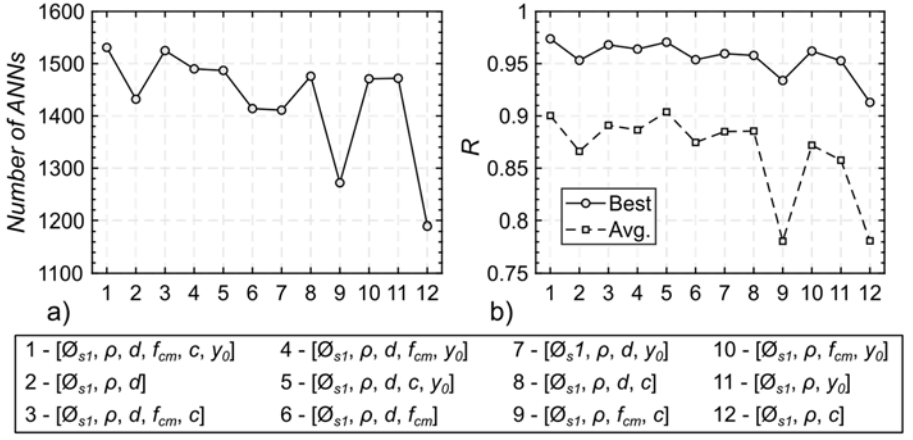

Fig. 4.9. Comparison of different combinations of input variables: a) number of neural networks with statistical significance $R \geq 0.6$ per input set; b) best and average R values

All the data was filtered in the same manner as previously calibrated ANNs, by counting only the statistically significant ($R > 0.6$) neural networks and removing cases where $R_{val} > R_{train}$. Although the number of well-performing ANNs is approximately similar for most cases, the input sets No. 9 and 12 have the least amount of them. The same observation can be extended to the most accurate individual neural networks from each group, where both No. 9 and No. 12 have lower maximum values of correlation coefficient R and more significantly, the average (of cases above $R > 0.6$) performance is significantly lower than the rest. A potential cause is a reliance on the cover of concrete and compressive strength in those sets. With compressive strength f_{cm} shown previously (Fig. 3.17) not to have a discernable impact on the crack spacing values, a similar observation was made for the cover of concrete (Fig. 3.19), although debatable due to the extreme scatter of results.

Following the present neural network study, it could be considered to substantiate the claims to a certain degree. Further comparing the R values between the best performing neural network configuration No. 1 and the other two configurations No. 4 and No. 5 where each of the variables (concrete cover c and compressive strength f_{cm}) were removed individually, reveals the influence of cover is greater than the compressive strength, $R_5 > R_4$. The discrepancies between No. 1 and No. 5 are marginal and can be attributed to randomness. It is important to note, that these observations are based on 2000 runs of each neural network, though deemed sufficient to cover for the effects of randomness in weight and bias initialisation, further investigation should be carried out with a significantly larger number of runs to discard any doubt. As for the relatively uniform high accuracy of all data sets, the limited amount of data will inherently yield higher

values of correlation *R* (Treves & Panzeri 1995). This can only be countered by extensively increased sample size, which is problematic for reinforced concrete beams and slabs, as the variation in experimental setups and the programme aims often results in incompatible results, that serve only the purpose of the initially designed study. On the other hand, the proposition of neural networks for modelling cracking of reinforced concrete elements can significantly improve the design of experimental programmes, when specific outcomes are desirable for validation purposes. Tests of large beams are costly both in terms of preparation and necessary equipment, the implementation of neural networks should alleviate these issues over time.

4.3.2. Crack Spacing Prediction Results and Comparison

In this subsection, the values predicted by the selected individual best performing ANN (with 6 variables) are compared against the proposed strain compliance approach, including the debonding effect, and design codes such as MC 2010 and EC2 (CEN 2004). The factual predicted spacing values and the normalised ones by the experimental ones are demonstrated in Figure 4.10. The horizontal axis represents the individual reinforced concrete elements as given in Tables 3.1, 3.4 and Annex C. Such a comparison was chosen, as it more easily highlights any existing patterns. The thick solid grey line depicts the experimental results. The proposed strain compliance method is shown by the thicker dash-dotted line. Design codes are represented by the thin dashed and dotted lines for the Eurocode 2 and Model Code 2010, respectively. The developed feed-forward ANN is given as the thick dashed line. It can be seen, that it follows the experimental values almost perfectly, with only a few cases, such as specimen No. 84, where the ANN shows as a spike, with greater spacing than actual, flatter shape. The same observation is true for the strain compliance approach, which on the overall is in very good agreement with the experimental results as well. Nevertheless, the performance of the neural network exceeds that of the proposed approach and the design codes, that display erratic behaviour and, on the whole, significantly underestimate the real crack spacing values, leading to unsafe predictions. Whereas the strain compliance approach leans on the safe side (Fig. 4.12b) and the neural network results are relatively evenly dispersed around the actual experimental values. The same observation can be made from Figure 4.8, therefore no clear tendency towards over- or underestimation is exhibited.

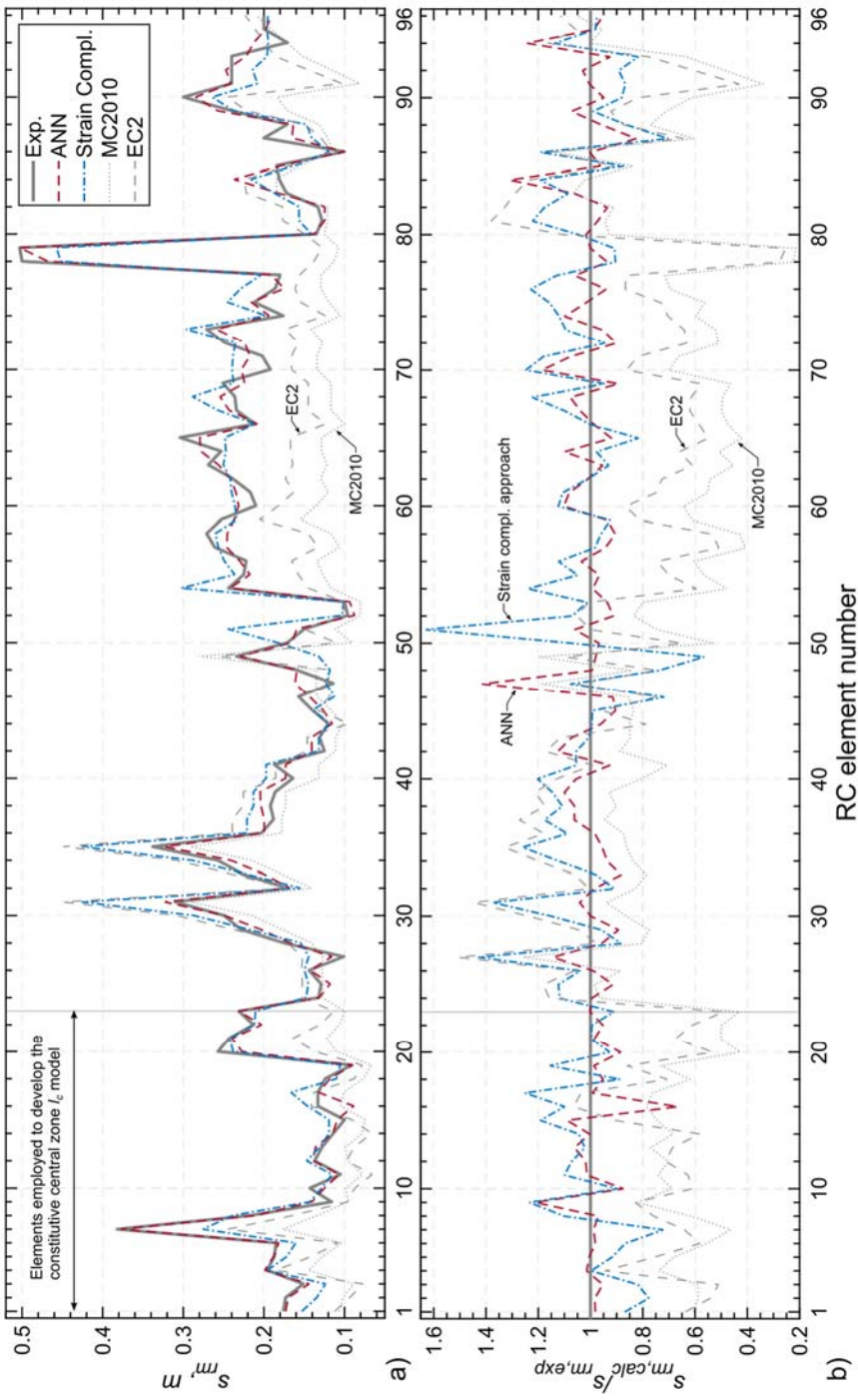

Fig. 4.10. Comparison of predicted mean crack spacing s_{rm} by the trained ANN, strain compliance approach, MC 2010 and EC2 (CEN 2004), per individual specimen: a) absolute spacing values; b) normalised by experimental spacing

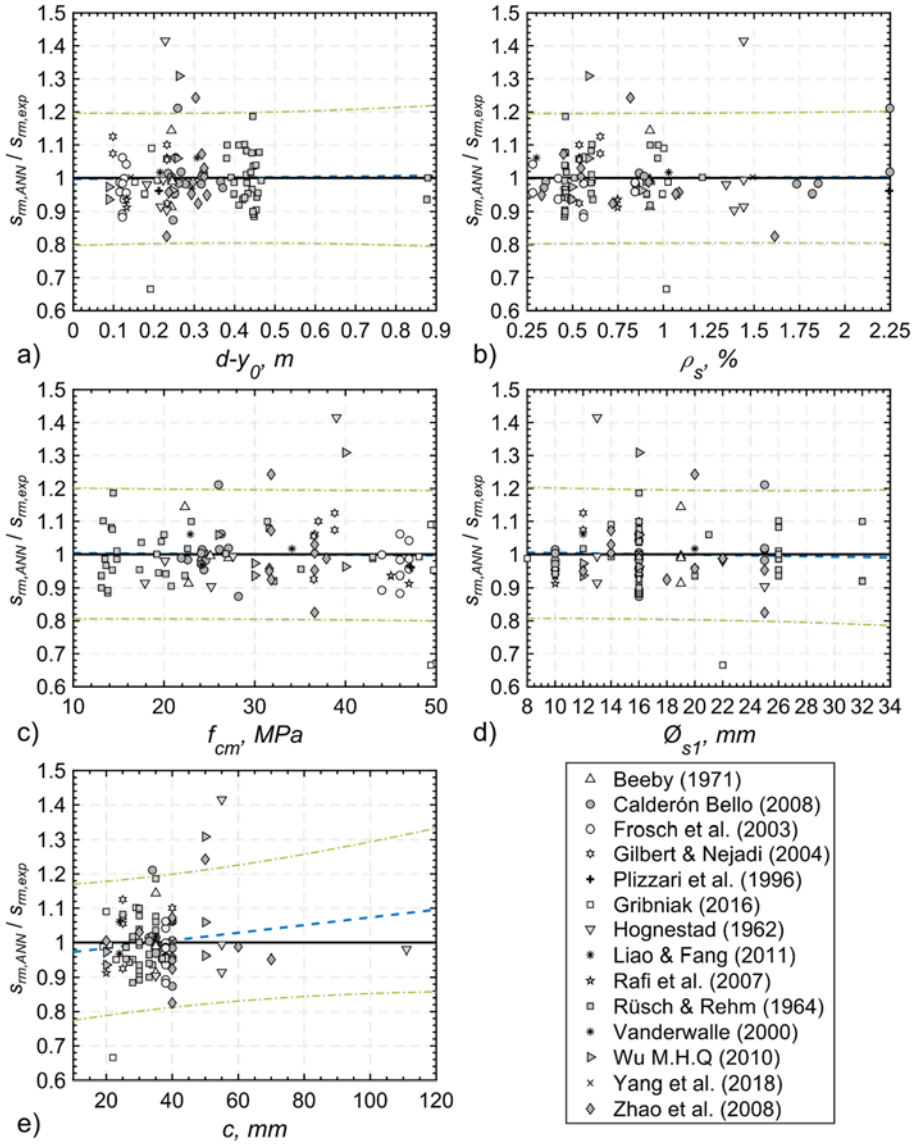

Fig. 4.11. Neural network predicted mean crack spacing values normalised by experimental spacing values: a) $d - y_0$ parameter; b) ratio of reinforcement ρ; c) concrete compressive strength f_{cm}; d) diameter of bar $Ø_{s1}$; e) concrete cover c

The crack spacing results have been segregated by the key physical parameters employed in Chapter 3, the size-dependent variable $d - y_0$, ratio of reinforcement ρ, concrete strength f_{cm}, diameter of the embedded tensile bars $Ø_{s1}$

and the cover of concrete c of the tensile bars. Further normalising the predicted crack spacing by the experimental spacings enables the evaluation of the performance of the neural network for each case. The scattered spacings are presented in Figure 4.11, where the solid horizontal line depicts the perfectly accurate scenario. The dashed thick line is the trend line and the offset dash-dotted lines depict the 0.05 and 0.95% confidence interval. The normalised neural network predictions against the $d - y_0$ parameter (Fig. 4.11a) confirm the network is highly tuned, with good generalisation capabilities, as no tendencies are present. The same observation applies to all parameters except the cover of concrete c (Fig. 4.11e), which is debatable due to the limited data points above 50 MPa.

4.4. Conclusions of Chapter 4

After developing and analysing the predictions by the feed-forward back propagation neural network, the following observations can be outlined:

1. The data sizes are inherently limited to reinforced concrete element experiments due to prohibitive costs and lack of compatibility between different testing programmes that have diverse aims and hence record different characteristics. Application of neural networks can potentially mitigate costs and reduce the number of experiments by predicting the outcomes with a higher degree of certainty than available approaches. Specifically, for validation tests when specific outcomes are anticipated.
2. The limited data set employed in the present research has been shown to be statistically significant by the multiple run and surrogate based approaches. The multiple run approach enabled to account for the randomness of the data and analyse the distributions, the surrogate data set provided insight on whether the data set is not too small and confirmed the existence of intricate relationships between the selected variables of the data samples.
3. The trained neural network model was shown to be significantly more accurate than design codes and slightly improved over the strain compliance approach. The general behaviour mimics the real data very well, as well as the strain compliance concept, which further demonstrates the robustness of the proposed mean crack spacing estimation approach. The developed neural network is free of tendencies when compared to distinct parameters such as $Ø_{s1}$, ρ, d, y_0, f_{cm}. With an exception for the cover parameter c, which seemed to have little impact on the crack spacing prediction accuracy and, similarly, the concrete strength f_{cm}, which did not impact the performance of the neural network in a significant way

General Conclusions

Originating from the literature review and the investigation of the background of reinforced concrete (RC) cracking, the following key points can be conveyed:

1. The existing RC element cracking analysis methods are varied in their reliance on physical parameters. Most include empirical notions. Methods are frequently not compatible in terms of estimating crack widths, spacing and strains. The bar diameter and the effective reinforcement ratio $Ø/\rho_{ef}$ is adopted in various techniques. It is empirical in nature due to the notion of the effective area of concrete in tension.
2. Application of neural networks for predicting cracking behaviour and particularly crack spacing is limited. The few studies that have attempted to predict crack spacing values are flawed, using few and mixed experimental results and not performing adequate neural network tuning, not mitigating risks of overfitting.

The investigation and analysis of tensile reinforced concrete elements have led to the development of a novel approach for the prediction of crack spacing of such elements, revealing:

3. The linear expression $\varepsilon_s(x) = Ax + \varepsilon_{s0}$, denoting the effective zone, is adequate in approximating the reinforcement strain behaviour at higher loading stages. The debonding zone features horizontal reinforcement strains due to the assumed damaged concrete adjacent to the primary

crack. The effective zone facilitates the entire transfer of stresses from the bar to the concrete encompassing it. The sum length of these zones equals to the distance between cracks.

4. The proposed strain compliance concept for predicting the mean crack spacing values of tensile elements is compatible in terms of strains and crack spacing results. This is ensured by the equality of the mean strain ε_{sm} as obtained by the stress transfer method with the mean strain estimated by a mean deformation method. It allows to take advantage of the knowledge of the strain distribution within an element from the stress transfer and knowledge of the average deformation behaviour from the mean strain techniques.
5. The technique minimally relies on empiricism only in the form of the denoted reference element, comprised of the reference ratio ρ_{ref} and bar diameter $Ø_{ref}$, with a known crack spacing value $s_{rm,ref}$.
6. The proposed approach results have been shown to be in good agreement with the experimental spacing values. With accuracy within –13% and +2% of the target and within –15% to +5% for the cases of using a tension stiffening model and Eurocode 2 as the mean strain techniques, respectively. The proposed concept provided bond stresses $\tau = 2.24f_{ct}$, comparable to the $\tau = 1.8–2.0f_{ct}$ range in design codes and research papers.

The findings and observations from the implementation of the strain compliance concept for the analysis of flexural RC elements can be summarised as follows:

7. Flexural RC element reinforcement strains are well approximated with three distinct strain representation zones, namely, the debonding, effective and central zones. The central zone is a newly introduced concept, governing the reinforcement strain behaviour in the middle of an investigated RC block, by averaging the reinforcement strains originating from secondary cracking. For simplicity the area can be well approximated by a flat strain profile.
8. A constitutive length model for the central zone l_c has been proposed, it relates the length to the distance between the neutral axis and the axis of the longitudinal tension bars. The expression $l_c = 0.44(d - y_0)$ has been suggested. The central zone length was found to be significantly extended for larger ratios of reinforcement ρ, resulting in shorter lengths of the effective zones.
9. The normalised prediction accuracy was on average 1.04 and 1.02 times the experimental value for the analysed 73 samples, respectively, for when debonding was considered and neglected. The estimations are on the safe side, i.e. exceeding ratio 1, whereas the Model Code 2010 and

Eurocode 2 estimations are underestimating the actual values at 0.91 and 0.74, respectively. The scatter was well controlled by the strain compliance approach.

10. As the classical approach parameter $Ø/\rho_{ef}$ implies, the spacing predictions decreased with larger ratios of reinforcement ρ. The impact of the diameter $Ø_{s1}$ of the tensile embedded bars was observed to be diminishing with greater ratios of reinforcement ρ. The influence of concrete compressive strength f_{cm} was marginal on the spacing predictions.

Artificial neural networks (ANN) have provided additional insights into the cracking phenomenon and the quality of the data employed for the development of the strain compliance approach, the analysis has revealed the following:

11. Applying a multiple run approach and comparing with surrogate data set trained ANN enables to calibrate a neural network to achieve good generalisation ability and accuracy from a limited and scattered RC flexural element data set.
12. The resulting neural network has been shown to predict the spacing between cracks accurately, with ~99.3% coverage shown to be within 0.83–1.18 range of the target and the mean normalised accuracy equal to 1.0. The 25% and 75% quartiles are within 0.95–1.05 range. Comparison against the strain compliance approach highlighted its robustness and its ability to capture the intricate features of flexural element cracking, much as the ANN. The investigation of input sets revealed the effective section height d, reinforcement diameter $Ø$ and ratio ρ to have the largest influence on the outcome, while the strength of concrete f_{cm} and cover of concrete c had a less pronounced impact on the crack spacing.

References

AIJ, A. I. of J. 1986. *Standard for structural calculation of RC structures*. Tokyo, Japan.

Ashtiani, M. S., Dhakal, R. P., Scott, A. N. and Bull, D. K. 2013. Cyclic beam bending test for assessment of bond-slip behaviour. *Engineering Structures*. Elsevier, 56, 1684–1697.

Balázs, G. L., Bisch, P., Borosnyoi, A., Burdet, O., Burns, C., Ceroni, F., Cervenka, V., Chiorino, M. A., Debernardi, P., Eckfeldt, L. and others 2013. Design for SLS according to fib Model Code 2010. *Structural Concrete*. Wiley Online Library, 14(2), 99–123.

Barre, F., Bisch, P., Chauvel, D., Cortade, J., Coste, J.-F., Dubois, J.-P., Erlicher, S., Gallitre, E., Labbé, P., Mazars, J. and others 2016. *Control of cracking in reinforced concrete structures: Research project CEOS. fr*. John Wiley & Sons.

Barrias, A., Casas, J. and Villalba, S. 2016. A review of distributed optical fiber sensors for civil engineering applications. *Sensors*. Multidisciplinary Digital Publishing Institute, 16(5), 748.

Beeby, A. W. 1970. An Investigation of Cracking in Slabs Spanning One Way. *Technical Report No. TRA 433*. London.

Beeby, A. W. 2004. The influence of the parameter φ/ρeff on crack widths. *Structural Concrete*. Thomas Telford Ltd, 5(2), 71–83.

Beeby, A. W. and Scott, R. H. 2005. Cracking and deformation of axially reinforced members subjected to pure tension. *Magazine of concrete research.* Thomas Telford, 57(10), 611–621.

Bigaj, A. J. 1999. Structural dependence of rotations capacity of plastic hinges in RC beams and slobs.

Bischoff, P. H. 2005. Reevaluation of deflection prediction for concrete beams reinforced with steel and fiber reinforced polymer bars. *Journal of structural engineering*. American Society of Civil Engineers, 131(5), 752–767.

Bischoff, P. H. and Maclaggan, D. A. 2006. Bond and Tension Stiffening in Concrete Tension Members with Plain Reinforcement. *1st International Structural Specialty Conference*, 800(2004), 1–10.

Borges, J. F. 1965. *Cracking and deformability of reinforced concrete beams*. Laboratório Nacional de Engenharia Civil.

Borosnyói, A. and Balázs, G. L. 2005. Models for flexural cracking in concrete: the state of the art. *Structural Concrete*. Thomas Telford Ltd, 6(2), 53–62.

Broms, B. B. 1965. Crack width and crack spacing in reinforced concrete members. *American Concrete Institute – Journal*, 62(10), 1237–1256.

Broms, B. B. and Lutz, L. A. 1965. Effects of arrangement of reinforcement on crack width and spacing of reinforced concrete members. in *Journal Proceedings*, 1395–1410.

Calderón Bello, E. 2008. *Estudio experimental de la fisuración en piezas de hormigón armado sometidas a flexión pura*. Caminos. (In Spanish).

CEB-FIP, C. E.-I. du B. 1978. *Model code for concrete structures, CEB-FIP international recommendations*. 3rd edn. Paris, France: Comité Euro-International du Béton.

CEB-FIP, C. E.-I. du B. 2012. *Model Code 2010 – Volume 1, bulletin 6.* Lausanne, Switzerland: International Federation for Structural Concrete (fib).

CEN, C. E. de N. 1992. *Eurocode 2: Design of concrete structures - Part 1–1: General rules and rules for buildings*. Brussels: European Committee for Standardization.

CEN, E. C. for S. 2004. *Eurocode 2: Design of concrete structures—Part 1–1*: *General rules and rules for buildings*. *EN 1992-1-1*.

Cha, Y.-J., Choi, W. and Büyüköztürk, O. 2017. Deep learning-based crack damage detection using convolutional neural networks. *Computer-Aided Civil and Infrastructure Engineering*. Wiley Online Library, 32(5), 361–378.

Choi, K.-Y. and Maekawa, K. 2003. Bond behavior in RC tension members based on the change of concrete fracture characteristics with temperature. *Proceedings of the Japan Concrete Institute*, 25(2), 991–996.

Danielius, G. 2014. Experimental and theoretical investigation of tension stiffening in tensile reinforced concrete members. *Tempiamų gelžbetoninių element tempiamojo sustandėjimo eksperimentiniai ir teoriniai tyrimai),* Master's thesis. Vilnius Gediminas Technical University, Lithuania. (In Lithuanian).

Davis, M. A., Bellemore, D. G. and Kersey, A. D. 1997. Distributed fiber Bragg grating strain sensing in reinforced concrete structural components. *Cement and concrete composites*. Elsevier, 19(1), 45–57.

Davis, M., Hoult, N. A. and Scott, A. 2017. Distributed strain sensing to assess corroded RC beams. *Engineering Structures*. Elsevier, 140, 473–482.

Debernardi, P. G. and Taliano, M. 2016. An improvement to Eurocode 2 and fib Model Code 2010 methods for calculating crack width in RC structures. *Structural Concrete*. Wiley Online Library, 17(3), 365–376.

Dietterich, T. G. 2000. An experimental comparison of three methods for constructing ensembles of decision trees: Bagging, boosting, and randomization. *Machine learning*. Springer, 40(2), 139–157.

Ekman, M., Warg, F. and Nilsson, J. 2005. An in-depth look at computer performance growth. *ACM SIGARCH Computer Architecture News*. ACM, 33(1), 144–147.

Elisseeff, A. and Paugam-Moisy, H. 1997. Size of multilayer networks for exact learning: analytic approach. in *Advances in Neural Information Processing Systems*, 162–168.

Elshafey, A. A., Dawood, N., Marzouk, H. and Haddara, M. 2013a. Crack width in concrete using artificial neural networks. *Engineering Structures*. Elsevier, 52, 676–686.

Elshafey, A. A., Dawood, N., Marzouk, H. and Haddara, M. 2013b. Predicting of crack spacing for concrete by using neural networks. *Engineering Failure Analysis*. Elsevier, 31, 344–359.

Farra, B. and Jaccoud, J. P. 1992. Bond behaviour, tension stiffening and crack prediction of high strength concrete. in *Proceedings of the International Conference of Bond in Concrete, Riga, Latvia*.

FIB, F. I. du B. 2000. Bond of reinforcement in concrete: state-of-art report. *Bulletin*, 10, 434.

Frosch, R. J., Blackman, D. T. and Radabaugh, R. D. 2003. *Investigation of bridge deck cracking in various bridge superstructure systems*.

Ghaboussi, J., Garrett Jr, J. H. and Wu, X. 1991. Knowledge-based modeling of material behavior with neural networks. *Journal of engineering mechanics*. American Society of Civil Engineers, 117(1), 132–153.

Gilbert, R. I. and Nejadi, S. 2004. *An experimental study of flexural cracking in reinforced concrete members under short term loads*. University of New South Wales, School of Civil and Environmental Engineering.

Goto, Y. 1971. Cracks formed in concrete around deformed tension bars. in *Journal Proceedings*, 244–251.

Gribniak, V., Caldentey, A. P., Kaklauskas, G., Rimkus, A. and Sokolov, A. 2016. Effect of arrangement of tensile reinforcement on flexural stiffness and cracking. *Engineering Structures*. Elsevier, 124, 418–428.

Hagan, M. T., Demuth, H. B., Beale, M. H. and De Jesús, O. 1996. *Neural network design*. Pws Pub. Boston.

Henault, J.-M., Quiertant, M., Delepine-Lesoille, S., Salin, J., Moreau, G., Taillade, F. and Benzarti, K. 2012. Quantitative strain measurement and crack detection in RC structures using a truly distributed fiber optic sensing system. *Construction and Building Materials*. Elsevier, 37, 916–923.

Hognestad, E. 1962. High-strength bars as concrete reinforcement, Part 2: Control of flexural cracking. *Journal of the PCA Research and Development Laboratories*, 46–63.

Houde, J. 1974. *Study of force-displacement relationships for the finite-element analysis of reinforced concrete*. Thesis (Ph.D.)-McGill University.

Yang, I.-H., Joh, C. and Kim, K.-C. 2018. A comparative experimental study on the flexural behavior of high-strength fiber-reinforced concrete and high-strength concrete beams. *Advances in Materials Science and Engineering*. Hindawi, 2018.

Ichinose, T., Kanayama, Y., Inoue, Y. and Bolander Jr, J. E. 2004. Size effect on bond strength of deformed bars. *Construction and building materials*. Elsevier, 18(7), 549–558.

Ince, R. 2004. Prediction of fracture parameters of concrete by artificial neural networks. *Engineering Fracture Mechanics*. Elsevier, 71(15), 2143–2159.

Jakubovskis, R. 2015. *Suderintas gelžbetoninių elementų pleišėjimo, deformacijų ir sukibimo modeliavimas*. VGTU leidykla „Technika “. (In Lithuanian)

Janovic, K. K. H. 1986. Rissbildung im Stahlbeton-und Spannbetonbau. *Betonw und Fert.*, 52(12), 161–169. (In German).

JSCE, J. S. of C. E. 1997. Recommendation for design and construction of concrete structrues using continuous fiber reinforceing materials. in Machida, A. (ed.) *Concrete Engineering Series*. Tokyo, Japan: JSCE.

Juknys, M. 2017. *Tempiamųjų gelžbetoninių elementų diskrečių plyšių modelio fizikinių parametrų eksperimentiniai ir skaitiniai tyrimai*. Vilnius Gediminas Technical University. (In Lithuanian)

Kaklauskas, G., Gribniak, V., Bacinskas, D. and Vainiunas, P. 2009. Shrinkage influence on tension stiffening in concrete members. *Engineering Structures*. Elsevier, 31(6), 1305–1312.

Kaklauskas, G., Tamulenas, V., Bado, M. F. and Bacinskas, D. 2018. Shrinkage-free tension stiffening law for various concrete grades. *Construction and Building Materials*. Elsevier, 189, 736–744.

Kankam, C. K. 1997. Relationship of bond stress, steel stress, and slip in reinforced concrete. *Journal of Structural Engineering*. American Society of Civil Engineers, 123(1), 79–85.

Kasperkiewicz, J., Racz, J. and Dubrawski, A. 1995. HPC strength prediction using artificial neural network. *Journal of Computing in Civil Engineering*. American Society of Civil Engineers, 9(4), 279–284.

Kenel, A., Nellen, P., Frank, A. and Marti, P. 2005. Reinforcing steel strains measured by Bragg grating sensors. *Journal of materials in civil engineering*. American Society of Civil Engineers, 17(4), 423–431.

Kurumatani, M., Soma, Y. and Terada, K. 2019. Simulations of cohesive fracture behavior of reinforced concrete by a fracture-mechanics-based damage model. *Engineering Fracture Mechanics*. Elsevier, 206, 392–407.

Kuuskoski, V. 1950. *Über die haftung zwischen Beton und Stahl (Doctoral Dissertation)*. (In German).

Lapi, M., Orlando, M. and Spinelli, P. 2018. A review of literature and code formulations for cracking in R/C members. *Structural Concrete*. Wiley Online Library, 19(5), 1481–1503.

Lawrence, S., Giles, C. L. and Tsoi, A. C. 1998. *What size neural network gives optimal generalization? Convergence properties of backpropagation*.

Li, H., Li, J. and Yuan, H. 2018. A review of the extended finite element method on macrocrack and microcrack growth simulations. *Theoretical and Applied Fracture Mechanics*. Elsevier, 97, 236–249.

Liao, H. P. and Fang, S. S. 2011. An experimental study on flexural behavior of reinforced concrete beams strengthened with high-performance ferrocement. in *Advanced Materials Research*, 3772–3776.

Lorrain, M., Maurel, O. and Seffo, M. 1998. Cracking behavior of reinforced high-strength concrete tension ties. *Structural Journal*, 95(5), 626–635.

Ma, F. J. and Kwan, A. K. H. 2015. Crack width analysis of reinforced concrete members under flexure by finite element method and crack queuing algorithm. *Engineering Structures*. Elsevier, 105, 209–219.

Maekawa, K. and Qureshi, J. 1996. Computational model for reinforcing bar embedded in concrete under combined axial pullout and transverse displacement. *Doboku Gakkai Ronbunshu*. Japan Society of Civil Engineers, 1996(538), 227–239.

Mains, R. 1951. Measurement of the distribution of tensile and bond stresses along reinforcing bars. *In Journal proceedings*, 48(11), 225–252.

Marti, P., Alvarez, M., Kaufmann, W. and Sigrist, V. 1998. Tension chord model for structural concrete. *Structural Engineering International*. Taylor & Francis, 8(4), 287–298.

Monsberger, C. M., Lienhart, W., Kluckner, A., Wagner, L. and Schubert, W. 2018. Continuous strain measurements in a shotcrete tunnel lining using distributed fibre optic sensing. in *Proc. 9th European Workshop on Structural Health Monitoring, July 10–13, 2018, Manchester, United Kingdom*.

Moon, H. and Kim, J. 2011. Intelligent crack detecting algorithm on the concrete crack image using neural network. *Proceedings of the 28th ISARC*, 1461–1467.

Murray, A., Castel, A., Gilbert, R. I. and Chang, Z.-T. 2016. Time-dependent changes in the instantaneous stiffness of reinforced concrete beams. *Engineering Structures*. Elsevier, 126, 641–651.

Ng, P. L., Ma, F. J. and Kwan, A. K. H. 2015. Crack analysis of concrete beams based on pseudo-discrete crack model. in *Proceedings of the Second International Conference on Performance-based and Life-cycle Structural Engineering, Brisbane, Australia*, 669–678.

Noakowski, P. 1985. Verbundorientierte, kontinuierliche Theorie zur Ermittlung der Rißbreite. Wirklichkeitsnaher und einfacher Nachweis unter Berücksichtigung der Verbundgesetze und der Betonzugfestigkeit sowie unter Verknüpfung des Erstriß-und Endrißzustands (Teil 1). *Beton-und Stahlbetonbau*. Wiley Online Library, 80(7), 185–190. (In German).

Oehlers, D., Visintin, P., Haskett, M. and Chen, J. 2012. Consequences and solutions to our abysmal neglect of the bond-slip behaviour in reinforced concrete. Publisher Creations.

Oh, B. H. and Kang, Y. J. 1987. New formulas for maximum crack width and crack spacing in reinforced concrete flexural members. *Structural Journal*, 84(2), 103–112.

Pérez Caldentey, A., Corres Peiretti, H., Peset Iribarren, J. and Giraldo Soto, A. 2013. Cracking of RC members revisited: influence of cover, $\varphi/\rho_{s,ef}$ and stirrup spacing – an experimental and theoretical study. *Structural concrete*. Wiley Online Library, 14(1), 69–78.

Plizzari, G. A., Marchina, E. and Giuriani, E. 1996. Experimental study of splitting and flexural cracks in a RC beam with overlapped splices. *Materials and Structures*. Springer, 29(1), 19.

Rafi, M. M., Nadjai, A. and Ali, F. 2007. Experimental testing of concrete beams reinforced with carbon FRP bars. *Journal of composite materials*. Sage Publications Sage UK: London, England, 41(22), 2657–2673.

Rehm, G. 1961. *Über die Grundlagen des Verbundes zwischen Stahl und Beton*. Ernst.Reineck, K.-H. 1991. Ultimate shear force of structural concrete members without transverse reinforcement derived from a mechanical model (SP–885). *Structural Journal*, 88(5), 592–602.

RILEM, T. C. 1982. RC 5 Bond test for reinforcement steel. 1. Beam test, 1982. *RILEM Recommendations for the Testing and Use of Constructions Materials*. E & FN SPON, 213–217.

RILEM, T. C. 1994. RILEM recommendations for the testing and use of constructions materials. *RC*, 6, 218–220.

Rimkus, A. and Gribniak, V. 2017. Experimental investigation of cracking and deformations of concrete ties reinforced with multiple bars. *Construction and Building Materials*. Elsevier, 148, 49–61.

Ruiz, M. F., Muttoni, A. and Gambarova, P. G. 2007. Analytical modeling of the pre- and postyield behavior of bond in reinforced concrete. *Journal of Structural Engineering*. American Society of Civil Engineers, 133(10), 1364–1372.

Rüsch, H. and Rehm, G. 1964. Versuche mit Betonformstahlen, Deutscher Ausschuss fur Stahlbeton. Berlin. (In German).

Saliger, R. 1936. High grade steel in reinforced concrete. in *Preliminary Publication, 2nd Congress of IABSE. Berlin–Munich: IABSE Publications*.

Saliger, R. 1950. *Die neue Theorie des Stahlbetons auf Grund der Bildsamkeit vor dem Bruch*. F. Deuticke. (In German).

Sanad, A. and Saka, M. P. 2001. Prediction of ultimate shear strength of reinforced-concrete deep beams using neural networks. *Journal of structural engineering*. American Society of Civil Engineers, 127(7), 818–828.

Scott, C. H. 1987. Efficiency/equity tradeoffs in banking regulation. *Business & Society*. Sage Publications Sage CA: Thousand Oaks, CA, 26(1), 39–43.

Scott, R. H. and Gill, P. A. T. 1987. Short-term distributions of strain and bond stress along tension reinforcement. *The Structural Engineer*, 65(2), 39–43.

Shaikhina, T. and Khovanova, N. A. 2017. Handling limited datasets with neural networks in medical applications: A small-data approach. *Artificial intelligence in medicine*. Elsevier, 75, 51–63.

Somayaji, S. and Shah, S. P. 1981. Bond stress versus slip relationship and cracking response of tension members. in *Journal Proceedings*, 217–225.

Srivastava, N., Hinton, G., Krizhevsky, A., Sutskever, I. and Salakhutdinov, R. 2014. Dropout: a simple way to prevent neural networks from overfitting. *The Journal of Machine Learning Research*. JMLR. org, 15(1), 1929–1958.

Stathakis, D. 2009. How many hidden layers and nodes? *International Journal of Remote Sensing*. Taylor & Francis, 30(8), 2133–2147.

Strauss, A., Wan-Wendner, R., Vidovic, A., Zambon, I., Yu, Q., Frangopol, D. M. and Bergmeister, K. 2017. Gamma prediction models for long-term creep deformations of prestressed concrete bridges. *Journal of Civil Engineering and Management*. Taylor & Francis, 23(6), 681–698.

Tepfers, R. 1979. Cracking of concrete cover along anchored deformed reinforcing bars. *Magazine of concrete research*. Thomas Telford Ltd, 31(106), 3–12.

Timmer, J. 1998. Power of surrogate data testing with respect to nonstationarity. *Physical Review E*. APS, 58(4), 5153.

Treves, A. and Panzeri, S. 1995. The upward bias in measures of information derived from limited data samples. *Neural Computation*. MIT Press, 7(2), 399–407.

Vandewalle, L. 2000. Cracking behaviour of concrete beams reinforced with a combination of ordinary reinforcement and steel fibers. *Materials and structures*. Springer, 33(3), 164–170.

Vanluchene, R. D. and Sun, R. 1990. Neural networks in structural engineering. *Computer-Aided Civil and Infrastructure Engineering*. Wiley Online Library, 5(3), 207–215.

Verleysen, M. and François, D. 2005. The curse of dimensionality in data mining and time series prediction. in *International Work-Conference on Artificial Neural Networks*, 758–770.

Wang, J.-J., Tao, M.-X. and Nie, X. 2017. Fracture energy-based model for average crack spacing of reinforced concrete considering size effect and concrete strength variation. *Construction and Building Materials*. Elsevier, 148, 398–410.

Wenkenbach, I. 2011. *Tension Stiffening in Reinforced Concrete Members with Large Diameter Reinforcement*. Durham University.

Windisch, A. 2016. Crack control: an advanced calculation model – Part I: Review of classic tests. *Concrete Structures*, 41–48.

Wu, H. Q. and Gilbert, R. I. 2008. An experimental study of tension stiffening in reinforced concrete members under short-term and long-term loads. *UNICIV Report no*.

Wu, H. Q. and Gilbert, R. I. 2009. Modeling short-term tension stiffening in reinforced concrete prisms using a continuum-based finite element model. *Engineering Structures*. Elsevier, 31(10), 2380–2391.

Wu, H. Q. 2010. *Tension stiffening in reinforced concrete – instantaneous and time-dependent behaviour*. University of New South Wales, Sydney.

Zhao, S. B., Guang, J., Zhang, X., Cheng, X. and Huang, C. 2008. Experimental study and statistical analysis of crack patterns of reinforced concrete beams. *Engineering Mechanics*, 25(12), 141–146. (In Chinese)

List of Scientific Publications by the Author on the Topic of the Dissertation

Publications in Reviewed Scientific Journals

Kaklauskas, G., Ramanauskas, R. and Jakubovskis, R. 2017a. Mean crack spacing modelling for RC tension elements. *Engineering Structures*. Elsevier, 150, 843–851. (Clarivate Analytics Web of Science) [IF: 2.755].

Kaklauskas, G., Ramanauskas, R. and Ng, P. L. 2019a. Predicting Crack Spacing of Reinforced Concrete Tension Members Using Strain Compliance Approach With Debonding. *Journal of Civil Engineering and Management*, 25(5), 422–430. (Clarivate Analytics Web of Science) [IF: 2.029].

Kaklauskas, G., Sokolov, A., Ramanauskas, R. and Jakubovskis, R. 2019b. Reinforcement Strains in Reinforced Concrete Tensile Members Recorded by Strain Gauges and FBG Sensors: Experimental and Numerical Analysis. *Sensors*. Multidisciplinary Digital Publishing Institute, 19(1), 200, 1–13. (Clarivate Analytics Web of Science) [IF: 3.031].

Publications in Other Editions

Gudonis, E., Kaklauskas, G., Bacinskas, D., Gribniak, V., Ramanauskas, R. and Tamulenas, V. 2015. Experimental investigation on short-and long-term deformations of

cracked reinforced concrete ties. *CONCREEP 10: 10th International Conference on Mechanics and Physics of Creep, Shrinkage and Durability of Concrete and Concrete Structures*, 958–962.

Gudonis, E., Ramanauskas, R. and Sokolov, A. 2017. Experimental investigation on strain distribution in reinforcement of RC specimens. in *Proceedings of the 2nd International RILEM/COST Conference on Early Age Cracking and Serviceability in Cement-based Materials and Structures (EAC–02)*. Brussels, Belgium: RILEM Publications, 573–578.

Kaklauskas, G., Juknys, M., Jakubovskis, R., Gudonis, E., Ramanauskas, R., Aleksandr, S. and Gribniak, V. 2016. Experimental investigation on strain distribution in reinforcement of RC specimens under tension loading. in *International RILEM Conference on Materials, Systems and Structures in Civil Engineering 2016 segment on Service Life of Cement-Based Materials and Structures*. Lyngby, Denmark: RILEM Publications S.A.R.L, 279–286.

Kaklauskas, G., Ng, P. L., Jakubovskis, R. and Ramanauskas, R. 2017b. Numerical modelling of cracked RC tension members using stress-transfer approach. in Hong, H. and Chunwei, Z. (eds) *Mechanics of structures and materials: advancements and challenges: proceedings of the 24th Australasian Conference on the Mechanics of Structures and Materials (ACMSM24)*. Perth, Australia: CRC Press Taylor & Francis Group, 137–142.

Kaklauskas, G. and Ramanauskas, R. 2016a. A new approach in predicting the mean crack spacing of flexural reinforced concrete elements. in *fib Symposium 2016. Performance-based approaches for concrete structures*. Cape Town, South Africa, 1–11.

Kaklauskas, G. and Ramanauskas, R. 2016b. A new analytical approach in modelling of cracking of RC members. in *International RILEM Conference on Materials, Systems and Structures in Civil Engineering 2016 segment on Service Life of Cement-Based Materials and Structures*. Lyngby, Denmark, 269–278.

Kaklauskas, G., Ramanauskas, R., Jakubovskis, R., Gribniak, V. and Juknys, M. 2015. A new method for formulating crack spacing models of RC ties. in *Proceedings of the second international conference on performance-based and life-cycle structural engineering (PLSE 2015)*. Brisbane, Australia, 620–629.

Kaklauskas, G., Ramanauskas, R., Ng, P. L., Jakubovskis, R. and Juknys, M. 2016. Crack spacing model for reinforced concrete tension members based on damage zone and strain compliance concepts. in *fib Symposium 2016. Performance-based approaches for concrete structures*. Cape Town, South Africa, 1–11.

Summary in Lithuanian

Įvadas

Problemos formulavimas

Betoninės konstrukcijos pasižymi ypatinga svarba mūsų šiuolaikiniame pasaulyje. Tačiau dėl jų specifikos, riboto tempiamojo stiprio, sukeliančio šių konstrukcijų pleišėjimą, gali sutrumpėti statinio eksploatacijos trukmė ir nepasiekti suprojektuotos. Tai turi ženklų poveikį šios medžiagos tvarumui. Siekiant užtikrinti gelžbetoninių konstrukcijų ilgaamžiškumą, vienas svarbiausių kriterijų yra pleišėjimo apribojimas. Tačiau šiai dienai šis reiškinys nėra iki galo išaiškintas. Tai atsispindi per pastaruosius kelis dešimtmečius išleistose įvairiose projektavimo normose ir mokslo publikacijose pateiktose pleišėjimo formuluotėse. Jos yra pilnos įvairių empirinių faktorių ir pasižymi nenuoseklumu bei suderinamumo trūkumu tarp vidutinių deformacijų ir pleišėjimo. Tai suteikė motyvaciją plėtoti šios disertacijos tyrimus, siekiant užtikrinti universalaus metodo sukūrimą, tinkamą tiek deformacinėms, tiek pleišėjimo elgsenoms analizuoti. Sparčiai besivystant skaitiniams metodams ir kompiuterių skaičiavimo efektyvumo galimybėms tampa vis lengviau pritaikyti seniau ypač sudėtingais laikytus metodus, kaip, pavyzdžiui, dirbtinius neuroninius tinklus. Šie metodai suteikia naujų galimybių pažvelgti į įvairius duomenų komplektus, tačiau gan ribotai yra taikomi statybos inžinerijoje, ypač tiriant gelžbetoninių konstrukcijų pleišėjimą. Šiuo tyrimu siekiama nustatyti, ar įmanoma gauti patikimus ir tikslius rezultatus naudojant neuroninų tinklų metodą atstumui tarp plyšių prognozuoti, kai turimų duomenų kiekis yra ženkliai ribotas ir pasižymintis nemaža sklaida, natūralia gelžbetoninėms konstrukcijoms.

Darbo aktualumas

Viena esminių ilgo tarpatramio statinių, kaip pavyzdžiui tiltų, problema yra išplėstinis jų pleišėjimas ir plyšių pločiai, kurie viršija normose numatytas tinkamumo ribinio būvio sąlygas. Prie šios problemos prisideda nepakankamas egzistuojančių skaičiavimo metodų tikslumas. Projektavimo normose pateikti metodai įtraukia labai daug empirinių koeficientų bei nuostatų, kurie tik prisideda prie didelės rezultatų sklaidos. Šie metodai taip pat pasižymi negebėjimu suderinti deformacijų ir pleišėjimo elgsenas. Siekiant išspręsti šiuos trūkumus reikalingas apjungtas metodas. Šiuolaikinėse formuluotėse plyšio plotis yra susietas su atstumu tarp gretutinių plyšių per armatūros ir betono sukibimo elgseną, todėl siekiant tikslesnių skaičiavimų plyšio pločiui nustatyti būtina iš pradžių suprasti ir adekvačiai prognozuoti vidutinius atstumus tarp plyšių. Tai leistų tiksliau įvertinti rezultatų išsibarstymą ir ateityje statistiškai išvesti metodus maksimalaus atstumo tarp plyšių apskaičiavimui su apibrėžtu patikimumu.

Tyrimo objektas

Disertacijos tyrimų objektas – vidutiniai atstumai tarp pagrindinių tempiamų bei lenkiamų armuotų betoninių elementų plyšių, apkrovimo lygiui esant stabilizuotų plyšių stadijoje.

Darbo tikslas

Disertacijos tikslas – naujo tempiamų bei lenkiamų gelžbetoninių elementų pleišėjimo analizės metodo sukūrimas bei jo patikrinimas taikant dirbtinius neuroninius tinklus.

Darbo uždaviniai

Disertacijos tikslams pasiekti suformuoti šie uždaviniai:

1. Apžvelgti gelžbetoninių elementų pleišėjimo metodus, nustatyti esamų metodų trūkumus, pagrindinius parametrus.
2. Skaitiškai ir analitiškai ištirti tempiamų bei lenkiamų gelžbetoninių elementų eksperimentinius duomenis, pagrindinį dėmesį skiriant atstumams tarp pagrindinių plyšių.
3. Sukurti teorinį modelį tempiamų gelžbetoninių elementų vidutinių atstumų tarp normalinių plyšių įvertinimui, kai yra pakankamas apkrovos lygis, užtikrinantis elemento elgseną atitinkančią stabilizuotų plyšių stadiją.
4. Pritaikyti teorinį modelį lenkiamiems gelžbetoniniams elementams.
5. Įvertinti pasiūlytų teorinių modelių tikslumą bei deformacinę elgseną juos palyginus su surinktais eksperimentiniais duomenimis, atliekant sisteminę analizę bei juos palyginus su projektavimo normomis.
6. Pritaikyti dirbtinį neuroninį tinklą atstumams tarp plyšių prognozuoti iš surinktų lenkiamų armuotų betoninių elementų eksperimentinių duomenų, patikrinti surinktus duomenis.

7. Palyginti dirbtinio neuroninio tinklo bei pasiūlyto fizikinio modelio prognozes bei charakteristikas.

Tyrimų metodika

Pasirinkta disertacijos tyrimų metodika daugiausiai orientuota į kiekybinę analizę, kuri apima statistinę surinktų eksperimentinių tempiamų bei lenkiamų gelžbetoninių elementų pleišėjimo duomenų analizę, egzistuojančių metodų analizę, naujo atstumų tarp plyšių įvertinimo metodo plėtojimą, jo lyginimą su skaitiniais ir analitiniais metodais. Išanalizuotos esminės mechaninės bei geometrinės savybės, turinčios ryškiausią poveikį atstumams tarp pagrindinių plyšių, ištirti šių savybių sąryšiai. Remiantis inžinerine logika bei siekiant paprastumo, išlaikant konstrukcijų mechanikos tvarumą plėtojamas suderintų deformacijų metodas. Šiems tikslams pasiekti buvo naudojama *Matlab* programa, joje atliekant regresijos analizes bei pritaikant skaitinius iteracinius metodus. Siekiant užtikrinti surinktų eksperimentinių duomenų tinkamumą disertacijos tyrimams bei pasiūlyto metodo patikrinimui buvo nuosekliai apmokytas ir kalibruotas dirbtinis neuroninis tinklas. Neuroninių tinklų mokymas, tikrinimas bei statistinė analizė buvo atliekama *Matlab* programoje.

Darbo naujumas

1. Pasiūlyta suderintų deformacijų koncepcija, kuri sulygina diskrečiųjų plyšių ir vidutinių deformacijų metodų vidutines armatūros deformacijas, taikoma tiek tempiamiems, tiek lenkiamiems gelžbetoniniams elementams. Paminėtų skaičiavimo metodų suderinimas užtikrina principų pritaikomumą deformacinei ir pleišėjimo elgsenai.
2. Sukurtas suderintų deformacijų metodas, taikant inžineriškai supaprastintus armatūros deformacijų profilius tarp gretutinių pagrindinių plyšių, užtikrinantis aukštą vidutinių atstumų tarp plyšių skaičiavimo tikslumą. Pasiūlytas metodas apibrėžia koncepciją, kuri yra labai lanksti, leidžianti įtraukti skirtingas armatūros deformacijų pasiskirstymo funkcijas, įvertinti lokalius reiškinius bei skirtingas geometrines skerspjūvio formas bei alternatyvias medžiagas. Rezultatai visada yra suderinti tiek deformacijų, tiek plyšių atžvilgiu, nes tai sąlygoja diskrečiųjų plyšių bei vidutinių deformacijų metodai, sudarantys pasiūlytos koncepcijos pagrindą.
3. Nuoseklia bei išsamia statistine procedūra apmokinto dirbtinio neuroninio tinklo rezultatai parodė, kad esminiai parametrai turintys reikšmingiausią poveikį armuotiems betoniniams lenkiamų konstrukcijų atstumams tarp pagrindinių plyšių yra efektyvus skerspjūvio aukštis, neutralios ašies padėtis, armatūros strypo skersmuo bei konstrukcijos armavimo procentas. Kiek mažesnį poveikį pagrindiniams plyšiams turi betono apsauginio sluoksnio aukštis, o minimalų poveikį turi betono gniuždymo stipris.

Darbo rezultatų praktinė reikšmė

1. Sukurtas naujas metodas iš anksto įvertinti vidutinį atstumą tarp plyšių suderinant vidutinę deformacinę bei pleišėjimo elgsenas. Metodas gali būti panaudotas tiek tempiamiems, tiek lenkiamiems elementams – dažniausiai sutinkamiems gelžbetoninių konstrukcijų tipams. Susiejant vidutinį atstumą tarp plyšių su maksimaliu atstumu tarp plyšių galima nustatyti maksimalų plyšio plotį elementui.
2. Apmokintas dirbtinis neuroninis tinklas pasitelkiant atrinktus lenkiamų gelžbetoninių sijų ir plokščių eksperimentinius duomenis. Neuroninio tinklo atstumų tarp plyšių prognozės ir jų sklaida geresnės už suderintų deformacijų metodą bei projektavimo normų rezultatus, todėl yra tinkamas tiek realioms konstrukcijoms prognozuoti, tiek planuojant eksperimentines gelžbetoninių konstrukcijų programas. Pasinaudojant tik šešiais pagrindiniais kintamaisiais – armatūros skersmeniu, armavimo procentu, efektyviu konstrukcijos aukščiu, neutraliosios ašies padėtimi, betono apsauginio sluoksnio aukščiu ir betono gniuždymo stipriu - galima suprojektuoti eksperimentinę programą su aukštu patikimumo lygiu ir pasiekti norimų rezultatų.

Ginamieji teiginiai

1. Išvystyta deformacijų suderinamumu pagrįsta koncepcija, tinkama taikyti tiek tempiamiems gelžbetoniniams elementams, tiek lenkiamoms konstrukcijoms, leidžianti tiksliai įvertinti vidutinius atstumus tarp pagrindinių plyšių. Metodas pagrįstas mechaniškai bei minimaliai remiasi empirinėmis nuostatomis. Pasiūlyta koncepcija užtikrinama per vidutinių armatūros deformacijų, apskaičiuotų įtempių perdavimo ir vidutinių deformacijų metodais, lygybę.
2. Užtikrinus nuoseklų kalibravimo procesą, galima apmokinti dirbtinį neuroninį tinklą iš riboto ir išsibarsčiusio duomenų kiekio, kuris pasižymės geresniu tikslumu ir sugebėjimu generalizuoti vidutinius atstumus tarp plyšių lenkiamose gelžbetoninėse konstrukcijose negu kiti metodai.

Darbo rezultatų aprobavimas

Iš viso buvo publikuota 11 mokslinių publikacijų, susijusių su šios disertacijos tema, iš kurių 3 – žurnaluose, turinčiuose cituojamumo rodiklį, 8 – įvairių tarptautinių konferencijų rinkiniuose. Doktorantūros studijų laikotarpiu (2015-2019) disertacijos rezultatai buvo paskelbti 5 konferencijose:

- 2017. 2-oji tarptautinė RILEM/COST *Early Age Cracking and Serviceability in Cement-based Materials and Structure*s (EAC–02), Briuselis, Belgija.
- 2016. 24-oji Australijos ir Azijos *Mechanics of Structures and Materials* (ACMSM24), Pertas, Australija.
- 2016. fib simpoziumas *Performance-based approaches for concrete structures*, Keiptaunas, Pietų Afrikos Respublika.
- 2016. Tarptautinė RILEM konferencija *Materials, Systems and Structures in Civil Engineering*, Lyngbis, Danija.

- 2015. 10-oji tarptautinė konferencija *Mechanics and Physics of Creep, Shrinkage, and Durability of Concrete and Concrete Structures* (CONCREEP 10), Viena, Austrija.

Disertacijos struktūra

Disertaciją sudaro įvadas, 4 skyriai, bendrosios išvados, literatūros sąrašas (105 šaltiniai), autoriaus mokslinių publikacijų sąrašas (11 publikacijų), santrauka lietuvių kalba bei 8 priedai. Darbo apimtis 145 puslapiai. Darbe pateikti 51 grafikai, 11 lentelių per keturis skyrius.

Padėka

Autorius be galo dėkingas už paramą, kantrybę bei paskatinimą šiame ilgame kelyje rengiant šią disertaciją savo žmonai Skaistei Ardavičiūtei-Ramanauskienei bei savo mamai Genovaitei Ramanauskienei.

Už konsultacijas, patarimus ir pagalbą rengiant šią disertaciją autorius išreiškia padėką savo mokslinio darbo vadovui – Gelžbetoninių konstrukcijų ir geotechnikos katedros profesoriui habil. dr. Gintariui Kaklauskui.

Taip pat, autorius išreiškia dėkingumą dr. Viktorui Gribniak iš Metalinių ir kompozitinių konstrukcijų katedros, už vertingus komentarus ir bendras patirtis dr. Pui Lam NG, taip pat prof. dr. Dariui Bačinskui bei dr. Eugenijui Gudoniui iš Gelžbetoninių konstrukcijų ir geotechnikos katedros, dr. Aleksandrui Sokolov iš Inovatyvių statybinių konstrukcijų mokslo laboratorijos. Autorius taip pat išreiškia dėkingumą visiems nepaminėtiems Gelžbetoninių konstrukcijų ir geotechnikos katedros darbuotojams, kolegoms doktorantams su kuriais teko dalintis šia doktorantūros patirtimi.

Už šios disertacijos pastabas ir atsiliepimus autorius dėkoja dr. Remigijui Šalnai, dr. Vladimirui Popov bei dr. Gintautui Skripkiūnui.

Autorius išreiškia padėką Lietuvos mokslų tarybai už finansinę paramą doktorantūros studijų metu.

1. Betoninių konstrukcijų pleišėjimo elgsenos ir tinkamumo analizės apžvalga

Pirmajame disertacijos skyriuje pateikta literatūros šaltinių disertacijos tematika apžvalga bei aptarti esminiai šiems tyrimams teoriniai aspektai. Išsamiai aptarta bendrinė gelžbetoninių konstrukcijų elgsena, ypač pleišėjimo kontekste. Pateikti pagrindiniai plyšių tipai ir jų klasifikavimas. Pabrėžiant gelžbetoninių konstrukcijų deformacinę elgseną, akcentuota stabilizuotų plyšių stadija ir jos svarba pleišėjimo procesui, plyšių charakteristikų nustatymui. Taip pat aprašyti pagrindiniai egzistuojantys armatūros sukibimo įtempių bei armatūros deformacijų nustatymų metodai bei jų trūkumai. Pateikta išsami mokslinėje literatūroje pateikiamų pleišėjimo metodų analizė, išanalizuotos jų formuluotės bei pagrindiniai teoriniai aspektai. Lygiagrečiai, išanalizuota populiariose projektavimo normose pateiktų vidutinių atstumų tarp plyšių apskaičiavimo formuluočių trūkumai. Pastebėta, kad egzistuojantys metodai nėra suderinti, pasižymi pritaikomumu

tik pleišėjimui, bet retai geba aprašyti deformacinę elemento elgseną pakankamu tikslumu. Pažymėtina, kad egzistuojančios formuluotės pagrinde remiasi tarp empirinių nuostatų dažnai pasitaikančia efektyvaus tempiamojo betono ploto sąvoka.

Išanalizuoti egzistuojančių dirbtinių neuroninių tinklų taikymo gelžbetoninėms konstrukcijoms tyrimai. Pateikta įvadinė teorinė neuroninių tinklų struktūra ir jos komponentai. Aptarti pagrindiniai esamų tyrimų trūkumai, pabrėžiant jų ribotas taikymo sritis arba akcentuojant pasirinktų pradinių duomenų neadekvatumą. Pastebėjimai pateikti ir gelžbetoninių konstrukcijų eksperimentinių programų atžvilgiu, kai dėl skirtingų tikslų dažnai gauti rezultatai nėra suderinami tarp skirtingų tiriamųjų programų. Tam poveikį turi tiek skirtingai atlikti eksperimentai, tiek skirtingi jų tikslai ir fiksuojami duomenys. Skyriuje aptarta galimybė dalinai išspręsti ženkliai ribotų duomenų problema taikant statistinę analizę ir kruopščiai apmokant neuroninį tinklą. Išanalizavus mokslinę literatūrą, suformuluoti darbo uždaviniai bei tyrimo objektas.

2. Suderintų deformacijų metodo pritaikymas tempiamų armuotų betoninių elementų atstumų tarp plyšių nustatymui

Antrajame disertacijos skyriuje pateiktas suderintų deformacijų metodo išvystymas ir pritaikymas gelžbetoniniams elementams, veikiamiems tempimo apkrovų, reprezentuojantiems dažnai sukibimo ir deformacijų eksperimentuose taikomus elementus. Pasiūlytas metodas remiasi supaprastinta armatūros deformacijų reprezentacija stabilizuotų plyšių stadijoje priimant, kad deformacijos kinta tiesiškai atskirose pakitusio sukibimo ir efektyviose zonose. Visi įtempiai perduodami tarp armatūros ir betono tik efektyviojoje zonoje, o likusioje dalyje priimama, kad bendras darbas nevyksta dėl pažeisto betono ties pagrindiniu plyšiu. Suderintų deformacijų metodo esmė yra lygybės tarp vidutinių armatūros deformacijų εsm , nustatomų iš diskrečiųjų plyšių, ir vidutinių deformacijų metodų užtikrinimas. Papildomai šis metodas reikalauja etaloninio elemento, kuris apibrėžiamas žinomu armavimo procentu ir armatūros strypu, kuriam taip pat žinomas vidutinis atstumas tarp gretutinių pagrindinių plyšių. Iš šio etaloninio elemento nustačius armatūros ir betono sukibimo įtempius juos galima pritaikyti alternatyvių konfigūracijų elementų atstumų tarp plyšių įvertinimui.

Remiantis supaprastinta armatūros deformacijų diagrama (S2.1 pav.) aprašyti atstumą tarp plyšių galima per atskiras jos zonas, pateiktas šiame darbe. Tai pakitusios armatūros ir betono sukibimo zonos ties pagrindiniais plyšiais ir efektyviąją zona, kurioje užtikrinamas bendras armatūros ir betono darbas. Visi įtempiai perduodami būtent šioje zonoje. Šių zonų suma sudaro vidutinį atstumą tarp plyšių:

$$0{,}5s_{rm} = l_d + l_{eff}. \quad \text{(S2.1)}$$

Efektyvi zona aprašoma tiese, todėl armatūros deformacijos gali būti aprašomas šia paprasta formule:

$$\varepsilon_{s0} + Al_{eff} = \varepsilon_{si}. \quad \text{(S2.2)}$$

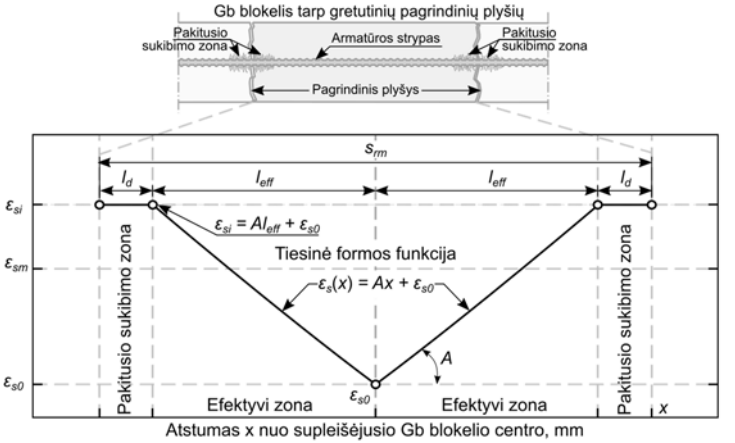

S2.1 pav. Tariama armatūros deformacijų pasiskirstymo išilgai tempiamo gelžbetoninio elemento gretutinių pagrindinių plyšių diagrama

Suderintų deformacijų metodas reikalauja, kad būtų užtikrinta diskrečiųjų plyšių ir vidutinių deformacijų metodų vidutinių tempiamos armatūros deformacijų lygybė. Išreiškiant šią lygybę pagal supaprastintas armatūros deformacijas, pateiktas S2.1 pav., gaunama lygtis:

$$\frac{0{,}5A\left(l_{eff}\right)^2 + \varepsilon_{s0} l_{eff} + \varepsilon_{si} l_d}{0{,}5 s_{rm}} = \varepsilon_{sm}. \tag{S2.3}$$

Parinktas apkrovimo lygis, atitinkantis stabilizuotų plyšių stadiją, kuris sudaro ~300 MPa įtempius tempiamoje armatūroje, arba armatūros deformacijas ε_{si} lygias 0,0015. Tai atitinka standartinę S500 armatūrą. Taikant metodą ne etaloniniam elementui, lygtyje S2.3 pateikta vidutinė armatūros deformacija ε_{sm} įvertinama per pasirinktą vidutinių deformacijų metodą, kuris gali būti įvertintas tiek projektavimo normomis, tiek skaitiniais metodais (kaip baigtinių elementų analize grįstais metodais). Turint šią reikšmę, galima nustatyti koeficientą A etaloniniam elementui jį išreiškus kaip:

$$A = \frac{\varepsilon_{si} l_{eff} + \varepsilon_{si} l_d - 0{,}5\varepsilon_{sm} s_{rm,ref}}{0{,}5 l_{eff}^2}. \tag{S2.4}$$

Efektyvi zona aprašoma tiese, todėl armatūros ir betono sukibimo įtempiai yra pastovūs, išreiškus juos iš diferencialinės išraiškos:

$$\tau(x) = \frac{E_s \text{Ø}_s}{4} \frac{d\varepsilon_s}{dx} = A \frac{E_s \text{Ø}_s}{4}. \tag{S2.5}$$

Žinant pasirinkto etaloninio elemento armatūros ir betono sukibimo įtempius τ bei minimalią armatūros deformacijų reikšmę ε_{s0}, nustatomą iš S2.2 lygties, galima įvertinti vidutinius atstumus tarp plyšių bet kuriam kitam armatūros skersmens ir armavimo procento konfigūracijos tempiamam gelžbetoniniam elementui.

Siekiant atlikti palyginimą, iš mokslinės literatūros buvo surinkti 170 tempiamų elementų eksperimentiniai duomenys. Visi bandiniai yra 100×100 mm skersmens, centriškai armuoti vienu armatūros strypu. Pritaikius pasiūlytą metodą, gautos atstumų

tarp pagrindinių plyšių reikšmės pateiktos S2.1 lentelėje. Etaloniniu elementu pasirinktas Ø14 mm skersmens strypas.

S2.1 lentelė Vidutinių atstumų tarp plyšių skaičiavimo reikšmės taikant Euronormas 2 kaip vidutinių deformacijų metodą, esant 100×100 mm skerspjūviui

$Ø_s$	ρ_s	$s_{rm,exp}$	$l_d \neq 0$		$l_d = 0$	
			s_{rm}	$s_{rm} / s_{rm,exp}$	s_{rm}	$s_{rm} / s_{rm,exp}$
mm	%	mm	mm		mm	
10	0,78	217,6	226,1	1,05	231,9	1,07
12	1,13	182,5	188,4	1,03	191,0	1,05
14	1,54	162,4	162,4	–	162,4	–
16	2,00	149,9	144,0	0,96	141,9	0,95
20	3.14	137,6	116,7	0,85	111,1	0,81

Pasiūlyto metodo palyginimas su projektavimo normomis ir eksperimentiniais duomenimis pateiktas grafiškai S2.2 paveiksle.

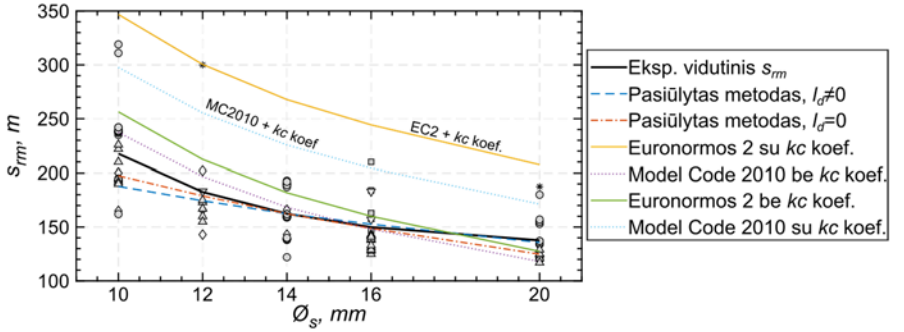

S2.2 pav. Skaičiavimo rezultatų palyginimas su eksperimentiniais duomenimis bei projektavimo normomis

Pasiūlyta suderintų deformacijų koncepcija pasižymėjo santykiniu tikslumu 0,85–1,05 rėžėse, lyginant su eksperimentiniais duomenimis. Tuo tarpu Euronormų 2 rezultatai viršijo daugiau nei 50 % vidutinį atstumą tarp pagrindinių plyšių. Armatūros ir betono sukibimo zonų ties pagrindiniais plyšiais įvertinimas šiek tiek pagerina rezultatus, bet visumoje pasižymi santykinai mažu poveikiu atstumams tarp plyšių.

3. Suderintų deformacijų metodo adaptavimas lenkiamų armuotų betoninių konstrukcijų atstumų tarp plyšių nustatymui

Trečiajame disertacijos skyriuje toliau išplėtotas pasiūlytas suderintų deformacijų metodas ir pritaikytas lenkiamiems armuotiems betoniniams elementams. Pagrindinės metodo prielaidos išlaikomos tos pačios, bet atsisakyta etaloninio elemento empirinės sąvokos, kas leidžia metodą pritaikyti tiesiogiai, be iteracinių skaičiavimų. Armatūros

deformacijų pasiskirstymas, išilgai elemento gretutinių pagrindinių plyšių, taip pat priimamas tiesinis, tačiau įtraukiama nauja centrinės zonos sąvoka. Ši zona reprezentuojama horizontalia linija viduryje nagrinėjamo gelžbetoninio elemento blokelio, kurį apriboja du pagrindiniai plyšiai, siekiantys neutraliąją ašį. Tiesiškas supaprastinimas atspindi vidutinę deformacinę elgseną dėl antrinių plyšių. Šiame skyriuje detaliai išnagrinėtas pasiūlyto metodo taikymas, palyginimas su projektavimo normomis bei kitais skaičiavimais.

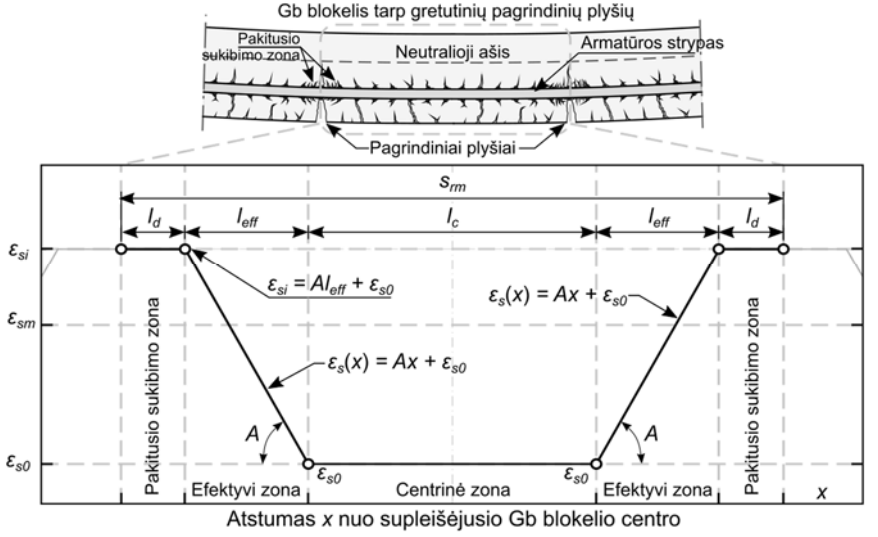

S3.1 pav. Taikoma supaprastinta armatūros deformacijų tarp gretutinių pagrindinių plyšių lenkiamuose gelžbetoniniuose elementuose schema

Pagal pasiūlytą metodą, vidutinis atstumas tarp plyšių nustatomas iš atskirų jį sudarančių zonų sumos – tai pakitusio sukibimo, efektyviųjų bei centrinės zonų:

$$s_{rm} = 2l_d + 2l_{eff} + l_c. \tag{S3.1}$$

Kaip ir tempiamiems elementams, suderintų deformacijų metodas pagrįstas vidutinių armatūros deformacijų lygybe tarp dviejų skaičiavimo koncepcijų: vidutinių deformacijų ir diskrečiųjų plyšių. Lenkiamiems elementams pritaikius S3.1 paveiksle pateiktą armatūros deformacijų supaprastinimo schemą, suderintų deformacijų sąlyga išreiškiama taip:

$$\frac{2\varepsilon_{si}l_d + 2\left(\varepsilon_{si} - 0{,}5Al_{eff}\right)l_{eff} + \varepsilon_{s0}l_c}{2l_d + 2l_{eff} + l_c} = \varepsilon_{sm}. \tag{S3.2}$$

Vidutinės armatūros deformacijos ε_{sm} nustatomos iš pasirinkto vidutinių deformacijų metodo (kaip Euronormos 2 arba Model Code 2010). Pasiūlytas modelis remiasi, kad pakitusio sukibimo zonos l_d ilgis yra nustatomas iš atskiro šios zonos modelio. Siekiant nustatyti efektyviosios zonos ilgį, galima išreikšti S3.2 lygtį kaip:

$$Al_{eff}^2 + (2\varepsilon_{sm} + l_cA - 2\varepsilon_{si})l_{eff} + (l_c\varepsilon_{sm} + 2l_d\varepsilon_{sm} - l_c\varepsilon_{si} - 2l_d\varepsilon_{si}) = 0, \tag{S3.3}$$

taip įmanoma toliau supaprastinti ją į kvadratinę lygtį:

$$Al_{eff}^2 + Bl_{eff} + C = 0, \quad \text{(S3.4)}$$

koeficientą B galima nustatyti iš lygties:

$$B = l_c A - 2(\varepsilon_{si} - \varepsilon_{sm}), \quad \text{(S3.5)}$$

ir koeficientą C iš:

$$C = -(\varepsilon_{si} - \varepsilon_{sm})(l_c + 2l_d). \quad \text{(S3.6)}$$

Koeficientas A nustatomas iš sukibimo įtempių priklausomybės nuo armatūros skersmens lygties S2.5. Taigi, efektyvios zonos ilgis l_{eff} išreiškiamas kaip kvadratinės lygties sprendinys:

$$l_{eff} = \frac{-B + \sqrt{B^2 - 4AC}}{2A}. \quad \text{(S3.7)}$$

Pateiktas bendras sprendimo algoritmas skirtas nustatyti vidutinį atstumą tarp plyšių bet kokios konfigūracijos gelžbetoniniam elementui. Tačiau norint nustatyti efektyvios zonos l_{eff} ilgį būtina žinoti centrinės zonos l_c ilgį. Šiame darbe buvo išvestas fizikinis šios zonos modelis, pasitelkiant 14 surinktų eksperimentinių lenkiamųjų elementų bandinių iš Calderón Bello (2008) bandymų programos. Įstačius eksperimentinį vidutinį atstumą tarp plyšių $S_{rm,exp}$ į S3.1 ir S3.2 formules galima išreikšti centrinės zonos ilgį l_c:

$$l_c = 2 \times \sqrt{\frac{\varepsilon_{sm} s_{rm,exp} - \varepsilon_{si} s_{rm,exp} + Al_d^2 + 0{,}25As_{rm,exp}^2 - As_{rm,exp} l_d}{A}}. \quad \text{(S3.8)}$$

Apskaičiavus centrinės zonos reikšmes atrinktiems elementams, jos buvo atidėtos pagal atstumą tarp neutraliosios ašies ir tempiamos armatūros ašies $d - y_0$ (S3.2 pav). Pastebėta aiški koreliacija tarp šių parametrų, todėl regresijos būdu išvestas fizikinis centrinės zonos l_c modelis, pateiktas lygtyje S3.9. Šis modelis pasižymi determinacijos koeficientu $R^2 = 0{,}9874$.

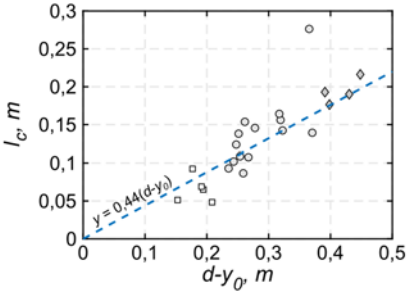

S3.2 pav. Centrinės zonos fizikinis modelis, išvesta priklausomybė nuo atstumo tarp neutraliosios ašies ir tempiamos išilginės armatūros ašies

$$l_c = 0{,}44(d - y_0). \quad \text{(S3.9)}$$

Ištyrus centrinės zonos priklausomybę nuo armavimo procento pastebėta, kad centrinė zona sudaro didesnę dalį bendro atstumo tarp plyšių, kai elementas yra stipriai armuotas (S3.3 pav.) lyginant su silpniau armuotais elementais. Tai paveikia ir efektyvios zonos ilgį, kas sąlygoja mažą skirtumą tarp maksimalių armatūros deformacijų, aptinkamų pagrindiniame plyšyje, ir minimalių armatūros deformacijų, esančių viduryje nagrinėjamo gelžbetoninio blokelio, apriboto dviem pagrindiniais plyšiais. Todėl nors centrinės zonos

dalis bendrame atstume tarp plyšių ir išauga, jos absoliuti ilgio reikšmė yra mažesnė. Silpnai armuotiems, kuriems skirtumas tarp maksimalios ir minimalios armatūros deformacijos $\Delta\varepsilon_s$ ženkliai išauga, efektyvi zona pailgėja. Ši elgsena gali būti siejama lenkiamų gelžbetoninių elementų antrinių plyšių atsiradimu. Labiau armuoti elementai pasižymi didesniu skaičiumi antrinių plyšių, kurie išsivysto iki apatinio sijos paviršiaus. Tose vietose, kur atsiranda plyšiai, armatūra pradeda pernešti didesnę apkrovos dalį, o tai reiškia išaugusias armatūros deformacijas. Centrinė zona būtent atspindi vidutinę šių antrinių plyšių veikiamą armatūros deformacinę elgseną. Būtina pabrėžti, kad antriniam pleišėjimui ženklų poveikį gali turėti ir betono apsauginio sluoksnio aukštis. Esant dideliam aukščiui, antriniai plyšiai gali nepasiekti betono paviršiaus, o esant labai mažam, antrinių plyšių gali būti labai daug.

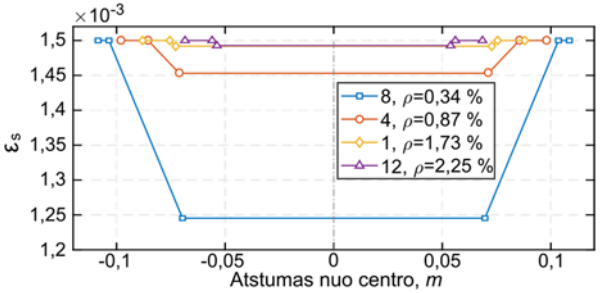

S3.3 pav. Armatūros deformacijų tarp gretutinių pagrindinių plyšių profiliai atrinktiems elementams 8, 4, 1 ir 12 iš Calderón Bello (2008) eksperimentų

Sukurtas suderintų deformacijų metodas bei pasiūlytas fizikinis centrinės zonos modelis buvo pritaikytas 96 surinktiems eksperimentiniams sijų ir plokščių bandiniams. Gautų vidutinių atstumų tarp plyšių reikšmės buvo palygintos santykiniu tikslumu su eksperimentiniais duomenimis bei projektavimo normomis (S3.4 pav.).

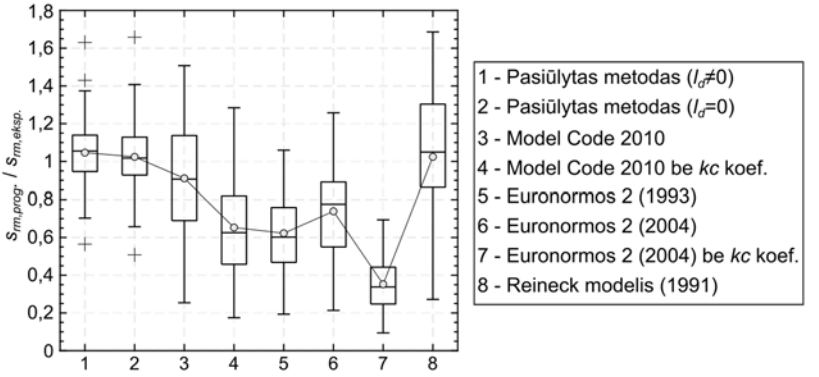

S3.4 pav. Skaičiavimų rezultatų, normalizuotų pagal eksperimentinius rezultatus, palyginimas tarp pasiūlyto metodo ir projektavimo normų

Pasiūlytas metodas pasižymi ženkliai patobulintu tikslumu taikant jį pagrindiniams plyšiams, pasiektas 1,04 tikslumas. Rezultatai šiek tiek geresni, kai neįvertinamos pakitusios sukibimo zonos ties pagrindiniais plyšiais. Pasiektas 1,02 tikslumas, bet sklaida šiek tiek išaugo. Lyginant su Euronormomis 2 arba Model Code 2010 rezultatais, vidutinės reikšmės yra saugios, t.y. pervertina tikrąjį plyšį, ko nepasiekia projektavimo normos. Bet būtina paminėti, kad normose nėra akcentuojama, kokiems plyšiams jos taikomos, todėl saugiau daryti prielaidą, kad normos vertina visus plyšius: tiek antrinius, tiek pirminius.

Pasiūlytos koncepcijos rezultatai pateikti lentelėse ir grafikuose, išanalizuotas atskirų parametrų poveikis. Pasiektas metodo tikslumas bei sklaida žymiai geresnė už projektavimo normų rezultatus. Santykinis tikslumas, normalizavus su eksperimentiniais duomenimis, pasiektas 1,04 ir 1,02, kai yra vertinama ir nevertinama pakitusio sukibimo zona. Pastebėta, kad armatūros skersmens poveikis atstumui tarp plyšių auga mažėjant armavimo procentui. Didžiausią poveikį vidutiniam atstumui tarp plyšių turi elemento efektyvus aukštis ir neutraliosios ašies padėtis.

4. Dirbtinių neuroninių tinklų pritaikymas atstumų tarp plyšių prognozavimui

Ketvirtasis disertacijos skyrius skirtas surinktų eksperimentinių lenkiamų gelžbetoninių elementų analizei pasitelkiant dirbtinius neuroninius tinklus bei siekiant išvystyti jų pagrindu paremtą vidutinių atstumų tarp plyšių modelį. Šiam tikslui buvo panaudoti duomenys iš trečio skyriaus, taip užtikrinant palyginamumą su pasiūlytų suderintų deformacijų metodu. Siekiant užtikrinti kokybišką neuroninių tinklų kalibravimą, ypač įvertinus gan mažą turimų duomenų kiekį, buvo pasirinktas daugiaiteracinis metodas. Šis metodas sudarė sąlygas statistiškai įvertinti atskirus neuroninius tinklus ir jų tikslumą bei elgseną apmokant didelį jų skaičių kiekvienai tiriamai konfigūracijai. Tam tikslui taikomi atsitiktiniai svoriai. Papildomai buvo panaudoti pakaitiniai duomenys, kurie buvo sugeneruoti imituojant tikrų duomenų statistinį pasiskirstymą, remiantis Kolmogorovo-Smirnovo testu. Šie duomenys leido įvertinti, ar gaunami rezultatai, neuroninio tinklo tikslumas, galimybė prognozuoti vidutinius atstumus tarp plyšių nėra atsitiktinumas. Patikrinta, ar surinkti eksperimentiniai duomenys pasižymi tikrais fizikiniais sąryšiais tarp reikšmių. Kadangi šie ryšiai yra žinomi iš gelžbetoninių konstrukcijų tyrimų, tikrinama, ar gautas pasiskirstymas atitinka tikėtiną. Neuroninių tinklų kalibravimui, kiekvienai konfigūracijai buvo atliekama po 2000 iteracijų, taikant atsitiktinius pradinius svorio koeficientus.

Palyginus pakaitinius duomenis patvirtinta, kad surinkti eksperimentiniai duomenys tikrai pasižymi fizikiniais ryšiais tarp parametrų reikšmių. Aukščiausia pasiekta regresijos koeficiento *R* reikšmė ~0,5, o dauguma išsidėsto tar p –0,1 ir 0,2. Šių neuroninių tinklų regresijos koeficientai ženkliai atitolę nuo nuo tikrų duomenų rezultatų skirstinio, kur prasčiausi neuroniniai tinklai pasižymi *R* reikšme apie 0,5 ir pasiekia iki ~0,99 (S4.1 pav.). Pakaitinių duomenų pasiskirstymas bendrai pasižymi didesne sklaida palyginus su tikrų duomenų atveju.

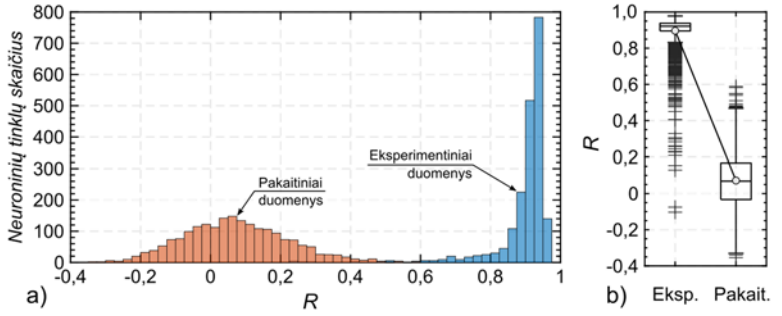

S4.1 pav. Nepriklausomam tikrinimui naudojamų eksperimentinių bei pakaitinių duomenų ir iš jų gautų prognozių pasiskirstymas: a) neuroninių tinklų regresijos koeficiento *R* pasiskirstymas tikriems bei pakaitiniams duomenims; b) duomenų statistika

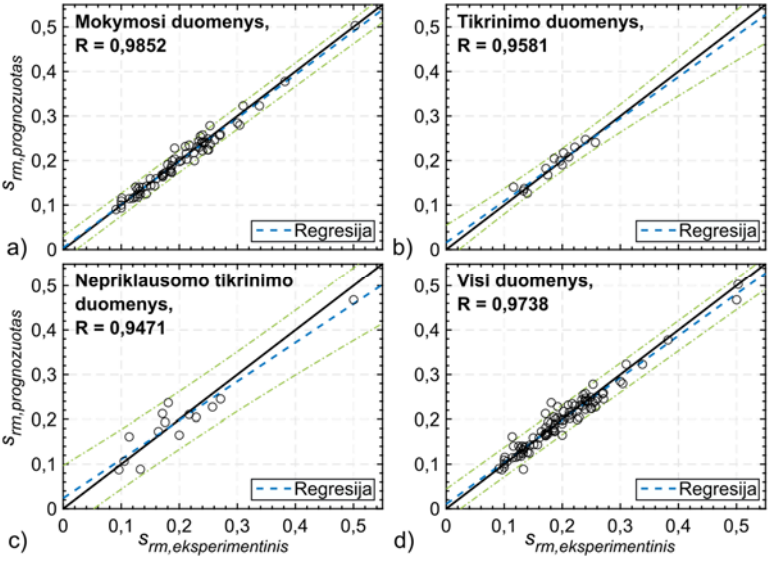

S4.2 pav. Tiesinė regresija tarp neuroninio tinklo prognozių ir eksperimentinių vidutinių atstumų tarp lenkiamų gelžbetoninių elementų pagrindinių plyšių duomenų: a) mokymosi duomenų rinkiniui, b) tikrinimo duomenų rinkiniui, c) nepriklausomo tikrinimo duomenų rinkiniui bei d) bendram visų duomenų rinkiniui

Atrinktas geriausias neuroninis tinklas pasižymi labai aukštu tikslumu. Žvelgiant į visus duomenis buvo pasiektas R = 0,9738, o analizuojant tik nepriklausomo tikrinimo duomenis, pasiektas R = 0,9471. Įvertinus mažą surinktų duomenų kiekį, pasiektas geras tikslumas nepriklausomiems duomenims, kurie nedalyvavo dirbtinių tinklų mokymo procese. Šie duomenys sudarė 15% nuo visų duomenų, taip pat 15% buvo atsitiktinai atrinkta dirbtinių neuroninių tinklų konvergavimui. Likę 70% buvo atsitiktinai atrinkti tinklo apmokymui. Regresijos grafikai pateikti S4.2 paveiksle.

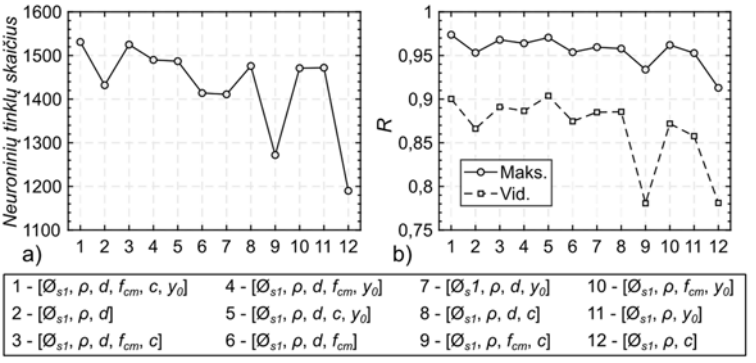

S4.3 pav. Tempiamojo elemento apkrovos ir deformacijų diagramos:
a) įvertinus pradines deformacijas dėl susitraukimo, b) neįvertinus susitraukimo

Siekiant pažvelgti į atskirų parametrų poveikį neuroninio tinklo elgsenai, pradiniai duomenys buvo sudalinti į 11 papildomų rinkinių iš tų pačių įvesties duomenų (S4.3 pav.). Pastebėta, kad prasčiausią tikslumą demonstruoja tie neuroniniai tinklų modeliai, kurie be pagrindinių armatūros skersmens Ø ir armavimo procento ρ reikšmių naudoja tik betono apsauginį sluoksnį c arba betono gniuždymo stiprį f_{cm}.

Apmokintas ir kalibruotas neuroninis tinklas pademonstravo labai aukštą tikslumą ir labai gerai sukontroliuotą sklaidą eksperimentiniams duomenims. Pasiektas idealus santykinis vidutinis tikslumas 1,0, o 25 % ir 75 % kvartiliai apriboti 0,95–1,05 ribose. 99,3 % procentų aprėpties ribose prognozės patenka į 0,83–1,18 ribas. Užfiksuotas aukštas generalizavimo lygis, nerodantis jokios ryškios tendencijos pervertinti arba pakankamai neįvertinti vidutinio atstumo tarp plyšių, išskyrus apsauginio betono c atžvilgiu. Prie šito gali prisidėti ribotas kiekis gelžbetoninių elementų, kurių apsauginis sluoksnis virš 60 mm.

Bendrosios išvados

Išanalizavus mokslinę literatūrą bei pleišėjimo teoriją, galima teigti, kad:

1. Esami gelžbetoninių konstrukcijų pleišėjimo modeliai yra ženkliai išsibarstę fizikinių parametrų atžvilgiu. Daugelis metodų priklauso nuo empirinių nuostatų. Metodai nėra suderinti plyšių pločio, atstumų tarp plyšių bei deformacijų analizės ažvilgiu. Armatūros skersmens ir armavimo procento santykis $Ø/\rho_{ef}$ yra dažnai naudojamas pleišėjimo metoduose. Šis faktorius yra empirinis dėl savo priklausomybės nuo efektyvaus tempiamojo betono ploto sąvokos.
2. Dirbtinių neuroninių tinklų pritaikymas tirti pleišėjimą, būtent vidutinius atstumus tarp plyšių yra ribotas. Keli tryimai, kurie bandė prognozuoti atstumus tarp plyšių, buvo nenuoseklūs atrenkant eksperimentinius duomenis, nesuderinant jų bei neužtikrinant tinkamą neuroninių tinklų kalibravimą.

Išanalizavus tempiamų gelžbetoninių elementų pleišėjimo elgseną buvo inovatyvus suderintų deformacijų metodas šių elementų atstumų tarp plyšių prognozavimui. Bevystant metodą, atskleista:

3. Tiesinė armatūros deformacijų $\varepsilon_s(x) = Ax + \varepsilon_{s0}$ išraiška leidžia pakankamu tikslumu aprašyti deformacijas aukštesniuose apkrovimo lygiuose. Tai leidžia aprašyti armatūros deformacijas tarp pagrindinių plyšių išskiriant dvi zonas: efektyviąją, kurioje egzistuoja armatūros ir betono sąveika, ir pakitusio sukibimo zoną, kurioje ši sąveika priimama kaip neegzistuojanti dėl pažeisto betono. Šių zonų bendras ilgis sudaro atstumą tarp pagrindinių plyšių.
4. Pasiūlytas suderintų deformacijų metodas vidutinių atstumų tarp gretutinių pagrindinių plyšių nustatymui pasižymi darnumu deformacinės bei pleišėjimo elgsenų atžvilgiu. Šį darnumą užtikrina vidutinių deformacijų lygybė tarp dviejų skirtingų pleišėjimo koncepcijų: vidutinių deformacijų ir įtempių perdavimo. Šių metodų apjungimas leidžia pasinaudoti abiejų metodų privalumais: aukšto tikslumo vidutinių deformacijų įvertinimu bei deformacijų pasiskirstymu erdvėje tarp dviejų pagrindinių plyšių.
5. Suderintų deformacijų metodas pasižymi maža priklausomybe nuo empirinių nuostatų, remdamasis tik etaloninio elemento sąvoka, kuri aprašoma armavimo procentu ρ_{ref}, armatūros skersmeniu $Ø_{ref}$ bei vidutiniu atstumu tarp plyšių $s_{rm,ref}$.
6. Suderintų deformacijų metodo rezultatai parodė gerą atitikimą eksperimentinėms reikšmėms. Taikant Euronormas 2 kaip vidutinių deformacijų metodą, tikslumas buvo nuo –13 % iki +2 % ribose. Taikant tempiamojo sustandėjimo modelį buvo pasiektas tikslumas nuo –15 % iki +5 % ribose. Pasiūlytu metodo nustatyti armatūros betono sukibimo įtempiai $\tau = 2{,}24 f_{ct}$ mažai skiriasi nuo mokslinėje literatūroje ir normose sutinkamų $\tau = 1{,}8–2{,}0 f_{ct}$ reikšmių.

Išplėtojus suderintų deformacijų metodą lenkiamoms gelžbetoninėms konstrukcijoms, buvo pastebėta, kad:

7. Tempiamos armatūros deformacijas tarp pagrindinių plyšių galima supaprastintai išreikšti per pakitusio sukibimo, efektyviąją bei centrinę zonas. Centrinė zona yra nauja koncepcija, kuri reprezentuoja vidutinę deformacijų elgseną viduryje tarp dviejų pagrindinių plyšių kaip horizontalią tiesę. Taip supaprastinami antriniai plyšiai, kurie įprastai būna išsiplėtoję šioje zonoje.
8. Centrinės zonos ilgiui l_c išvestas fizikinis modelis, kuris susieja šios zonos ilgį su efektyviuoju skerspjūvio aukščiu bei neutraliąja ašimi. Pasiūlyta $l_c = 0{,}44(d - y_0)$ išraiška. Nustatyta, kad ši zona yra ženkliai ilgesnė stipriau armuotoms lenkiamoms gelžbetoninėms konstrukcijoms, taip sumažinant efektyvios zonos ilgį.
9. Normalizuotas metodo tikslumas, įvertinant pakitusio sukibimo zonas ties pagrindiniais plyšiais, siekiantis 1,04 santykinio tikslumo, lyginant su eksperimentinėmis reikšmėmis. Nevertinant pakitusio sukibimo zonų santykinis tikslumas yra 1,02. Prognozės yra saugios, viršijančios 1,0 santykinį tikslumą. Taikant Euronormas 2 ir Model Code 2010 projektavimo normas pagrindiniams plyšiams, santykinis tikslumas buvo atitinkamai 0,91 ir 0,74.

10. Pagal klasikinių metodų parametrą $Ø/\rho_{ef}$, armatūros skersmens $Ø_{s1}$ poveikis atstumui tarp pagrindinių plyšių mažėja su augančia armavimo procento ρ reikšme. Betono gniuždymo stiprio f_{cm} poveikis atstumams tarp plyšių minimalus.

Pritaikius dirbtinius neuroninius tinklus atstumų tarp plyšių skaičiavimui buvo galima patikrinti surinktus eksperimentinius duomenis bei palyginti sukurto diskrečiųjų plyšių metodo tikslumą. Atlikus šiuos skaičiavimus bei palyginimu, galima teigti, kad:

11. Pritaikius statistinius metodus, generuojant didelį skaičių neuroninių tinklų, bei lyginant su netikrais duomenimis apmokintais neuroniniais tinklais galima apmokinti dirbtinį neuroninį tinklą pasižymintį aukštu tikslumu ir geru generalizavimu mažam, išsibarsčiusiam gelžbetoninių elementų duomenų kiekiui.
12. Pasiektas 1,0 santykinis tikslumas apmokintam neuroniniam tinklui su sukontroliuota sklaida 0,83–1,18 ribose, apimančiose ~99,3 % visų rezultatų sklaidos. 25 % ir 75 % kvartilių rėžės, atitinkamai, 0,95–1,05. Palyginus su pasiūlytu deformacijų suderinamumo metodu, tiek neuroninis tinklas, tiek pasiūlytas metodas pasižymi tvirtumu bei gebėjimu atkartoti sąryšius tarp lenkiamų gelžbetoninių elementų parametrų. Efektyvus gelžbetoninės konstrukcijos aukštis d, armatūros skersmuo $Ø$ bei armavimo procentas ρ pasižymi didžiausiu poveikiu vidutiniam atstumui tarp pagrindinių plyšių. Mažiau svarbūs buvo betono apsauginis sluoksnis c ir betono gniuždymo stipris f_{cm}.

Annexes[1]

Annex A. Experimental data employed for the analysis of tensile reinforced concrete elements
Annex B. *Matlab* code for the analysis of tensile reinforced concrete elements
Annex C. Experimental data and results from the analysis of flexural reinforced concrete elements
Annex D. *Matlab* code of flexural reinforced concrete element analysis
Annex E. Surrogate data set for artificial neural network comparison
Annex F. Declaration of academic integrity
Annex G. The co-authors' agreements to present publications material in the dissertation
Annex H. Copies of scientific publications by the author on the topic of the dissertation

[1]The annexes are supplied in the enclosed compact disc

Regimantas RAMANAUSKAS

PRIMARY CRACK SPACING MODEL OF REINFORCED CONCRETE ELEMENTS

Doctoral Dissertation

Technological Sciences,
Civil Engineering (T 002)

ATSTUMO TARP PAGRINDINIŲ PLYŠIŲ ARMUOTO BETONO ELEMENTUOSE MODELIS

Daktaro disertacija

Technologijos mokslai,
statybos inžinerija (T 002)

2019 10 07. 13,0 sp. l. Tiražas 20 egz.
Vilniaus Gedimino technikos universiteto
leidykla „Technika“,
Saulėtekio al. 11, 10223 Vilnius,
http://leidykla.vgtu.lt
Spausdino BĮ UAB „Baltijos kopija“,
Kareivių g. 13B, 09109 Vilnius